ISTANBUL TECHNICAL UNIVERSITY ★ GRADUATE SCHOOL OF SCIENCE ENGINEERING AND TECHNOLOGY

DUAL-CURABLE TEXTILE ADHESIVES FOR CORD/RUBBER APPLICATIONS

Ph.D. THESIS

Zehra YILDIZ

Department of Polymer Science and Technology

Polymer Science and Technology Programme

FEBRUARY 2017

ISTANBUL TECHNICAL UNIVERSITY ★ GRADUATE SCHOOL OF SCIENCE ENGINEERING AND TECHNOLOGY

DUAL-CURABLE TEXTILE ADHESIVES FOR CORD/RUBBER APPLICATIONS

Ph.D. THESIS

Zehra YILDIZ
(515112007)

Department of Polymer Science and Technology

Polymer Science and Technology Programme

Thesis Advisor: Prof. Dr. Hacer Ayşen ÖNEN

FEBRUARY 2017

İSTANBUL TEKNİK ÜNİVERSİTESİ ★ FEN BİLİMLERİ ENSTİTÜSÜ

ÇİFT-KÜRLENEBİLEN TEKSTİL YAPIŞTIRICILARININ KORD KUMAŞ/KAUÇUK UYGULAMALARI

DOKTORA TEZİ

Zehra YILDIZ
(515112007)

Polimer Bilim ve Teknolojisi Anabilim Dalı

Polimer Bilim ve Teknolojisi Programı

Tez Danışmanı: Prof. Dr. Hacer Ayşen ÖNEN

ŞUBAT 2017

Zehra YILDIZ, a Ph.D. student of İTU Graduate School of Science Engineering and Technology student ID 515112007, successfully defended the thesis/dissertation entitled “DUAL-CURABLE TEXTILE ADHESIVES FOR CORD/RUBBER APPLICATIONS”, which she prepared after fulfilling the requirements specified in the associated legislations, before the jury whose signatures are below.

Thesis Advisor :	**Prof. Dr. Hacer Ayşen ÖNEN** İstanbul Technical University	....
Jury Members :	**Prof. Dr. İ. Ersin SERHATLI** İstanbul Technical University	....
	Prof. Dr. İsmail USTA Marmara University	....
	Prof. Dr. Yeşim GÜRSEL Istanbul Technical University	....
	Prof. Dr. M. Vezir KAHRAMAN Marmara University	....

Date of Submission : 06 February 2017
Date of Defense : 28 February 2017

To my precious family and dearest friends,

FOREWORD

This thesis is the result of my five years of studying in several different laboratories; Polymeric Materials Research and Development Laboratory (POLMAG) in the faculty of Arts and Sciences, Istanbul Technical University, Chemical Tests Laboratory, in the Faculty of Technology, Marmara University, and School of Materials Science and Engineering Research Laboratory in Georgia Institute of Technology. This research was funded by the Research Fund of Istanbul Technical University. I feel myself lucky for having the opportunity to work in those well-appointed laboratories with precious people and to be a graduate student in Polymer Science and Technology Programme. First of all, I would like to thank to my supervisor Prof. Dr. H. Ayşen Önen for her patience and colloborative efforts on my research. She helped me to overcome all difficulties during my research and supplied a great impact on my future career. I would like to give my sincere thanks to Prof. Dr. Atilla Güngör for his valuable and enlightening contribution on my research. He is one of my scientific idols and I will never forget his kind supports. I also would like to thank his dearest wife Prof. Dr. Günay Güngör for the arrangement of all Skype meetings during my research in US. Many thanks to my doctoral committee members; Prof. Dr. İ. Ersin Serhatlı and Prof. Dr. İsmail Usta for their valuable contribution on my work. I owe special thanks to Prof. Dr. Youjiang Wang and Prof. Dr. Karl Jacob for having me a chance to be in Georgia Tech as visiting researcher.

I would like to express my sincere appreciation to my colleagues; Res. Asst. Onur Atak, Dr. Tuba Çakır Çanak, Dr. Emrah Çakmakçı, Res. Asst. Nergis Demirel Gültekin and her husband Dr. Bekir Cenkkut Gültekin for their kind assistance for my research and analysis. I wish to thank to my friends from Georgia Tech; Dr. Wail Fallah, M.Sc. Bandu Kale, Dr. Iryna Davydenko and her husband Dr. Kosta Ziabrev for their help and friendship during my research. Also I wish to thank Ms. Zuhal Nart (Izomas Co.) due to her valuable consultancy and support in cord fabric supplement.

My final appreciation goes to my beloved family; my mom Ayşe Yıldız, my dad Ekrem Yıldız, my mother-in-law Müzeyyen Yıldız, my father-in-law Naci Yıldız, and my dearest husband Asst. Prof. Dr. Kazım Yıldız for their patience and encouragement during all stages of my life.

December 2016

Zehra YILDIZ
(Research Assistant)

TABLE OF CONTENTS

Page

ABBREVIATIONS

AA	: Acrylic acid
AETO	: Acrylated epoxidized tung oil
AIBN	: Azobisisobutyronitrile
Ar	: Argon
AV	: Acid value
$CDCl_3$	: Deuterated chloroform
CO_2	: Carbon dioxide
CS	: Chondroitin sulfate
DGEBA	: Diglycidyl ether of bisphenol-A
DMSO-d6	: Deuterated dimethylsulfoxide
DPGDA	: Dipropylene glycol diacrylate
DS	: Degree of swelling
DSC	: Differential scanning calorimetry
EA	: Epoxy acrylate
EB	: Electron beam
EDS	: Energy dispersive X-ray spectroscopy
EEW	: Epoxy equivalent weight
ETO	: Epoxidized tung oil
FTIR	: Fourier transform infrared
GF	: Gel fraction
HCl	: Hydrochloric acid
$HClO_4$	: Perchloric acid
HDDA	: 1,6-Hexanediol diacrylate
HDI	: Hexamethylene diisocyanate
He	: Helium
HEA	: 2-Hydroxyethyl acrylate
HEMA	: 2-Hydroxyethyl methacrylate
HQ	: Hydroquinone
^1H NMR	: Proton nuclear magnetic resonance
H_2O_2	: Hydrogen peroxide
IPDI	: Isophorone diisocyanate
KOH	: Potassium hydroxide
LCD	: Liquid-crystal display
LOI	: Limiting oxygen index
MAA	: Methacrylic acid
MEHQ	: Hydroquinone monomethyl ether
MEK	: Methyl ethyl ketone
MMA	: Methylmethacrylate
MWCNT	: Multi-walled carbon nanotube
N_2	: Nitrogen
$NaHCO_3$	: Sodium bicarbonate
NaOH	: Sodium hydroxide
NVP	: N-vinylpyrrolidone
O_2	: Oxygen

PET	**:** Polyethylene teraphthalate
PUA	**:** Polyurethane acrylate
PVB	**:** Polyvinyl butyral
PVC	**:** Polyvinyl chloride
RFL	**:** Resorcinol fomaldehyde latex
SBR	**:** Styrene butadiene rubber
SEM	**:** Scanning electron microscopy
TCDDA	**:** Tricyclodecane dimethanol diacrylate
TDI	**:** 2,4-Toluene diisocyanate
TGA	**:** Thermogravimetric analysis
THF	**:** Tetrahydrofuran
TMPTA	**:** Trimethylolpropane triacrylate
TMPTMA	**:** Trimethylolpropane trimethacrylate
TO	**:** Tung oil
TPP	**:** Triphenyl phosphine
UV	**:** Ultraviolet
VPA	**:** Vinylphosphonic acid
VPAMETO	**:** Vinylphosphonic acid modified epozidized tung oil

SYMBOLS

°C	: Celcius degree
h	: Hour
kJ/mol	: Kilojoule per mole
M	: Molarity
min	: Minute
mL	: Mililiter
mL/min	: Mililiter per minute
mm	: Milimeter
MPa	: Megapascal
N	: Normality
N/cm	: Newton per centimeter
nm	: Nanometer
ppm	: Partical per million
w	: Weight
µL	: Microliter
s	: Second
%	: Percentage
Ɵ	: Theta angle
ƟY	: Youngs' contact angle
γ	: Surface free energy

LIST OF TABLES

Page

LIST OF FIGURES

Page

DUAL-CURABLE TEXTILE ADHESIVES FOR CORD/RUBBER APPLICATIONS

SUMMARY

Cord fabric reinforced rubber composites have been widely used in some industrial applications such as car and bicycle tires, hoses, conveyor belts etc. A good adhesion between the polar cord fabric and non-polar rubber surfaces is the most crucial factor determining the product life and quality. In tyre production process, the tyre cord (polyester, polyamide, etc.) is treated first with a resorcinol formaldehyde latex (RFL) and then with a terpolymer of 2-vinylpyridine-styrene-butadiene to adhere the cord onto the rubber surface. This treatment gives a close bonding of tyre cord to rubber essential in the production of tires. Since the formaldehyde usage causes adverse effect on human health and environment, its usage has been restricted in many countries. Some manufacturers tried to use epoxy resin as adhesive instead of formaldehyde in tyre production. Because of this process is solvent-based, another danger can be seen resulting from the accumulation of high amounts of solvent in the factory roof which can cause explosion by the effect of any electrical leakage. Considering the mentioned tyre production processes and their dangers, a new process is desired without any formaldehyde and solvent usage.

UV-curing technology became so important and popular recently due to its superior properties such as instant drying, being ecofriendly and solvent-free process, requiring less energy and so on. UV-curable coating formulations consist of three basic components; oligomer, photoinitiator, and reactive diluent. The reactive diluents in the process help to lower the viscosity of the oligomer and improve the overall structural properties of the end product. Oligomers are macromolecular complexes that can be polymerized by photolysis of photoinitiators with the exposure of UV light. Epoxy acrylate (EA), polyester acrylate, polyurethane acrylate (PUA) are mostly used oligomers in UV-curable coatings.

In order to reduce the UV energy and increase the polymerization rate, a dual-curable oligomer having both UV-curable and thermal-curable functional groups in one resin is desirable such as monoacrylate-terminated EA oligomers. EA oligomers having vinyl ester groups with carbon-carbon double bonds at the end of the epoxy resin, are generaly used in industrial applications because of excellent adhesive and non-yellowing properties, flexibility, hardness, and chemical resistance. The epoxy part gives toughness to the cured films whilst carbon-carbon and ether bonds give chemical resistance to the structure. The reaction between epoxy and an acid produces hydroxyl groups, thereby introducing polarity which can improve the wettability of adhesive. UV-curable PUAs are formed by the reaction of two chemical species containing an isocyanate group (toluene 2,4-diisocyanate (TDI), isophorone diisocyanate (IPDI), etc.) and a hydroxyl group (2-hydroxyethyl methacrylate (HEMA), 2-hydroxyethyl acrylate (HEA), etc.). The isocyanate groups are responsible for the stiffness and hardness properties whereas hydroxyl groups give flexibility to the oligomer. PUA

oligomers are favored due to the excellent chemical resistance, good adherence and durability, superior thermo-mechanical properties.

The aim of the present thesis work is to develope new types of formaldehyde-free adhesive formulations that will show a good bonding in textile cord fabric/rubber composites. In the first stage, bisphenol-A type epoxy was reacted with acrylic acid (AA) at various molar concentrations. The effects of carboxyl/epoxide ratio and vinylphosphonic acid (VPA) content on the thermal characteristics and adhesion properties of coatings were investigated. The obtained EA oligomers were characterized by Fourier transform infrared (FTIR) and proton nuclear magnetic resonance (^{1}H NMR) spectroscopies. The completion of photopolymerization was proven by FTIR analysis by observing the disappearance of acrylate absorption peak after UV curing. Adhesive formulations were prepared by using the synthesized EA oligomers and then coated on cord fabrics via dip-coating process. The unsaturated groups of the oligomer were crosslinked onto the cord fabric by using UV light. The thermal properties of EA coated UV-cured cord fabric samples were searched by thermogravimetric analysis (TGA) and differential scanning calorimetry (DSC). After coating and UV-curing stage, thermal stability increased because of the increment in carbon amount. The EA layer provided more amorphous structure thus lower melting temperature values were observed compared to the cord fabric. Scanning electron microscopy (SEM) images showed that EA coated fiber surface gained a smoother structure without any agglomeration. Contact angle measurement of the UV-cured cord surface proved that AA increment in oligomer caused a more hydrophobic behavior because hydroxyl groups of the acid form hydrogen bonding with the oxygen atom of the polyester cord fabric. After UV-curing stage, cord fabrics were put between two styrene-butadiene-rubber (SBR) layers and thermally cured by using heat and pressure in order to adhere the treated cord surface to the rubber layer. After dual-curing process, peel test was applied to evaluate the adhesion property of the oligomer. Peel testing results showed that the best peel strength with 18.0 N/cm has been obtained when the carboxyl/epoxide ratio was set as 1. The highest acrylate functionality in the oligomer structure allows more connection point between the double bonds of SBR during the thermal curing process. When VPA was included to the adhesion formulation as adhesion promoter higher adhesion strength values were obtained with flame resistant property. This result can be explained by the flame retardant property of the phosphorous in VPA inherently. Furthermore, when VPA amount in the formulation increases, thermal stability and char formation also increases. ECE washing process and NaOH treatment were applied on cord fabrics before coating process, in order to increase wettability character of the surface with a more functionalized property. The highest adhesion strength value (50.8 N/cm) was recorded in the sample having 10 % VPA in the formulation.

In the second stage of the thesis, bio-based adhesive formulations were designed to adhere textile cords and rubber. Tung oil (TO) was chosen as a bio-source due to the high degree of unsaturation compared to other vegetable oils, providing opportunity to design new oligomeric structures. For the oligomer synthesis, TO was firstly epoxidized and then reacted with AA. The obtained epoxidized tung oil (ETO) and acrylated epoxidized tung oil (AETO) oligomers were characterized by FTIR, ^{1}H-NMR spectroscopies, thermal analysis and then applied between the textile cord and rubber surfaces as adhesive. Contact angle measurement was performed from the coated UV-cured cord fabric surfaces. Peel test was used to evaluate the adhesion strength between coated UV-cured cord and rubber surfaces. Results showed that thermo-oxidative stability of TO increased after the inclusion of epoxide groups to the structure. Contact angle values decreased with increasing AETO amount in the adhesive formulation due to the hydrophilic character of epoxidized free fatty acids. The highest peel strength values of 26.0 N/cm and 20.5 N/cm were obtained with the inclusion of 50 % AETO and 75 % VPAMETO to the formulation.

In the last stage of the thesis, dual-curable formaldehyde-free adhesive formulations were prepared with the reaction of TDI and HEMA and then the obtained PUA oligomers were included into the formulations by using different types of reactive diluents. Polyvinyl butyral (PVB) was also included to the formulation as an adhesion promoter. All oligomers were characterized by FTIR and ^{1}H NMR spectroscopies. The adhesion formulations were applied on cord fabrics upon adhere onto the rubber surfaces. The effects of PVB ratio, NCO:OH molar ratio, and reactive diluent types on adhesion strength in cord/rubber composites were all investigated. Results showed that after coating and UV curing stages, both thermal stability and melting temperature of the cord fabric decreased due to the inclusion of amorphous regions into the fabric structure. PVB gives strong binding ability and acts as adhesion promoter in cord fabric/rubber composites so the peel strength value increases with increasing PVB amount in the formulation. The best adhesion strength value of 94.7 N/cm was observed when 5 % PVB was included in the formulation. Trimethylolpropane trimethacrylate (TMPTMA) and tricyclodecane dimethanol diacrylate (TCDDA) were used as reactive diluents in the adhesive formulations. The bulky and cyclic nature of tricyclodecane unit in TCDDA gives to the coating formulation a higher thermal stability, higher rigidity, with a better peel strength compared to the TMPTMA included samples. The highest adhesion strength value of 100.4 N/cm was recorded when TCDDA was used as reactive diluent in the formulation. Considering the NCO:OH molar ratio in the oligomer, thermal stability, gel fraction, glass transition and melting temperatures, adhesion strength were all increased whilst swelling degree and weight loss with chemical exposure decreased with increasing NCO:OH ratio. This result can be explained by the trimerization reactions and formation of intermolecular hydrogen bonding resulting a highly crosslinked, three dimensional structure with less molecular mobility and higher adhesive strength. The highest adhesion strength of 103 N/cm was obtained when the NCO:OH ratio was set as 4. Furthermore, TCDDA and TMPTMA were used together as reactive diluent in various ratios. The adhesion strength was investigated in terms of reactive diluent composition. Accordingly, the highest adhesion strength value of 111.6 N/cm was recorded in the sample having only TCDDA as reactive diluent. As mentioned before, this result can be explained by the increase in surface functionality due to the cyclic, bulky nature of tricyclodecane units in TCDDA.

ÇİFT-KÜRLENEBİLEN TEKSTİL YAPIŞTIRICILARININ KORD KUMAŞ/KAUÇUK UYGULAMALARI

ÖZET

Kord kumaşı ile güçlendirilmiş kauçuk kompozitleri, araba ve bisiklet lastikleri, hortum, taşıyıcı bantlar gibi pek çok endüstriyel alanda kullanılmaktadır. Polar yapıdaki kord kumaşı ile polar olmayan kauçuk yüzeyler arasında iyi bir yapışmanın olması, ürünün ömrünü ve kalitesini belirleyen en önemli faktördür. Araba lastiği üretiminde kord kumaşlar (polyester, polyamit, vb.) kauçuk yüzeylere yapıştırılmak amacı ile ilk olarak rezorsinol formaldehit lateks (RFL) ile ve sonra 2-vinilpiridin-stiren-bütadien terpolimeri ile muamele edilmektedir. Bu işlem kumaşın kauçuk yüzeye, lastik üretimi için gerekli olan şekilde yapışmasını sağlamaktadır. Formaldehit kullanımı, insan sağlığı ve çevre üzerindeki yan etkilerinden dolayı pek çok ülkede yasaklanmıştır. Bazı üreticiler araba lastiği üretiminde formaldehit yerine epoksi reçine kullanımını denemişlerdir. Fakat bu yöntemin solvent bazlı oluşu, büyük miktarlarda buharlaşan solventin tesis içinde birikip herhangi bir elektrik kaçağı ile patlamalara sebep olabileceği ihtimali ile diğer bir tehlikeyi beraberinde getirmektedir. Lastik üretimindeki bu tehlikeler göz önünde tutulduğunda, formaldehit ve solvent içermeyen yeni bir sisteme ihtiyaç duyulmaktadır.

Son yıllarda UV-kürleme teknolojisi, hızlı kuruma, çevre dostu olma, solvent içermeme, daha az enerji gerektirme gibi üstün özelliklerinden dolayı önemli ve popüler hale gelmiştir. UV-kürlenebilir kaplama formülasyonları, oligomer, fotobaşlatıcı ve reaktif seyreltici olmak üzere üç temel bileşenden oluşmaktadır. Proseste kullanılan reaktif seyrelticiler oligomer viskozitesini düşürmede ve son ürünün yapısal özelliklerini geliştirmede yardımcı olurlar. Oligomerler, UV ışınlarının etkisi altında parçalanan fotobaşlatıcılar varlığında polimerleşen makromoleküler yapıdaki bileşiklerdir. Epoksi akrilat (EA), polyester akrilat, poliüretan akrilat (PUA) UV-kürlenebilir kaplamalarda en çok kullanılan oligomerlerdir.

UV-enerji kullanımını azaltmak ve polimerizasyon hızını arttırmak amacı ile, monoakrilat sonlu EA oligomerleri gibi UV ve termal kürlenebilen fonksiyonel grupları aynı anda bulunduran, dual-kürlenebilir oligomerlerin üretimi önem kazanmaktadır. Epoksi reçinenin bir ucunda karbon-karbon çift bağlı vinil ester grupları bulunduran EA oligomerler endüstriyel uygulamalarda, üstün yapışma ve sararmama özellikleri, esneklik, sertlik ve kimyasal dayanım özelliklerinden dolayı sıklıkla kullanılmaktadır. Kürlenen filme epoksi grubu sertlik verirken karbon-karbon ve eter bağları kimyasal dayanım sağlamaktadır. Epoksi ve bir asit arasındaki reaksiyon sonucu hidroksil grupları oluşmakta, dolayısı ile yapıştırıcının ıslanabilirlik özelliği polaritenin artması sonucu iyileşmektedir. UV-kürlenebilir PUAlar, izosiyanat grup (toluen diizosiyanat (TDI), izofron diizosiyanat (IPDI) vb.) ve hidroksil grup (2-hidroksietil metakrilat (HEMA), 2-hidroksietil akrilat (HEA) vb.) içeren iki farklı kimyasal bileşiğin reaksiyonu ile üretilirler. Oligomerdeki izosiyanat grubu sertlik ve sağlamlık özelliklerinden sorumlu iken hidroksil grupları esneklik sağlamaktadır.

PUA oligomerler yüksek kimyasal dayanımları, iyi yapışma özelliği, dayanıklılık ve üstün termo-mekanik özelliklerinden dolayı tercih edilmektedir.

Sunulan bu tez çalışmasının amacı, tekstil kord kumaşı ve kauçuk yüzeyler arasında iyi bir yapışma gösteren, formaldehit içermeyen yeni tipte yapıştırıcı formülasyonları geliştirmektir. Tezin ilk aşamasında, bisfenol-A tipi epoksi, farklı mol oranlarında akrilik asit (AA) ile reaksiyona sokulmuştur. Karboksil/epoksit oranı ve VPA miktarının kaplamaların termal ve yapışma özelliklerine olan etkileri incelenmiştir. Elde edilen EA oligomerler Fourier transform kızılötesi (FTIR) ve proton nükleer manyetik rezonans (^{1}H NMR) spektrometreleri ile karakterize edilmiştir. Fotopolimerizasyonun tamamlanması, FTIR analizi ile, UV-kürlemeden sonra akrilat absorpsiyon pikinin kaybolmasını izleyerek ispatlanmıştır. Bu EA oligomerler yapıştırıcı formülasyonlarına eklenmiş ve dip-kaplama ile kord kumaş yüzeylerine uygulanmıştır. Oligomer üzerindeki doymamış grup UV ışınları ile kord kumaş üzerinde sertleştirilmiştir. EA kaplı, UV-kürlenmiş kord kumaş numunelerinin termal özellikleri termogravimetrik analiz (TGA) ve diferansiyel taramalı kalorimetre (DSC) ile incelenmiştir. Kaplama ve UV-kürleme işlemleri sonrası artan karbon miktarı ile termal kararlılık artmıştır. EA kaplama daha amorf bir yapı kazandırdığından, ham kord kumaşa göre daha düşük erime sıcaklık değerleri gözlenmiştir. Taramalı elektron mikroskobu (SEM) fotoğrafları, EA kaplamanın lif yüzeyini aglomere olmadan daha düzgün hale getirdiğini göstermiştir. UV-kürlenmiş kord kumaş yüzeyinden temas açısı ölçümleri, AA artışı ile, polyester kumaş üzerindeki oksijen atomu ve asidin hidroksil grupları arasında oluşan hidrojen bağları sonucu, daha hidrofobik bir yapının oluştuğunu ispatlamıştır. UV-kürlemeden sonra kord kumaşlar kauçuk yüzeylere yapıştırılmak üzere, iki stiren-bütadien-kauçuk (SBR) tabaka arasına konmuş, sıcaklık ve basınç uygulanarak termal olarak kürlenmiştir. Çift-kürleme işleminden sonra, oligomerin yapışma özelliğini incelemek amacı ile yapışma testi yapılmıştır. Yapışma testi sonucuna göre en yüksek yapışma kuvveti 18.0 N/cm ile karboksil/epoksit oranı 1 olduğunda elde edilmiştir. Oligomerdeki akrilat fonksiyonel gruplarının artması termal kürleme işlemi sırasında SBR'ın çift bağları ile daha çok bağlanma noktası oluşumunu sağlamıştır. Yapıştırıcı formülasyonuna, yapışmayı arttırıcı olarak VPA eklendiğinde, daha yüksek yapışma kuvveti değerleri ve fosfor gruplarının doğasından gelen güç tutuşur özelliğinden dolayı yanma dayanımlı yapılar elde edilmiştir. Ayrıca, fosforun yapısından dolayı VPA artışı, termal kararlılık ve kül oranlarının artmasını sağlamıştır. Yapıştırıcının uygulanmasından önce kord kumaşları, daha hidrofilik ve fonksiyonel özellik kazandırmak amacı ile, ECE deterjanı ile yıkanmış ve sodyum hidroksit (NaOH) ile muamele edilmiştir. En yüksek yapışma kuvveti 50.8 N/cm değeri ile % 10 VPA içeren formülasyonda elde edilmiştir.

Tezin ikinci aşamasında, tekstil kordlarını kauçuğa yapıştırmak için biyo-tabanlı yapıştırıcı formülasyonları hazırlanmıştır. Diğer bitkisel yağlar ile kıyaslandığında, yeni oligomerik yapıların dizayn edilmesine olanak sağlayan, daha yüksek doymamışlık oranına sahip tung yağı (TO) biyo-kaynak olarak tercih edilmiştir. Oligomer sentezi için ilk olarak TO epokside edilmiş, sonra AA ile reaksiyona sokulmuştur. Elde edilen epokside tung yağı (ETO) ve akrillenmiş epokside tung yağı (AETO) oligomerleri, FTIR, 1H NMR spektrometreleri, termal analiz yöntemleri ile karakterize edilmiş, ve daha sonra tekstil kordları ve kauçuk yüzeyler arasında yapıştırıcı olarak uygulanmıştır. Dip-kaplamalı UV-kürlenmiş kord kumaşları temas açısı ölçümleri ile karakterize edilmiştir. Kord kumaş ve kauçuk yüzeyler arasındaki yapışma kuvveti yapışma testi ile değerlendirilmiştir. Epoksit grupların TO yapısına eklenmesi ile termo-oksidatif kararlılık artmıştır. Yapıştırıcı formülasyonundaki artan

AETO miktarı ile, epokside olmuş serbest yağ asitlerinin hidrofilik yapısından dolayı, temas açısı değerleri düşmüştür. En yüksek yapışma kuvveti değerleri olan 26.0 N/cm ve 20.5 N/cm, formülasyona % 50 AETO ve % 75 VPAMETO ilaveleri ile elde edilmiştir.

Tezin son aşamasında, formaldehit içermeyen çift-kürlenebilen oligomerler, TDI ve HEMA reaksiyonu ile hazırlanmış ve daha sonra elde edilen PUA oligomerler farklı reaktif seyrelticiler ile birlikte yapıştırıcı formülasyonlarında kullanılmıştır. Formülasyonlara polivinil bütiral (PVB) yapışmayı arttırıcı olarak ilave edilmiştir. Tüm oligomerler FTIR ve ^{1}H NMR spektrometreleri ile karakterize edilmiştir. Yapıştırıcı formülasyonları kord kumaşa, kauçuğa yapıştırılmak üzere uygulanmıştır. PVB miktarı, NCO:OH mol oranı ve reaktif seyreltici türünün, kord ve kauçuk yüzeyler arasındaki yapışma kuvveti üzerine olan etkileri incelenmiştir. Dip-kaplamalı UV-kürlenmiş kord kumaşların, termal kararlılık ve erime sıcaklıkları, kaplama sonrası amorf yapıların ilavesi nedeni ile düşmüştür. PVB, güçlü bir bağlanma yeteneği vererek, kord kumaş ve kauçuk yüzeyler arasında yapışmayı arttırıcı olarak rol almıştır. Formülasyondaki PVB miktarı arttıkça yapışma kuvveti artmıştır. En yüksek yapışma kuvveti olan 94.7 N/cm değeri, formülasyona % 5 PVB ilavesi ile elde edilmiştir. Trimetilolpropan trimetakrilat (TMPTMA) ve trisiklodekan dimetanol diakrilat (TCDDA) formülasyonlarda reaktif seyreltici olarak kullanılmıştır. TCDDA’daki trisiklodekan grubunun hacimli ve halkalı yapısı, yapıştırıcı formülasyonuna, TMPTMA içeren numunelere göre daha yüksek termal kararlılık, sertlik ve daha iyi yapışma kuvveti değerleri sağlamıştır. En yüksek yapışma kuvveti olan 100.4 N/cm değeri, reaktif seyreltici olarak TCDDA kullanıldığında elde edilmiştir. Oligomerdeki NCO:OH mol oranının etkisi incelendiğinde, NCO:OH oranı arttıkça, termal kararlılık, jel fraksiyonu, camsı geçiş ve erime sıcaklıkları, yapışma kuvveti artmış, şişme derecesi ve kimyasal çözeltiye maruziyet sonucu ağırlık kaybı değerleri azalmıştır. Tüm bu sonuçlar, trimerizasyon reaksiyonları sonucu oluşan moleküller arası hidrojen bağlarının, yüksek çapraz bağlanmış, üç boyutlu, düşük moleküler hareketliliğe sahip, yüksek yapışma kuvveti gösteren yapıların oluşması ile açıklanabilir. En yüksek yapışma kuvveti olan 103 N/cm değeri, NCO:OH mol oranı 4 olduğunda elde edilmiştir. Ayrıca, TCDDA ve TMPTMA reaktif seyrelticileri farklı oranlarda karıştırılarak da yapıştırıcı formülasyonlarına eklenmiş, yapışma kuvveti incelenmiştir. Buna göre en yüksek yapışma kuvveti değeri olan 111.6 N/cm reaktif seyreltici olarak tek başına TCDDA kullanılan formülasyonda elde edilmiştir. Bu sonuç daha önce belirtildiği gibi, TCDDA içerisinde bulunan hacimli ve halkalı grupların yüzey fonksiyonelliğini arttırması sonucu kord kumaş/kauçuk arasındaki etkileşimin artmasına ile açıklanabilmektedir.

1. INTRODUCTION

Textile cords are used as textile reinforcements for rubber products, primarily in automotive industry and especially in the tyre production industry. Other usage areas of textile cords are vehicle tyres, hoses, conveyor belts, airsprings etc. The main raw materials of cord fabrics are polyamide, polyester, aramid and rayon. First stage of cord fabric production is twisting of raw yarns as single or multi layers. Second stage is weaving of these twisted yarns by using fine weft yarns. Finally, the obtained cord fabric in this manner is applied hot stretching process and then treated by some chemicals in order to gain desired properties suitable for its usage areas.

Vehicle tyres are multi-component, composite materials consisting of cord fabric, rubber and an adhesive. The performance of the adhesive material that is used to bond cord and rubber together, directly affects the tyre quality. For this reason, academic researches to obtain the best adhesion degree with the most effective production stage have gained so much importance recently.

1.1 Purpose of Thesis

Conventional tyre production process contains some risks such as excessive amount of formaldehyde and solvent evaporation process. The objective of the present thesis work is to develop new types of formaldehyde-free adhesive formulations, which have a strong bonding ability between the textile cord and rubber material. For this purpose, epoxy ester oligomers were synthesized by using various acids such as acrylic acid, vinylphosphonic acid and fatty acids of tung oil. Polyurethane acrylate oligomers were synthesized in various NCO:OH molar ratio with the inclusion of PVB as adhesion promoter and different types of reactive diluents. The obtained oligomers were included in adhesive formulations, coated on textile cords via dip-coating, and then the adhesives were cured between cord/rubber surfaces by using UV and thermal energy. Spectroscopic analysis, physical characterization techniques, and peel test were applied to evaluate the adhesive properties and performance. This type of adhesive has dual-curable character due to the presence of both UV- and thermo-curable functional groups on its backbone. This dual-curable adhesive is newly born in literature, and just a few studies have been made about it. In this thesis work, the targeted adhesive will be the first that is used to bond textile cords to rubber surfaces.

1.2 Literature Review

The adhesion strength of rubber composites reinforced with textile cord fabrics is one of the deterministic properties for the vehicle tires quality and performance. RFL dipping formulation is widely used to adhere the cord onto the rubber surfaces [1, 2]. Since the formaldehyde usage causes adverse effect on human health and environment, its usage has been restricted in many countries [3-5]. Thus, a formaldehyde-free adhesive system is needed in the tire industry.

UV curing is a photochemical process in which high-intensity ultraviolet light is used to instantly “harden” or “dry” inks, coatings or adhesives. UV-curing can be classified into two major types; free radical and cationic. Free radical polymerization of acrylate functional resins is more common than cationic. Cationic polymerization involves the formation of Bronstead or Lewis acid during the UV initiation step, and then this acid polymerize such functionalities as an epoxide or vinyl ether. UV curing formulation consists of reactive oligomers, reactive diluents, and photoinitiators. The reactive diluents in the process help to lower the viscosity of the oligomer and improve the overall structural properties of the end product. Oligomers are macromolecular complexes that can be polymerized by photolysis of photoinitiators with the exposure of UV light. Commonly used oligomers are epoxy acrylates, polyester acrylates, urethane acrylates, and silicone acrylates. Liquid monomers and oligomers are mixed with a small percent of photoinitiators, and then exposed to UV energy. In a few seconds, the products - inks, coatings or adhesives instantly harden. In UV curing, there is no solvent to evaporate, no environmental pollutants, no loss of coating thickness, and no loss of volume. This results in higher productivity in short time, with a reduction in waste, energy use and pollutant emissions. The other advantages of UV-curing are good adhesion to various substrates, high curing rate, controlled elasticity, and high stability at storage [6, 7].

In order to reduce the UV energy and increase the polymerization rate, a dual-curable oligomer having both UV-curable and thermo-curable functional groups in one resin is desirable such as monoacrylate-terminated epoxy oligomers. By changing the equivalent ratio of acid and epoxy groups, it is possible to obtain monoacrylate-terminated EA with only one double bond at one end, while the other end has an epoxide group. Thus, a monoacrylate-terminated epoxyacrylate can be prepared, allowing both UV and thermal curing (dual-curing) processes [8-12].

EA oligomers having vinyl ester groups with carbon-carbon double bonds at the end of the epoxy resin, are generally used in industrial applications because of excellent adhesive and non-yellowing properties, flexibility, hardness and chemical resistance. The epoxy part gives toughness to the cured films, whilst carbon-carbon and ether bonds give chemical resistance to the structure. The reaction between epoxy acrylate and an acid produces hydroxyl groups, thereby introducing polarity which can improve the wettability of the adhesive. A number of studies have been made considering the epoxy acrylate usage for various adhesive applications. For instance, a dual-curable oligomer for liquid-crystal display (LCD) cell assembly, containing both double bond and epoxide group on the same molecule (monoacrylate-terminated epoxyacrylate), from the reaction of AA and diglycdylether of bisphenol-A (DGEBA) was synthesized. The reaction of AA and DGEBA catalyzed by triphenyl phosphine (TPP) in the temperature range of 60-120 ^{o}C [11, 13]. The adhesion strength on glass substrate for the UV-induced epoxies containing various monomers such as polyol, vinyl ether, and acrylate has been investigated. Additionally, the reactivity of the hydroxyl groups on the polymer chain and its effect on adhesion strength have been evaluated [14]. In another study, to develope a cycloaliphatic diepoxide crosslinkable acrylic latex coating; methylmetacrylate (MMA) for carboxyl functionality, HEMA for hydroxyl functionality were used, respectively. The crosslinking of the latexes with the diepoxide was catalyzed by using sulphonic or phosphonic acids [15]. A series of dual-curable adhesives was prepared by blending bisphenol A type methacrylate, glycidyl methacrylate, acrylic acid, a trifunctional monomer, a photoinitiator and a catalyst. The reaction was performed between these monomers to form a crosslinked structure wherein the epoxy groups reacted with the carboxyl groups in the presence of UV and thermal stimuli [16].

In literature, the effects of HEMA and NCO:OH ratio on the mechanical and physicochemical properties of UV-curable isophorone diisocyanate-based polyesterurethane methacrylates have been reported. Results have showed that an increase in NCO:OH ratio and HEMA percentage improves the hardness, thermal stability, and tensile strength due to the increase in crosslinking density and intermolecular interaction [17]. The effects of acryl-polyol concentration and NCO:OH ratio on the gelation process and micro-phase separation of polyurethane gels have also been investigated. A high NCO:OH ratio increases the formation of isocyanurates that act as crosslinking points, resulting in a higher gelation temperature [18]. Another study finds that swelling of the natural rubber/polyurethane block copolymers decreases with increasing NCO:OH ratio due to the formation of allophanate linkages with the help of the excess isocyanate groups [19]. The effects of NCO:OH ratio of polyurethane polyester elastomer [3], and castor oil based polyurethane [20] adhesives in wood-to-wood adhesion strength have been also discussed.

2. THEORETICAL PART

2.1 Tyre Industry

The first tyre was manufactured by John Boyd Dunlop in 1888 by using the Irish flax as reinforcing component. In 1923, rayon fiber was started to be used as fiber layer in tyres. Tyres have a great industrial importance since they represent a connection between the car and the road. They must be durable under extreme conditions during their lifetime and provide dimensional stability with a low rolling resistance. They must absorp minimum noise and vibration while transmitting the driving and braking torque. The quality of a tyre can affect driving comfort and safety, and it is also effective on fuel saving. A simple tyre consists of 19-25 different components with up to 200 raw materials and a perfect combination amoung the tyre components is needed for a high quality tyre. The basic components of a tyre can be seen in Figure 2.1. The tyre tread gives abrasion resistance to the whole tyre and the casing. The steel belt serves protection to the plies and transfers the stress from the steel to the fabric components and side wall. The side wall protects the ply with an excellent weathering, tearing, abrasion, ozone, and fatigue resistances [21-26].

Figure 2.1 : Basic components of a tyre [22].

2.1.1 Rubber chemistry

Rubbers are long and regular macromolecular chains with small substituents in spatially orientation. They show reversible deformation behavior namely elastic deformation under external forces. The deformation ratio depends on the backbone structure and molecular weight of the rubber. The structural units of rubber are easily movable even at low temperatures due to having low glass transition temperatures. For instance poly-cis-1,4-butadiene and poly-cis-1,4-isoprene have glass transition temperatures (T_g's) around -110 and -70 ^oC, respectively. The Tg value increases with increasing the irregularity in polymer chain (trans-1,4, 1,2 3,4 positions) and implementation of large pendant groups (styrene-butadiene-rubber). Rubber is converted into three-dimensional network via curing during the vulcanization process. Rubbers can be made by natural vegetable sources that is called as natural rubber latex or can be man-made such as butadiene rubber, styrene-butadiene rubber, isoprene rubber, chloroprene rubber, ethylene-propylene rubber, epichlorohydrin rubber, silicone rubber, polysulfide rubber etc.

Rubber can be participated in chemical reactions due to the presence of some reactive functional groups which allow to be modified by some chemical species. For instance, natural rubber latex has been epoxidized with the presence of performic acid and then *in-situ* polymerization reaction of methyl methacrylate monomer has been performed on the rubber surface. The obtained modified natural rubber latex films can be used in glove, balloon, and tubing manufacturing processes with a better surface roughness and less friction coefficient values [27]. The adhesion properties of sulphur-vulcanized styrene butadiene rubber have been improved by modifying the surface atmospheric pressure plasma treatment [28]. The surface of the ground rubber tire, that were generated from recycled car tires, has been modified by bulk polymerization of AA in order to be used in paving applications as asphalt binder [29]. Natural rubber surface has been epoxidized in order to obtain a self-healing property which is important for ballistic applications [30]. The rubber reactions can be also performed during the vulcanization (curing, crosslinking) process via the unsaturated double bonds on its structure. The unsaturated double bonds in both their cis- and trans-1,4 structural units in polymer backbone and situated in 1,2 positions (pendant vinyl groups) allow the chemical reactions. Double bonds in pendant groups are more reactive in radical reactions whilst double bonds in cis- and trans-1,4 positions are more reactive towards halogens, oxygen, sulphur, and peracids. Double bond reactivity in trans-1,4 position is lower than cis-1,4 position [31].

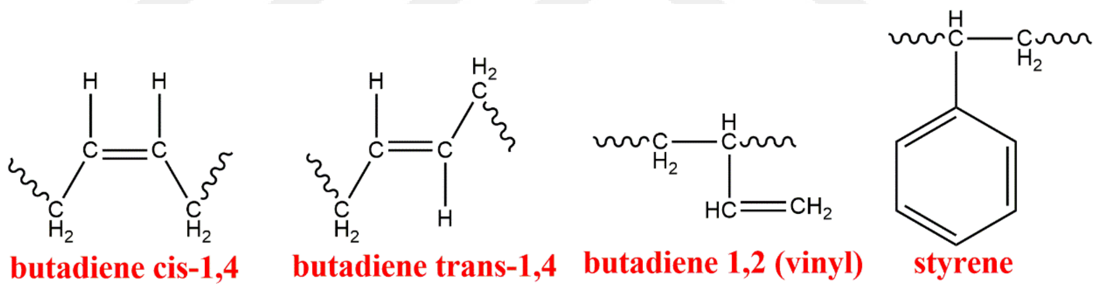

Figure 2.2 : Structural units of SBR.

2.1.2 Textile cords

Textile cords are being used in tyre industry to give dimensional stability to tyres, to reinforce the rubber compound, and to provide strength for heavy loads. Cords can be made from polyester, nylon, aramide, rayon yarns with high twist values in various fiber amount per cross section of yarn. The cord properties can be changed by the raw material of the cord, the number of plies and twist value of the yarn. Nylon gives a very good fatigue resistance and high toughness with a high tenacity due to its highly crystalline regions. Aramid fiber gives a very strong reinforcement to tyres, rubber hoses, and belts however they show very low elongation at break values. Polyester shows a good physical combination with high strength, low shrinkage, high modulus, and a good extensibility with a most competitive price for rubber industry. Rayon shows a high initial modulus with a wide range of testing temperature (30-70 ^oC). Some properties of textile cord fibers with their historical data can be seen in Table 2.2 [21, 32].

Table 2.1 : Properties of textile cord fibers with their historic data [21].

	Polyester	**Polyamide 6**	**Polyamide 6.6**	**Rayon (Viscose)**	**Aramid (Aromatic polyamide)**
Density (g/cm^3)	1.38	1.14	1.14	1.52	1.44
T_g (^oC)	69	50	57	--	>300
T_m (^oC)	285	255	255	--	--
T_d (^oC)	--	--	--	210	500
Moisture Content (%)	0.4	4	4	12-14	1.2-7
E-Modulus (cN/tex)	850	300	500	600-800	4000
Tensile Strength (MPa)	1100	850	850	685-850	2750
Year of Invention	1941	1938	1935	1885	1969
Introduction in Tyre Reinforcement	1962	1947	1947	1938	1974

(T_g Glass transition temperature, T_m Melting temperature, T_d Decomposition temperature)

2.1.3 Functionalization of textile surfaces

Adhesion is a phenomenon in textile materials/rubber composites due to the inherent non-polar property of textile surfaces and lack of the desired functionality. Surface functionalization of textile fibers has great importance since it determines the fiber-matrix interaction strength, and effects the chemical, mechanical, and physical properties of the composite. Textile surfaces should be functionalized with various techniques in order to gain some specific properties such as antibacterial, hydrophobic/hydrophilic/oleophobic, electrically conductive, flame resist properties etc. Functioanlity of a surface illustrates the number of groups that are suitable for bonding to other molucules under proper conditions. There are several ways to give the desired functionality to a textile surface. These techniques can be seen in Figure 2.1 [33-35].

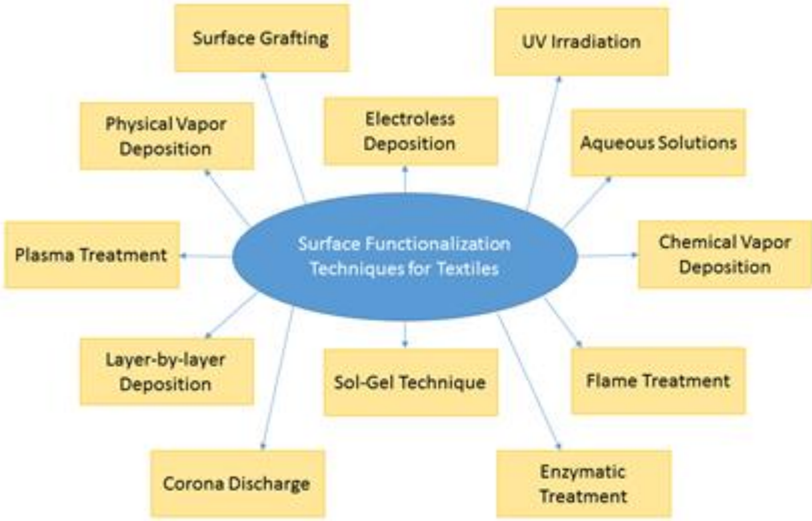

Figure 2.3 : Basic surface functionalization techniques in textile industry.

In literature, textile surfaces can be modified by aqueous solutions such as acids, alkaline, enzymatic, and isocyanate or by grafting some chemical species such as polyacrylic acid to the surface [36-39]. In a previous study, concentrated NaOH solution was used to functionalize the surface of poly(ethylene teraphthalate) (PET) films, in order to be used for cell proliferation via layer-by-layer assembly of chitosan and chondroitin sulfate (CS). Accordingly, the adhesion of endothelial cells onto the CS/chitosan assembled PET layers increased with increasing alkali treatment time [40]. The effect of cutinase enzyme and NaOH solution on the modification of amorphous and crystalline PET films have been also discussed and compared. FTIR spectroscopy and contact angle testing have been used to characterize the samples. Changes in peak intensities and carbonyl stretching peak areas have the evidence for alkali treatment. According to the contact angle testing, hydrophilicity of the surface was affected by alkali treatment more than enzymatic treatment. FTIR spectroscopy proved that conformational arrengement and chain orientation were affected by both enzymatic and alkali treatments [36].

In plasma treatment, textile surfaces are exposed to gas plasmas such as Ar, He, N_2, CO_2, O_2 etc. in various pressure, power, and time conditions to form radical sites on the surface [41]. Plasma treatment in N_2 atmosphere on polyester cord fabrics has been slightly improved the adhesion property of cord/rubber surfaces [42]. Aramid fiber surfaces have been modified by atmospheric air plasma technique with various plasma processing parameters. Application of the plasma treatment has improved the wettability and surface roughness of the fibers. Pull-out forces with the rubber matrix have been increased after plasma treatment [43]. Polypropylene nonwoven fabrics have been treated by low-pressure oxygen plasma in various plasma discharge power and exposure times, in order to see the changes in wettability and peel strength of the fabrics. Due to the formation of polar groups on the fabric surface, and the surface cleaning effect with plasma, the wettability property has been increased after plasma treatment. The functional reactive hydroxyl groups formed by plasma, may caused formation of covalent bonding with the isocyanate groups of polyurethane coating resulting in a better peel strength [44]. The advantages of plasma process are a being solvent free process and not having any chemical waste. In corona discharge process, an electrically induced stream of ionised air bombards the textile surface to form functional groups. Textile surfaces can also be modified upon UV irradiation in various wavelengths and flame treatment by burning the surface with reactive oxygen under ionised air. Sol-gel technique is also one of the most important one that consists of hydrolization of silica, application of the sols, and curing steps. Sol-gel can be applied with the combination of some textile finishes having different properties such as antiwrinkle, self cleaning, UV protection, controlled released, antistatic properties and so on [34].

2.1.4 Cord/rubber composites

Cord fabric reinforced rubber composites have been widely used in some industrial applications such as conveyor belts, hoses, car and bicycle tires, membranes etc. Considering the industrial applications of cord/rubber composites, adhesion between the two components is the most crucial factor, determining the product life and quality of the material. The modulus, elongation and polarity of both cord and rubber surfaces are completely different that means the adhesive material is so important. In literature a number of studies have been made regarding the adhesion issue between cord/rubber. Furthermore, the fatigue behaviors of cord/rubber composites have been investigated in terms of the material composition, after exposure to the various temperature, stress, and strain conditions [45]. The adhesion methods for cord/rubber composites can be seen in Figure 2.3. Cord fabrics have been treated by some chemical formulations such as RFL [1, 46, 47], cobalt boron acrylate [48], hydrated silica-resorcinol-hexamethoxymethylmelamine [49], prior to the adherence onto rubber surfaces [2, 50-53]. For instance, aramid cord fabrics have been treated with an epoxy-amine based oily finish and RFL dipping system prior to the adhesion to rubber [54]. A bonding combination of resorcinol formaldehyde, hexamethylene tetramine, and hydrated silica has been used to adhere nylon cord fabrics to the nitrile rubber [55]. Nylon cord fabrics have been also treated with RFL then adhered to the rubber in various vulcanization temperatures [1]. All these works represent formaldehyde usage in the process that has the potential to cause some health and environment related problems because of its toxicity. Therefore, preparation of formaldehyde-free adhesive formulations for cord fabric/rubber composites is crucial for tire industry.

Very few studies have been reported on the synthesis of dual-curable epoxyacrylate [11, 13, 16, 56, 57] and there was no research considering their application between textile cords and rubber surfaces as an adhesive. Therefore development of formaldehyde free adhesive formulations for cord/rubber application seemed as an innovative approach for tire industry.

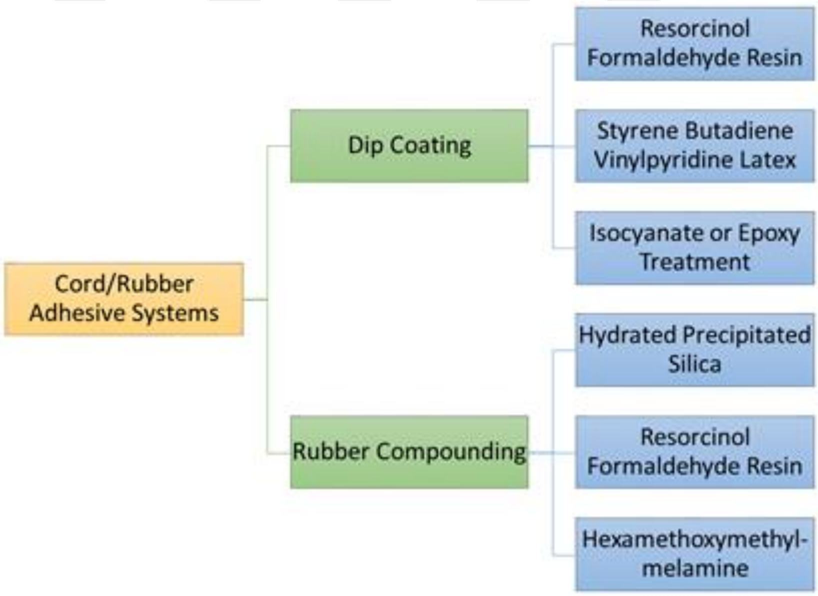

Figure 2.4 : Adhesion methods for cord/rubber surfaces.

The RFL system is the most widely used dipping solution in tyre industry. Resorcinol and formaldehyde helps bonding to the cord whilst latex bonds to the rubber surface during vulcanization. During the RFL treatment, resorcinol is dissolved in water and then formaldehyde and sodium hydroxide are added to the solution as condensation catalyst to form methanol groups (resole). Finally, latex is introduced to the solution. The cord fabric is immersed into the RFL solution and then passed through an oven under tension for curing of the coating material and drying of the solvents. The formaldehyde/resorcinol ratio, pH of the solution, resin/latex ratio, and the vulcanization temperature are variables of the RFL treatment that are effective on the adhesion strength of cord/rubber composites. The drawbacks of RFL treatment is being a multistep processing, which is costly and time consuming, and using toxic chemicals (formaldehyde) in the process [52, 58]. Hydrated precipitated silica is used as inorganic filler in rubber compounding in order to improve the cord/rubber adhesion and to reinforce the composites. Hexamethoxymethylmelamine is also used in cord/rubber adhesion systems as methylene donors that can be reacted with the resorcinol compound [32].

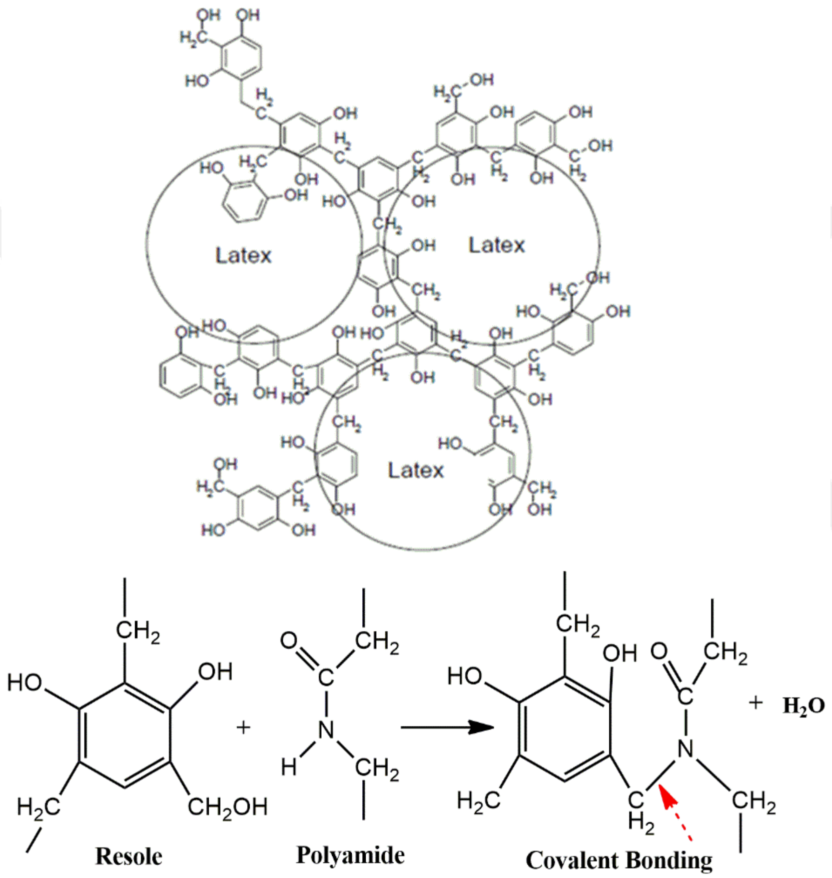

Figure 2.5 : The RFL dipping structure and covalent bonding between resole/polyamide molecules [21].

2.2 Adhesives for Textile Industry

Textile fibers are made from either natural sources (cotton, wool, silk, etc.) and chemical sources (polyester, polyamide, aramide, viscose, etc.). These fibers are being used in various industries such as automobile, aerospace, apparel, filtration, sports, geotextiles, furniture industry etc. Adhesion phenomenon of textile fiber onto a different surface is important to design high perfromance products. In textile based products, besides holding substrates together, adhesives, can also be used as a sealant, coating material, insulator, vibration damper, or a gap filler. Textile adhesives play an important role in manufacturing of lightweighted swimwears, protective clothings for fire-fighters and military applications, hot air baloons and so on. Adhesives in textile industry should present additional properties such as;

- ✓ Improvement in textile handling (wearable textiles),
- ✓ Water/vapor/air permeability (sportswear),
- ✓ Resistance to washing/dry cleaning,
- ✓ Tear and abrasion resistance (parachute materials),
- ✓ Barrier properties againist liquids/noise (rainwear clothes, automotive industry),
- ✓ Sterilization (medical textiles),
- ✓ Flame retardancy (furnitures, interior) [59].

Durability of a joint depends on several factors such as type of the adhesive, chemical and physical aging, moisture/temperature of the environment, curing conditions, surface treatment of the adherents, the amount and the application time of the load etc. All these variations should be considered while determining the adhesion performance [60].

Textile materials and all any types of adherent surfaces should be cleaned prior to the adhesion process. More than trace amount of dirt, grease, or any impurities may cause loss in adhesion strength and performance. Some pretreatments (chemical washing, flame treatment, corona, plasma) can be applied to the adherents before the adhesive application process.

Flexibility is one of the other problems in textile-based adhesion systems. Textile materials are inherently flexible so the interaction between the textile surface and adhesive material must be durable to any deformation.

The hydrophilicity of textile fibers (cotton, nylon, etc.) is the other problem that can affect the adhesion performance negatively. Textile fibers can absorp water/moisture from the atmosphere/environment resulting a dimensional change (swelling or shrinkage). This dimensional changes increase the stress on adhesion bonding so decrease the adhesion strength [59].

Textile adhesives can be classified based on the adhesive type. Solvent-based adhesives present high bonding strength and durability with a wide range of formulation selection. During the evaporation of solvent, large amounts of combustible gases can be accumulated in plants and may cause explosions. Waterborne adhesives are inexpensive comparing to the solvent-based adhesives. But evaporation of water requires high energy and time as well as it is not cost effective. Thermoplastic hot melt adhesives (polyamide, polyester, etc.) show instant bonding and require low energy usage. But specially designed equipments are needed for the application of the hot melts. Reactive liquid adhesives (polyurethane, etc.) are also needed low energy meanwhile they are expensive and require long curing times [59].

2.2.1 Adhesion theory

When two different surfaces come into contact, some attraction forces may occurred. If the contact is in molecular scale, there will be adhesion between these surfaces. Adhesion can be understood well with the knowledge of thermodynamic theory of wetting and spreading. Adhesives must present two different missions together; first they should wet the contacted surface and secondly they should make some bondings with the surface by hardening. Superhydrophobic surfaces show non-wetting and slippery properties against liquid droplets that is caused by air entrapment into the surface pores. This state is called as “Lotus effect” and is useful for some application areas such as biotehnology, micro/nano devices, self-cleaning surfaces, anti-icing, hydro-dynamic friction reduction etc. However, in some surfaces, liquid droplets do not roll off and they get pinned on the surfaces by wetting it. These kind of sticky surfaces are important in coating/adhesive applications, ink-jet printing, microfluidics, textile finishes etc. The liquid droplet behavior onto the surfaces can be investigated either by measuring the contact area between the droplet and surface (by means of contact angle) and by observing the effective contact length. Three interfacial energies can be seen in Figure 2.6 when a liquid droplet takes place on a surface; solid-liquid (SL), solid-vapor (SV), and liquid-vapor (LV). A high solid-vapor energy in other words a low Ɵ angle, causes wetting of the surface, whilst a low energy with a high Ɵ angle means a non-wetting surface, respectively [61-63].

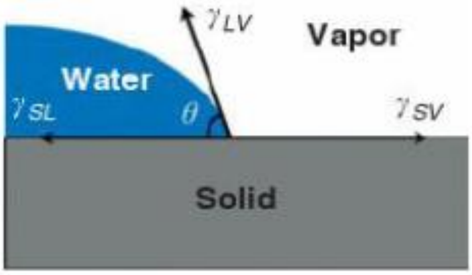

$$cos\theta = (\gamma_{SV} - \gamma_{SL})/\gamma_{LV}$$

Figure 2.6 : Liquid droplet onto a surface with three phases (S, solid; L, liquid; V, vapor) [63].

The type of adhesion between the adhesive and the substrate can occur by various types such as mechanical interlocking, diffusion, electronic bonding or chemically. The interaction type in a system depends on the roughness of surface and chemical structure of the adhesive. Due to the highly porous structure of textile surfaces, adhesive material can easily penetrate into the fabric pores, resulting an increment in interfacial contact area. When the adhesive material solidifed/cured, a mechanical locking between the adhesive and surface is occurred. The adhesive strength is the function of interfacial area and mechanical locking. An optimum adhesive penetration is needed to achieve a high adhesive strength since the penetration limits the fiber movement so decreases the strength and makes the textile surface rigid [59, 64].

“Wetting” in other words “the extent of the surface coverage” can be defined by the value of the contact angle of a liquid on a solid surface. A low contact angle (lower than 90^o) refers to a high wettability whilst a high contact angle (higher than 90^o) means poor wettability. A poor wetting causes interfacial defects consequently lowers the adhesive strength. Whereas a good wetting increases the work of adhesion that is directly proportional to the interfacial interactions. When the contact angle between the coating liquid and surface is zero, it means the coating liquid spreads out onto the surface completely and forms a film [62, 65-67].

The adhesion strength between the coating layer and substrate increases whenever the surface roughness increases. This result is stemming from the wetting effect of the coating liquid by penetrating through the surface and filling all grooves and pores. The wetting effect of a coating liquid with poor and good wettabilities can be seen in Figure 2.7. As mentioned before the penetration of the coating liquid cause mechanical locking because of the high interface area resulting an interlayer adhesion. The other properties that are effective on penetration except wetting are as follows; viscosity of the coating liquid, structure of the surface, temperature, pressure and type of the coating method. The fabric structural properties of openness, yarn/fiber fineness, surface finishes, roughness directly affect the wettability and penetration of the coating layer, thus affect the adhesion. Additionally, weak mechanical strength of the coating layer and big differences in thermal shrinkage between the layers cause decline in adhesion strength [66].

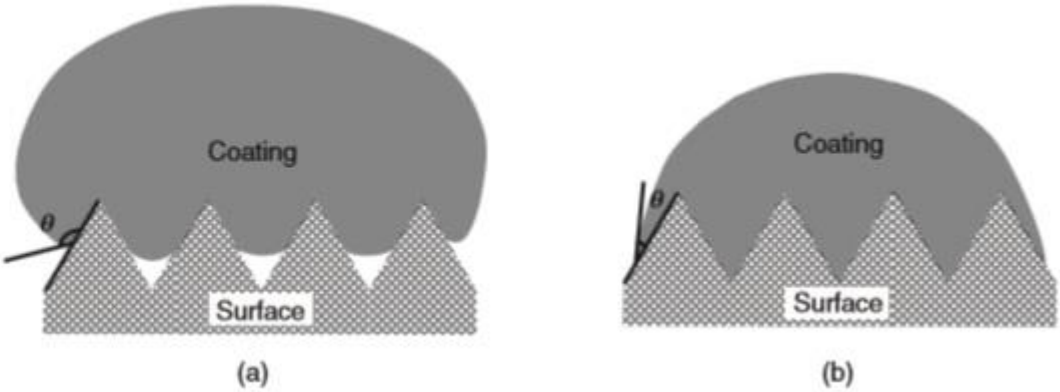

Figure 2.7 : Drops of the coating liquid with (a) poor wettability, (b) good wettability [66].

The adhesion theory can be described as several interactions between the adherents. These are; chemical bonding, mechanical interlocking, physical adsorption, diffusion, electrostatic interactions, and weak boundary layers [59].

2.2.2 Chemical bonding

Chemical bonding (60-700 kJ/mol) includes the chemical reaction of functional groups (hydroxyl, carbonyl, isocyanate etc.) in both substrate surface and adhesive material. Covalent, ionic, hydrogen bondings and Lewis acid-base interactions are the types of chemical bondings (Table 2.3). The term of "chemisorption" can be used for chemical bonding due to the combination of adsorption first following by the chemical reaction [59, 61].

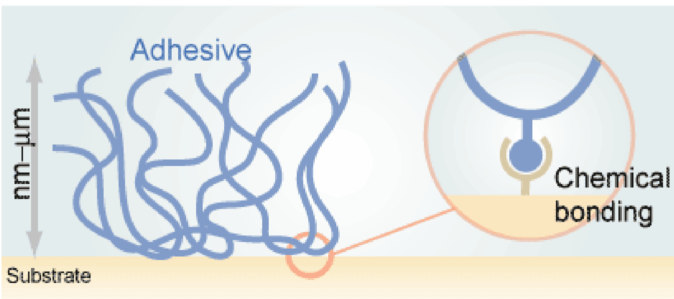

Figure 2.8 : Adhesion by chemical bonding [68].

Table 2.2 : Energies of typical chemical bonds [61].

	Type of Chemical Bonding	Energy (kJ/mol)
Covalent Bond	C-C	368
	C-O	377
	C-N	291
	Si-O	368
Ionic Bond	$Na^{+}Cl^{-}$	503
	$Al^{3+}O^{2-}$	4290
	$Ti^{4+}O^{2-}$	5340
Hydrogen Bond	-OH….OH (methanol)	32±6
	-OH…..O=C- (Acetic acid)	30±2
	-OH……N (Phenol-trimethylamine)	35±2
Lewis Acid-Base	BF_3+$C_2H_5OC_2H_5$	64
	C_6H_5OH+NH_3	33

2.2.3 Mechanical interlocking

Mechanical interlocking occurs via penetration of the adhesive material into the micro-voids of the adherents. So, after the curing of adhesive, adherents are bonded together mechanically. Surface roughness and irregularity of the adherents are the key factors for an effective mechanical interlocking interaction [59].

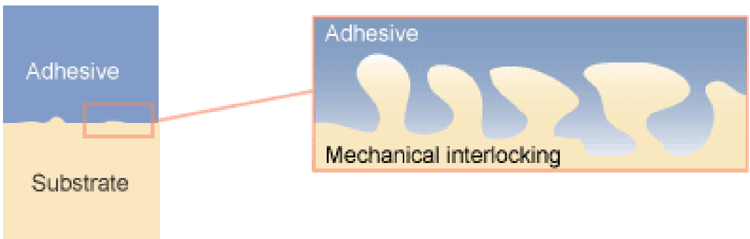

Figure 2.9 : Adhesion by mechanical interlocking [68].

2.2.4 Physical adsorption

During the physical adsorption, after the molecular contact of the adherents, adhesive molecules adsorp some molecules from the adherent surface via van der Waals forces. Dipole-dipole interaction is a kind of van der Waals forces with a low energy (≥2 kJ/mol). Molecules having permanent dipoles show stronger van der Waals forces. Molecular contact so as wetting is needed for physical adsorption interaction. In order to achieve a good wetting property, the surface energy of the adherent should be high and the surface tension of the liquid should be low [59, 61].

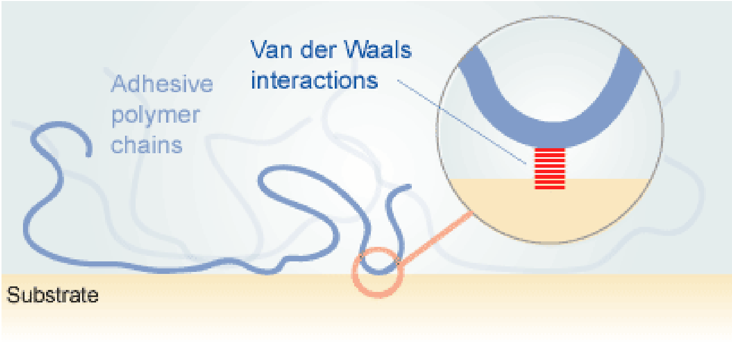

Figure 2.10 : Adhesion by physical adsorption [68].

2.2.5 Diffusion

In diffusion theory, the adhesive and adherent should be both polymeric and chemically compatible. Diffusion interaction takes place via the interdiffusion of the movable long-chain molecules between the adherent and adhesive material usually in a molten form. The schematic presentation of interdiffusion can be seen in Figure. The interdiffusion of polymer chains is affected by the physical form, time, temperature, and chemical properties [59].

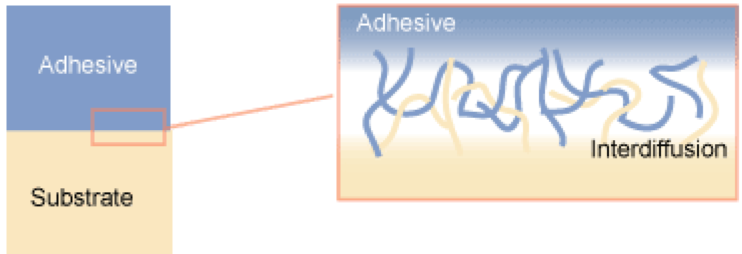

Figure 2.11 : Adhesion by interdiffusion [68].

2.2.6 Basic components of adhesive formulations

The main component of an adhesive formulation is the resin that provides the main structural and chemical properties. Catalysts/hardeners are added to accelerate/initiate the chemical curing process. In order to prevent side reactions, inhibitors are used. Solvents are used in adhesive formulations in order to increase the wettability of the fabric by lowering the viscosity of the resin. Thickeners provide increment in formulation viscosity. Reactive diluents act like solvents in adhesive formulation in lowering the viscosity but diluents do not evaporate instead they participate into the crosslinked resin structure by affecting the end product properties. Fillers are added to enhance specific properties of the end product such as flame retardant, coloring agent, durability, etc. Plasticizers provide flexibility to the adhesive system. Tougheners for toughness and tackifiers for self-adhesion are also added to the adhesive formulation.

Surfactants and wetting agents help to achieve a better dispersion of fillers and wetting property [59].

2.2.7 Adhesive application methods

A coated fabric can be accepted as a composite or hybrid textile. It means that hybrid textiles can provide functionality which cannot be performed by just a single component. Hybrid textile materials can be produced by using wide range of materials and processing methods for numerous structures with specific performances. "Coating" is one of the best known technique to produce hybrid textiles [69].

The textile surface needs to be clean before the coating process, because any surface contamination changes the surface characteristics thus affects the adhesion. Scouring/washing processes should be applied on textile surface before coating for removal of unwanted contamination. Furthermore, textile materials should be stabilized under a temperature higher than processing temperature in order to prevent shrinkage-related problems as a result of mechanical stress, heat, moisture and pressure during the coating process.

Coating process gives fabric surface some unique properties, that cannot be provided by using just fabric layer, including impermeability, flame retardancy, barrier, antistatic, antibacterial and insulation properties, conductivity, printability etc. Coated fabrics are used in a wide range of areas such as medical, apparel, automotive, architectural, ecological, agricultural textile applications, packaging materials and in synthetic leather. Adhesives are applied between the subtrates during coating process in order to provide good adhesion. The adhesive material should be compatible with the fabric layer and coating process. Selection of the coating process can be carried out considering several factors such as cost, production rate, environmental impacts, material properties, viscosity of the coating liquid, versatility etc.[69, 70]. The main coating techniques that are used in industrially and laboratuary scaled are explained briefly below.

Dip coating (impregnating) is the simplest amd most widely used coating method in textile industry. It is widely used to form very thin films onto the textile surfaces. The coating performance mainly depends on coating liquid, surface and process variables such as substrate and applicator, geometry, viscosity and surface tension of the coating liquid, coating velocity, surface roughness, wettability of fiber etc. For instance, a coating liquid with higher viscosity yields a thicker film on the surface [66].

In blade coating process, an excess of coating material is applied to the surface and the desired coating thickness is set and controlled by a metering blade. The blade is positioned above the surface and touches to the subtrate. The process variables are the shape and sharpness of the blade, alignment angle, and the degree of blade depression into the surface.

In air knife coating process, instead of a blade, excess coating material is applied to the surface and blown off by an air jet located on the air knife.

In metering rod coating process, the amount of coating material is controlled by a wire wound metering rod. Excess coating material is removed by a rod thus only the desired amount of coating liquid can pass through the wires. This method gives a precise coating thickness at relatively low cost. Rod coating method works best with coating liquid having low viscosity, because of the ease of flow between the wire levels. The process variables are surface speed and tension, metering rod rotation and penetration, coating liquid viscosity, wire shapes etc.

In transfer coating process, the coating material is first applied to a silicone release paper and then dried. The obtained paper passes through the laminating rollers together with the substrate by means of heat and pressure. After coating, the paper release peels away from the subtrate. The main advantage of this method is to obtain smooth and flexible coated fabrics.

Roll coating is the most well-known method in coating industry, and it can be catergorized according to the some variations such as the number, surface shape and rotating direction of the rolls.

In engraved roll coating method, the engraved roll is partially positioned in the coating bath. As it rotates, the coating liquid fills into the graves and is being carried by the engraved roller to the back-up roller. A doctor blade, that is existing upon the engraved roll, helps to remove the excess coating liquid from the surface.

Screen coating method can be mostly used in electrical applications and interlining production for textile fabrics. It provides an exact coating thickness and patterns even for the delicate surfaces. The coating material is applied through a mesh screen with squeezing roller. The coating properties can be changed by the screen mesh number, squeeze pressure, the angle between blade and the screen, viscosity of the coating material.

In the extrusion coating method, thermoplastic resin or reactive adhesives are fed directly to the surfaces. A wide range of coating thicknesses can be obtained by extrusion coating. The coating quality depends on the shape and contact angle of the lip, the position and pressure of the die, flow rate, melt temperature, compatibility between the coating layer and surface, speed of the coating line and the temperature of the coating roll.

In curtain coating method, the coating liquid freely falls onto a moving subtrate without any pressure or penetration force. The film thickness is in the range of just a few microns and does not affected from the surface roughness.

The powder coating method is an environmentally friendly process since it does not contain solvent, it forms just a few waste chemicals. It is also energy saving method because of no drying is existing. Solid powders are added to a fluidized bath, and the substrate passes through this bath. The solid powders are adhered to the subtrate with the help of electrostatic charges or pre-heated surface line. Sometimes the powder coating onto the substrate can be performed by means of an engraved roller.

The mostly used spray coating method is compressed air vaporization in which the air and coating material are pressed out through a nozzle. In this method a uniform coating thickness cannot be achieved but it can be applied even onto the irregular shapes. The other common spray coating methods are; airless pressure spray, hot flame spray, electrostatic spray, dry powder resin spray.

There are various coating methods apart from the commercially available and widely used processes such as electrospun coatings, electroless plating, sputter coating, chemical vapor deposition, supercritical fluid, and sol-gel coating [66, 71].

2.3 UV-Curing Technology

UV curing is a photochemical process in which high-intensity ultraviolet light is used to instantly "cure" or "dry" inks, coatings or adhesives. UV radiation is the strongest type of radiation that is invisible by human eye and can be divided into three groups based on the wavelength; UVA (320-400 nm), UVB (280-320 nm), and UVC (180-280 nm). The reactivity and concentration of the functional groups, the UV-light intesity, and the overall resin viscosity are effective parameters on the rate of polymerization in UV-curing technology. In order to limit the radical formation by controlling the polymerization rate during the photochemical process of EA's, any impurities and air should be eliminated. In literature, many studies were subjected to solve the adhesion problems of EA coatings considering the double bond conversion and surface energy differences between the adherent components [72].

Considering the polymerization type, UV-curing can be divided into two types; free radical and cationic. UV light initiates both radical and cationic polymerization but doesn't interfere with the propagation and termination stages. Free radical polymerization of acrylate functional resins is more common than cationic. In radical polymerization, molecules with an alkene group (unsaturated) take part such as vinyl ether, acrylates. In cationic polymerization, cation forming photoinitiators are used. Cationic polymerization involves the formation of Bronstead or Lewis acid during the UV initiation stage, and then this acid polymerize such functionalities as an epoxide or vinyl ether. Initiation and propagation stages are similar to radical polymerization but no termination with neutralization stage is observed in cationic polymerization. Instead, termination is performed by the nucleophilic impurities. The radical formation is inhibited by the oxygen in radical polymerization whilst cationic polymerization is insensitive to oxygen existence. In both radical and cationic polymerization the obtained polymer is insoluble. Figure 2.12 and 2.13 show the reaction steps of a photoinitiated free radical and cationic polymerizations, respectively [73-75]. Accordingly, R• radical is generated by the photo decomposition of the initiator. M and M• represent the monomer and monomeric radical, respectively.

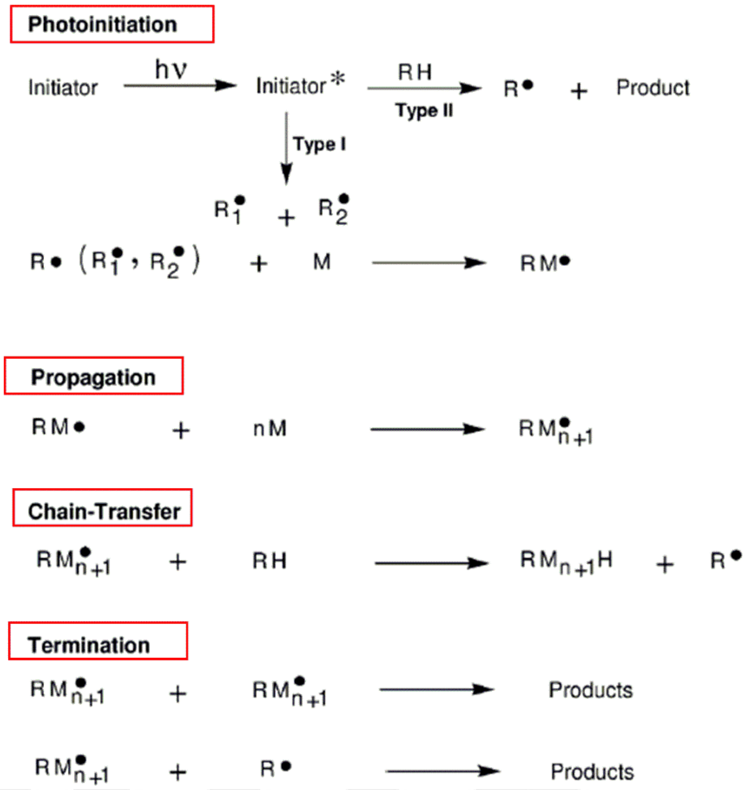

Figure 2.12 : Reaction scheme of free radical photopolymerization.

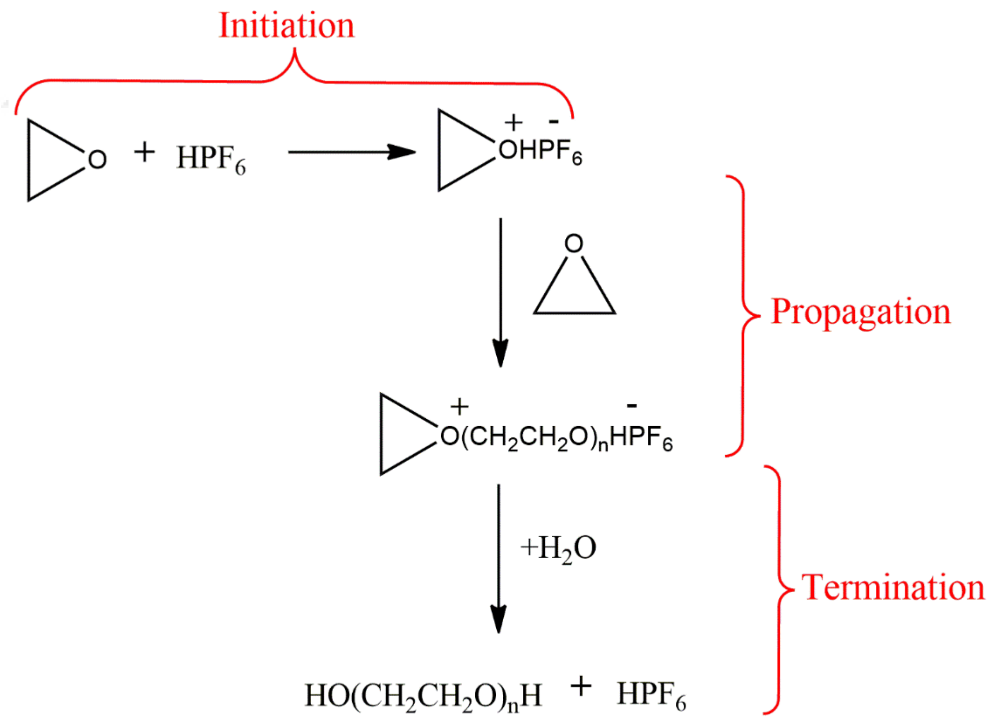

Figure 2.13 : Reaction scheme of cationic ring-openning photopolymerization.

UV curing system consists of reactive oligomers, reactive diluents, and photoinitiators. Commonly used oligomers are acrylic acid esters such as epoxy acrylates, polyester acrylates, urethane acrylates, and silicone acrylates. Liquid monomers and oligomers are added with a small percent of photoinitiators, and then exposed to UV energy. In a few seconds, the products, inks, coatings or adhesives instantly harden. In UV-curing, there is no solvent to evaporate, no environmental pollutants, no loss of coating thickness, and no loss of volume. This results in higher productivity in less time, with a reduction in waste, energy use and pollutant emissions at low temperatures. The other advantages of UV-curing are good adhesion to various substrates, high curing rate, controlled elasticity, and high stability at storage [8-10, 70, 76-79]. It supplies to the surface a high scratch resistance property with high optical clarity so as a good surface quality [70, 80-82]. It can be applied onto the surfaces in a wide temperature range that is important for heat-sensitive materials. Despite all these advantages, there are some drawbacks existing of UV-curing technology such as difficulties during the application on complex shapes, high shrinkage after curing, and continuous absorption of UV light resulting in poor weatherability. Moreover, only illuminated areas can be cured by UV-light, so at least one of the adherents should be transparent in UV-curing systems [61, 72, 83, 84].

2.3.1 Photoinitiators

Photoinitiators are thermally stable compounds which are capable of absorbing light in UV/visible wavelengths with high absorption coefficients. Industrial photoinitiators typically absorb light in 200-400 nm wavelength range. Some industrial photoinitiators can absorp light in near-visible region (around 400 nm) also known as blue light. 320-400 nm, 280-320 nm, and 200-280 nm in the electromagnetic spectra refer to the UV A, UV B, and UV C that are also known as long-wave UV, mid UV, and short-wave UV (Figure 2.13). When the photon energy is absorbed by a photoinitiator or a photosensitive compound, radicals are formed by a homolytic bond rupture. Most photoinitiators produce reactive species (free radicals or protonic acids) from the triplet state according to the polymerization mechanism (radical or cationic). Some widely used radical photoinitiators are as follows; hydroxy-2-methyl-1-phenyl-propanone, 2-methyl-1-[4-(methylthio) phenyl]-2-morpholinopropan-1-one, 2,2-dimethoxy-1,2-diphenylethan-1-one, 2-benzyl-2-dimethylamino-1-(4-morpholino phenyl) butan-1-one, etc. Free radical polymerization can be photoinitiated by using two types of photoinitiators; type I and type II. The type of the photoinitiator is effective on the rate of initiation and the penetration depth of the UV-light. After absorption of UV light, a rapid bond cleavage is observed in type I initiators. Durable excited triplet states are formed during type II initiator usage that are subjected to hydrogen abstraction or electron transfer stages [61, 76, 85-87].

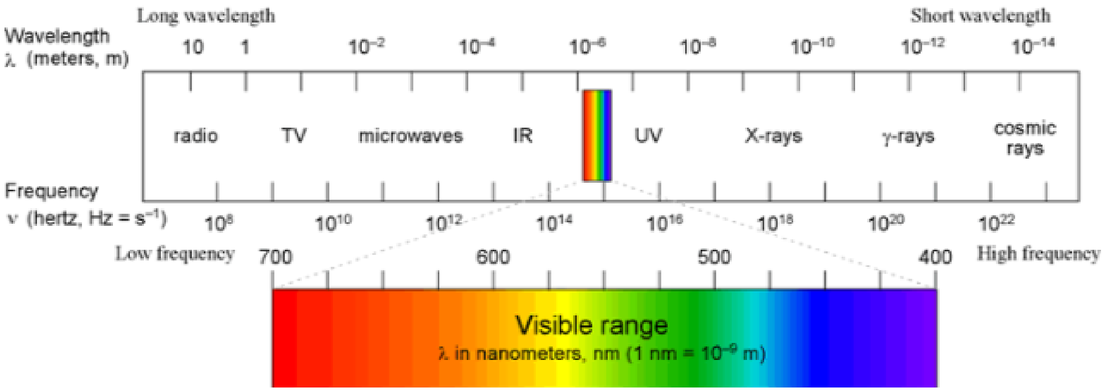

Figure 2.14 : The electromagnetic spectrum [88].

2.3.2 Reactive diluents

Reactive diluents are one of the most important component of a UV-curable formulation which are used to reduce the viscosity, control the crosslinking density, improve mechanical properties and chemical resistance etc. Acrylic based reactive diluents are commercially favored because of their high clarity and optical transparency with non-yellowing properties. In literature a number of studies have been made considering the effects of the type and percentage of the reactive diluent in the formulations, on the properties of the end product. For instance, urethane acrylate oligomer has been synthesized and then mixed with 1,6-hexanediol diacrylate (HDDA) and trimethylolpropane triacrylate (TMPTA). The effects of reactive diluent functionality on the coating properties have been searched. Results proved that the higher crosslinking density of the formulation with TMPTA, has increased the glass transition temperature and thermal stability of the coating material [89]. In another research, the effect of reactive diluent concentration on thermal degradation properties of N-(4-hydroxyl phenyl) maleimide derivatives has been studied. N-vinylpyrrolidone (NVP) has been chosen as reactive diluent. The highest thermal stability with a 30 % char yield has been obtained in 80 % maleimide derivative-20 % NVP composition [90]. The effect of reactive diluent (dipropylene glycol diglycidyl ether) on the mechanical properties of the multi-walled carbon nanotube (MWCNT) composites has also been studied [91].

2.3.3 Additives

Additives are chemical species which are used to enhance the overall formulation properties, give additional functionalities to the resin, and improve specific properties of the end product. Plasticisers are one of the additives in UV-curing systems that are used to adjust the viscosity and rheology of the adhesive formulations. Commonly used additives are as follows; antioxidants, antistatic/antifogging agents, thermal/UV stabilizers, flame retardants, color pigments, tackifiers [61, 62].

2.3.4 Applications of UV-curing

There is a growing demand for the usage of UV-curing technology in both academic and industrial scale due to its superior properties that are mentioned before. UV-curing techniques has found wide spread applications in automotive, aerospace, printing, wood, dentistry, biomedical, optical, packaging, and microelectronic industries, and metal, optical pick-up coatings etc. In that mentioned fields it can be used as lacquers, varnishes, printing inks, adhesives for plastic/glass bonding and so on. In the adhesive industry, UV-curing technique is used in two different classes. In the first class, the crosslinking of the adhesive is performed by the UV-light, and the end product is directly occurred. This type of adhesive is used in sealants, composites, lamination process etc. Whilst in the second class, a tacky polymer is formed by UV-light to be used as a pressure sensitive adhesive or hot-melt adhesive. So the main crosslinking step is occurred after the application of pressure or heat [56, 61, 85, 92-97].

2.4 Dual-Curing Mechanism

In literature, dual-curable vinyl ester resins have been synthesized by changing the equivalent ratio of the acid and epoxy. So the obtained oligomer has one double bond at one end allowing to be cured by UV-light. Whereas at the other end of the oligomer an epoxide group exists that can undergo with thermal curing mechanism. The schematic representation for this kind of oligomer can be seen in Figure 2.15 [98-100].

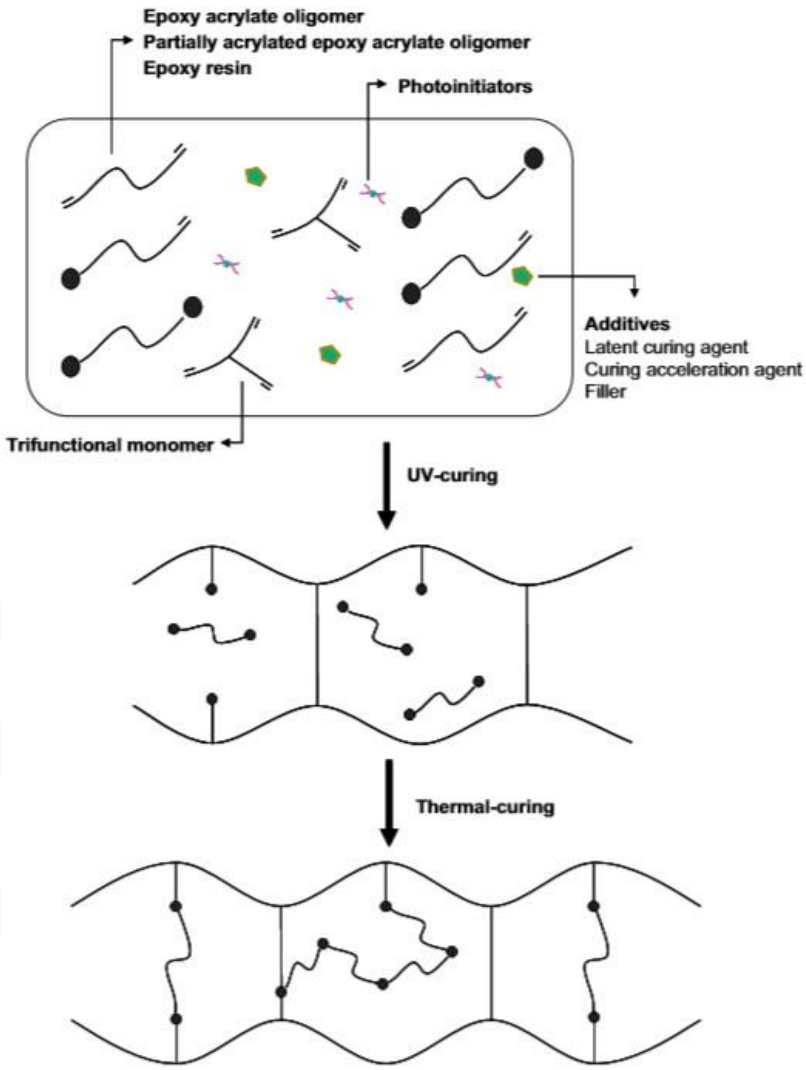

Figure 2.15 : Schematic diagram of dual-curable EA oligomers [13].

Dual-cure systems are needed when the adherents are not well-illuminated due to their complex shapes. In these systems, at least two functional species are presented such as isocayanates (thermally curable), acrylate double bonds (UV-curable) etc. The second curing mechanism can be heat or moisture sensitive. In dual-curing process, two crosslinking mechanisms exist, these can be combination of;

- ✓ UV-curing + thermal curing,
- ✓ UV-curing + anaerobic curing,
- ✓ UV-curing + moisture curing.

Thermal free radical initiators are mostly azo (AIBN) or peroxo (benzoyl peroxide) compounds, and dissociate into radicals with the exposure of thermal energy generally at 40-80 ^{o}C temperature range. After dissociation stage monomers are added to this radicals in propagation stage. The termination step can be occured in both two ways; combination or disproportionation. Polymerization may also be initiated thermally without using any initiator as in polymerization of styrene, methyl metacrylate, vinyl acetate etc. [101]. The basic dual-curing mechanism between a hydroxyl-functionalized diacrylate and diisocyanate can be seen in Figure 2 .16 [61, 70, 94].

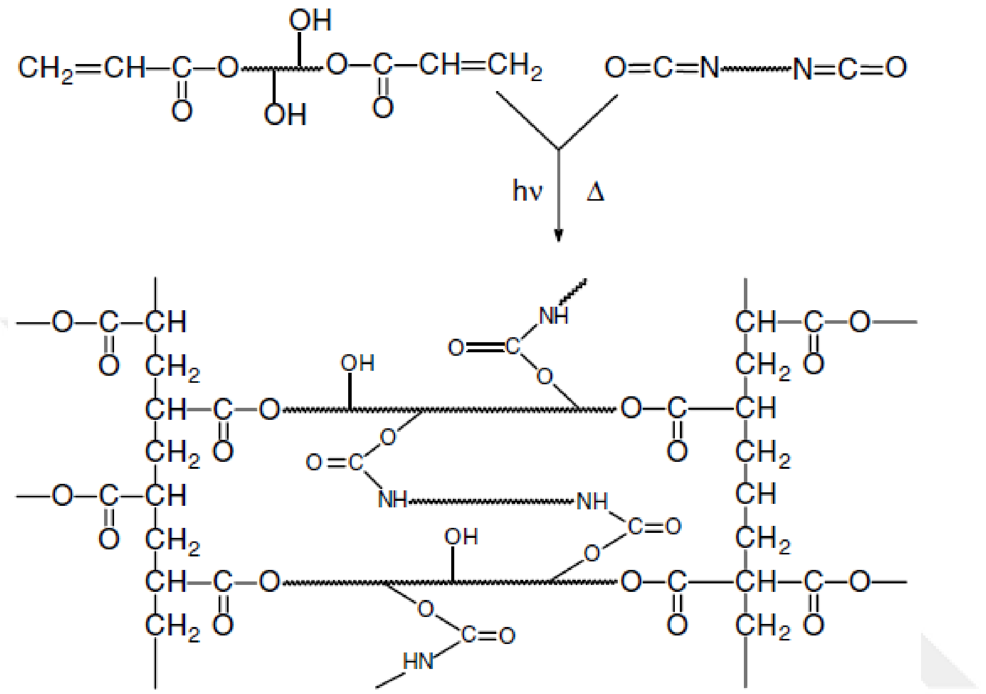

Figure 2.16 : Crosslinking mechanism in dual-curing systems [61].

2.5 Epoxyacrylates

The word "epoxy" illustrates the characteristic three-membered ring structure and is the combination of the Greek prefix "ep" that means "over and between" and the beginning three letters of "oxygen". Epoxy resins are widely used in many applications such as OLED technologies, metal can coatings, space, automotive, aviation industries, printed circuit boards, etc. Due to the excellent mechanical and chemical properties even at high temperatures, they can be used in composite materials as matrix component. Crosslinking reactions of the epoxy resins can be performed by carboxylic acids, amines, and anhydrides depending on the type of functional groups in the epoxy resin [94, 102-105]. Synthesis of UV-curable epoxy based vinyl ester resins can be performed with the reaction of the acid (acrylic acid, methacrylic acid, etc.) and epoxide groups. AA modified epoxy vinylesters compose of one epoxide group at one end and an unsaturated group at the other end. They show excellent chemical resistance, flexibility, non-yellowing properties, hardness, and good adhesion property. The unsaturated group gives flexibility and wettability properties whereas the epoxide group is responsible for the toughness. The epoxy-acid reaction forms hydroxyl groups that gives polarity so wettability character to the surface resulting a better adhesion properties [11-13, 105, 106]. Acid modified UV-curable oligomers are used to enhance the surface hardness, and tear resistance of the material by increasing the crosslinking density [107].

EA coatings have been widely used in many applications such as wood, automotive, and electrical industries, inks, varnishes, architectural coatings, optical fibers etc. They are favored due to their excellent weather durability, chemical, solvent, and corrosion resistance, good adhesion, and high stiffness properties [108-113]. In literature, improvement of the performance and adhesion property of EA coatings have been investigated. For instance, in order to enhance the scratch resistance with a better mechanical performance, alumina nano-particles have been included into the EA adhesive formulations. Accordingly, after inclusion of the alumina particles, hardness of the coating layer decreased whereas scratch resistance increased, and no remarkable change has been recorded about the gloss properties [56]. In another research, nano-siloxane methacrylate particles have been used in EA coating formulations. The scratch and abrasion resistance of the coating layers increased with increasing nano-siloxane methacrylate particles in the formulation. No change has been observed in gloss properties [57]. Nanosilica and nano-ZnO particles have been also included in EA adhesive formulations to enhance the abrasion, thermal, and scratch resistance of the materials [114]. Only a few studies regarding the flame resist property of the EA coating formulations with phosphorylation have been made. A flame retardant monomer has been synthesized by the reaction of ethylenediamine, phenyl dichlorophosphate, and HEA, then the obtained monomer has been used in EA coatings. Results proved that the thermal stability of the coating layer increased with increasing nitrogen and phosphorous amount in the formulation. The optimum flame retardant property of the coating layer has been observed in the sample containing 20 wt.% monomer with phosphorous atoms [115]. UV-cured flame retardant EA films have been prepared with the inclusion of tri(acryloyloxyethyl) phosphate and triglycidyl isocyanurate acrylate as flame resist additives [116]. VPA is favored in biomaterial industry, and in halogen-free flame retardant formulations due to having phosphonate group, and a high phosphorous content (29%), with a hydrophilic nature [117, 118]. In a previous study, epoxidized soybean oil has been reacted with VPA resulting the formation of phosphorylated epoxidized soybean oil monomer with flame retardant property. Results showed that the char formation and LOI value have increased with increasing phosphorous ratio in the coating formulation [92]. Moreover, VPA has been also used as photochemical finishing material in manufacturing of flame retardant cotton, polyester, and polyamide fabrics. Accordingly, VPA treatment in textile finishes allows to obtain flame retardant textile fabrics which have durability againist a few laundering steps [119].

2.6 Epoxidized Vegetable Oils

Vegetable oils are important biodegradable resources because of being universally available, non-toxic, non-volatile, non-depletable, domestically abundant and their low price. Synthesis of vegetable oil-based polymers are very significant research area, involving the modification of these fatty acids/triglyceride molecules as starting monomers. They can be used in several industrial applications such as lubricants, adhesives, printing inks, paints and polymeric coatings, biomedical applications, packaging materials etc. Fatty acids are the fundamental components that determine the physical and chemical properties of the vegetable oil. They improve the flexibility and impact resistance of the structure. For instance the major fatty acid of TO is the α-eleostearic acid and it has three double bonds on its backbone enabling production of different types of polymers [120, 121].

TO composes of various fatty acids including 4% oleic acid, 5.5% palmitic acid, 8.5% linoleic acid, and 82% α-eleostearic acid. The main usage area of TO is wood coatings. The main advantages of TO compared to other unconjugated oils (soybean, linseed oil, etc.) are better water resistance, higher hardness, and faster drying times. Recently, Larock et. al. has reported cationic and thermal copolymerization of TO with aromatic comonomers such as styrene and divinylbenzene to obtain a variety of new polymers ranging from rubbery to tough and rigid plastics. UV-curable TO resins have been prepared by the reaction of TO and phenolic resin in the presence of TMPTMA. TO modified polyol has been cationically UV-cured and the formation of smooth films has been observed by Thames et. al. [122-127].

Epoxidation of vegetable oil is performed by adding oxygen to the alkene groups of unsaturated fatty acids of vegetable oil. The unsaturation sites of vegetable oil can be converted to oxirane ring in the presence of catalysts and hydrogen peroxide in a process that is known as epoxidation. Then these epoxy groups can be reacted with highly reactive functional groups such as acids, amines, anhydrides in order to get the desired polymeric structure. Epoxyacrylates from epoxidized vegetable oils are generally used to reduce the viscosity of the formulations. The utilization of vegetable oil epoxies in paints and coatings may reduce the dependence of petrol-based chemicals and give rise to environmental recovery. Mostly commercially used vegetable oils are soybean, sunflower, rapeseed, castor, rubberseed, tung, safflower, olive, and linseed oil. Epoxidized vegetable oils can be used as plasticizers, toughening agents, lacquers, lubricants, reactive modifiers, stabilizers for polyvinyl chloride (PVC), and additives for wood coating. In the literature, epoxidized fatty acids have been used in various applications. For instance, in a previous study, epoxidation of canola oil has been carried out by using two different carboxylic acids (formic and acetic acid). Accordingly, it was found that acetic acid was much more effective then formic acid for peroxycarboxylic acid generation during the epoxidation process. In another study, karanja oil has been epoxidized by in situ peroxyacetic acid formation and then mathematically modelled to predict the kinetic parameters of the reaction. Results showed that optimum reaction condition was achieved at 70 ^{o}C, with 16 % catalyst loading, in a 1500 rpm stirring speed when the hydrogen peroxide-to-ethylenic unsaturation molar ratio was kept as 1.5. Epoxidation of soybean oil has been investigated by using formic acid as catalyst and hydrogen peroxide as oxygen donor. The highest epoxy content of 6.1 % in weight was observed at 50 ^{o}C, with 550 rpm stirring speed in 10h [128-133].

2.7 Polyurethane Acrylates

Typically, UV-curable urethane acrylate oligomers can be synthesized by using an isocyanate such as TDI [134], hexamethylene diisocyanate (HDI) [135], IPDI [136, 137] and an acrylate functional monomer such as HEA and HEMA. Acrylate functionality in the structure, gives the ability to be cured by UV-light. During the reaction some of the isocyanate groups intentionally left unreacted allowing to react with a polyol to form UV-curable urethane acrylate oligomer. Instead of a polyol, the isocyanate groups can be also reacted with PVB which gives a strong binding and adhesion property on many surfaces. In literature, UV-curable urethane acrylate oligomers have been synthesized by using an isocyanate, acrylate functional monomer and a polyol [138-140] but there was no research considering the usage of PVB instead of a polyol as reactive site for isocyanate group.

TDI-HEMA reaction is a common way to obtain UV-curable coating formulations [134, 136, 141]. HEMA gives acrylate functionality to the oligomer so the ability to be cured by UV-curing technique which represents a time and cost effective, solvent- and dash-free process [13, 142]. During the reaction, some of the isocyanate groups can be intentionally left unreacted allowing to react with some other groups to get additional functionality. In a previous study, a UV-curable polymer for bio-microelectromechanical devices has been obtained via a three-step in situ polymerization. First, carbon nanotubes has been modified by potassium permanganate then TDI has been reacted with functionalized carbon nanotubes. The excess of isocyanate groups in the reaction has been reacted with HEMA. Results have proved that carbon nanotubes can be chemically bonded to UV-curable polymers with a good dispersion by using TDI-HEMA reaction [81]. In another study, TDI-HEMA adduct has been reacted with butyl acrylate in order to obtain hybrid latexes. The decrease of butyl acrylate amount in the formulation caused an increase of hardness and glass transition temperature of final UV-cured products [143]. TDI-HEMA adduct has been also used in epoxy acrylate coatings to improve the surface, dielectric and tribological properties. A graft copolymer has been obtained first with the reaction of dicarboxyl terminated poly(2,2,3,4,4,4-hexafluorobutyl acrylate) oligomer with poly(dimethylsiloxane). Then TDI-HEMA adduct has been reacted with the graft copolymer. Results showed that inclusion of the obtained vinyl-terminated functional fluorinated siloxane graft copolymer to the coating formulation caused high hydrophobic and oleophobic properties, decease in surface energy, and reduction in the abrasion weight loss even in small amounts [37]. PVB has been primarily developed for safety glass lamination in automotive industry at the beginning of twentieth century. It is a random terpolymer composed of vinyl alcohol, vinyl acetate, and vinyl butyral monomeric units. The hydroxyl groups on vinyl alcohol unit are responsible of structural and functional properties of PVB. It has a good water and heat resistance, excellent thin-film forming ability with optical clarity, and high mechanical strength. It can be widely used as binder in coating formulations owing to its superior adhesion and bonding properties. The other usage areas are acoustic, solar applications, building industry etc. [144-147].

3. EXPERIMENTAL PARTS

3.1 Materials and Chemicals

3.1.1 Monomers and resins

Dipropylene glycol diacrylate (DPGDA, Allnex Corp.):

It was used as received. It is a difunctional reactive diluent with low viscosity and good moisture resistance. It can be used in UV/EB (electron beam) curable inks and coatings, wood/metal/plastic adhesives etc.

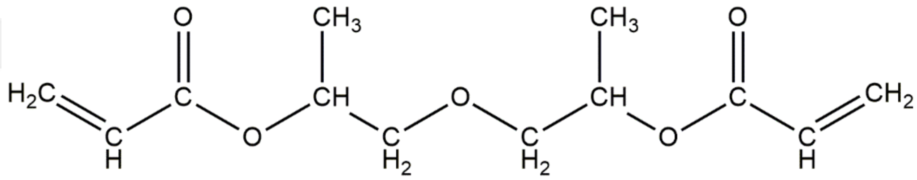

Figure 3.1 : Dipropylene glycol diacrylate.

Trimethylolpropane trimethacrylate (TMPTMA, stabilized with hydroquinone monomethyl ether (MEHQ), TCI Co.):

It was used as received. It is a three functional reactive diluent with high chemical/heat/weather/abrasion resistance, high crosslink density, and impact strength. It can be used in wire/cable coating formulations, paints, hard rubber objects etc.

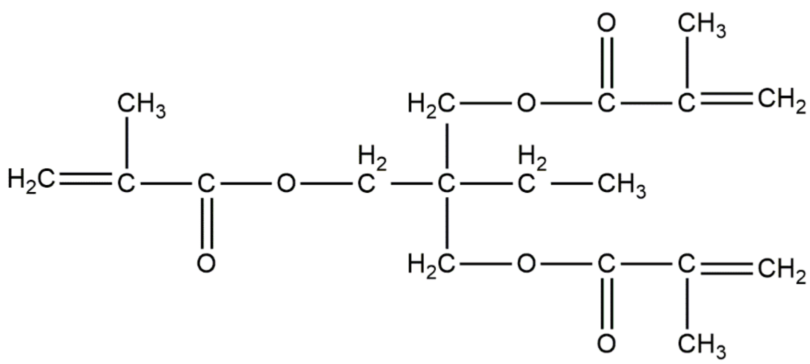

Figure 3.2 : Trimethylolpropane trimethacrylate.

Tricyclodecane dimethanol diacrylate (TCDDA, Rahn USA Corp.):

It was used as received. It is a reactive diluent for radically curable inks, coatings, adhesives, fillers, etc.

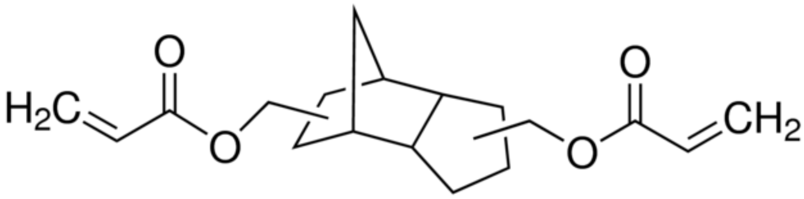

Figure 3.3 : Tricyclodecane dimethanol diacrylate.

N-vinyl pyrrolidone (NVP, ≥ 99 %, Sigma-Aldrich):

It was used as received. It is a reactive diluent that can be used in UV/EB curable inks, coatings, adhesives, etc.

Polyurethane acrylate (PUA) resin (Ebecryl 8210, Allnex Corp.):

It was used as received.

Epoxy resin (Epikote Resin 162, based upon diglycidiyl ether of bisphenol-A, EEW=167-171 g/equiv.):

It was used as received.

3.1.2 Solvents

Ethanol (≥ 99.8 %, Sigma-Aldrich):

It was used as received.

Methyl ethyl ketone (MEK, ≥ 99 %, Sigma-Aldrich):

It was used as received.

Toluene (≥ 99.5 %, Sigma-Aldrich):

It was dried and distilled.

Tetrahydrofuran anhydrous (≥ 99.9 %, THF, Sigma-Aldrich):

It was dried and distilled.

3.1.3 Other materials and chemicals

Acrylic acid (AA, 99 %, Sigma-Aldrich):

It was used as received. It contains 200 ppm MEHQ as inhibitor.

Vinylphosphonic acid (VPA, 97 %, Sigma-Aldrich):

It was used as received.

Triphenyl phosphine (TPP, 99 %, Sigma-Aldrich):

It was used as received.

Hydroquinone (HQ, ≥ 99 %, Sigma-Aldrich):

It was used as received.

Potassium hydroxide (KOH, 90 %, Sigma-Aldrich):

It was used as received.

Sodium hydroxide (NaOH, ≥ 98 %, Sigma-Aldrich):

It was used as received.

Sodium bicarbonate ($NaHCO_3$, ≥ 99.7 %, Sigma-Aldrich):

It was used as received.

Phenolphthalein (Indicator, Sigma-Aldrich):

It was used as received.

Crystal violet (Indicator, Sigma-Aldrich):

It was used as received.

Tetraethylammonium bromide (98 %, Sigma-Aldrich):

It was used as received.

Perchloric acid (70 %, Sigma-Aldrich):

It was used as received.

Acetic acid (≥ 99.7 %, Sigma-Aldrich):

It was used as received.

Hydrochloric acid (HCl, 37 %, Sigma-Aldrich):

It was used as received.

Tung oil (TO, Sigma-Aldrich):

It was used as received. It is also known as China wood oil. Its' components are 4 % oleic acid, 5.5 % palmitic acid, 8.5 % linoleic acid, and 82 % α-eleostearic acid.

Hydrogen peroxide (H_2O_2, ≥ 30 %, Sigma-Aldrich):

It was used as received.

Amberlite IRA 400 chloride form (Sigma-Aldrich):

It is an acidic ion exchange resin, and it was used as catalyst.

Di-n-butyltin dilaurate (T12, 95 %, Alfa Aesar):

It was used as received. It is used as catalyst in synthesis of polyurethanes and in transesterification reactions.

1-hydroxycyclohexyl phenyl ketone (Irgacure 184, Ciba Specialty Chemicals):

It was used as received. It is an efficient photoinitiator that is used for photopolymerization of acrylates, mono/multi-functional vinyl monomers with non-yellowing property.

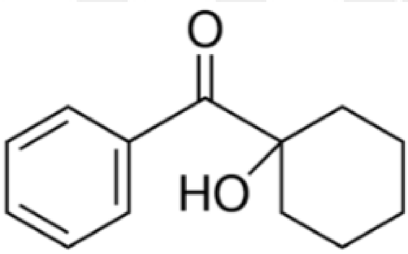

Figure 3.4 : Irgacure-184.

Tert-butyl monoperoxymaleate (Empions Co. Ltd.):

It was used as received. It is used as hardener, thermal initiator, curing agent for manufacturing of kitchenware, bathroom items, etc.

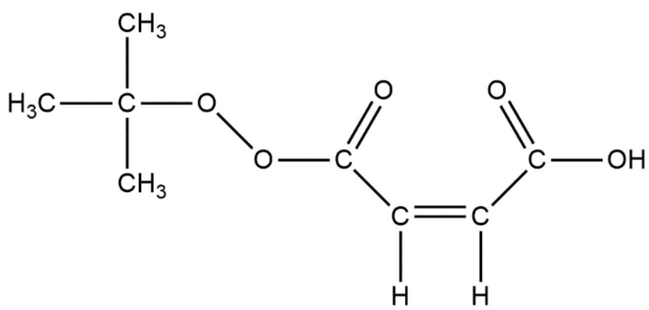

Figure 3.5 : Ter-butyl monoperoxymaleate.

Azobisisobutyronitrile (AIBN, 98 %, Sigma-Aldrich):

It was used as received.

2,4-Toluene diisocyanate (TDI, 95 %, TCl Co.):

It was used as received.

2-Hydroxyethyl methacrylate (HEMA, ≥ 99 %, TCl Co.):

It was used as received. It contains ≤ 50 ppm monomethyl ether hydroquinone as inhibitor.

Polyvinyl butyral (PVB, Mowital B 60H, Kuraray Europe GmbH):

It was used as received. Its' hydroxyl content is 18-21 %.

Polyester cord fabric (Izomas Co.):

360 g/m^2, 12 warp per cm, 5 weft per cm, 360 fibers per warp, 360 fibers per weft.

Polyester/polyamide cord fabric (Izomas Co.):

520 g/m^2, 8 warp per cm, 4 weft per cm, 540 fibers per warp, 400 fibers per weft.

Styrene butadiene rubber (SBR) sheets (Grainger Co.):

60 and 70 Shore A, 1.5 mm thickness.

3.2 Characterization Methods, Equipments and Analysis

3.2.1 Epoxy equivalent weight (EEW) and acid value (AV) measurements

Epoxy equivalent weight (EEW) refers to a certain amount of resin in grams containing a 1 g equivalent of an epoxy group. The EEW value can be determined by using perchloric acid ($HClO_4$) titration method. First, certain amount of EA resin is dissolved into MEK, then 5 mL tetraethylammonium bromide solution and 3 drops of crystal violet indicator solution is added to the main flask. The titration is made by $HClO_4$ solution until a purple-to-green color is obtained. EEW is calculated according to the equation 3.1 where m is the weight of the sample in gram, V1 and V2 refer to the volumes of $HClO_4$ solutions in mL that is required to titrate the sample and blank solution, respectively, and N is the normality of the $HClO_4$ solution (0.1 N) [103, 105].

$$EEW = \frac{1000xm}{(V_1 - V_2)xN} \tag{3.1}$$

The acid value (AV) shows the KOH amount in milligram required to neutralize one gram of EA oligomer. AV of the oligomers is measured by KOH titration method [108]. A certain amount of resin is dissolved in a suitable solvent, 6 drops of phenolphthalein indicator solution is added and then titrated by KOH solution until a pink color is obtained. AV is calculated according to the equation 3.2 where V is the KOH solution that is required to titrate the sample, M is the molarity of KOH solution, W is the sample used in gram.

$$AV = \frac{\mathrm{VxMx56.1}}{\mathrm{W}} \tag{3.2}$$

3.2.2 Fourier transform infrared (FTIR) spectroscopy

FTIR analyzes were carried out in Perkin Elmer Spectrum 100 FTIR spectroptometer in mid-infrared range (600-4000 cm^{-1}), that uses a ZnSe ATR-crystal with a variable angle accessory. Omnic software was used to record the spectral data at a resolution of 8 cm^{-1} and 64 co-added scans.

3.2.3 Nuclear magnetic resonance (NMR) spectroscopy

^{1}H NMR spectroscopy was carried out on Agilent VNMRS 500 MHz NMR instrument, by using deuterated chloroform ($CDCl_3$) and deuterated dimethylsulfoxide (DMSO-d6) as solvents and tetramethylsilane (TMS) as an internal standard. The measurement was performed with 3 s acquisition time, 20 ppm spectral width, 125 transients of 65k data points obtained over a 15 min data accumulation time.

3.2.4 Differential scanning calorimetry (DSC)

Thermal transition temperatures were measured by DSC, TA DSC Q10, at a heating rate of 10°C/min, from −80°C to 400°C under 50 mL/min nitrogen flow rate.

3.2.5 Thermogravimetric analysis (TGA)

TGA analysis was performed with a TA TGA Q50 instrument under nitrogen atmosphere at a heating rate of 10°C/min from room temperature to 600°C. Nitrogen flow rate was 30 mL/min.

3.2.6 Gel content

The gel fraction (GF %) of the UV-cured free films was measured by dipping the films into THF for one week at room temperature. After that the films were dried on a filter paper at 30 ^oC for 24 h. The GF (%) values were calculated by using the equation 3.3 where *W1* and *W2* show the weights of the films before and after swelling [17].

$$GF\ (\%) = \left[\frac{W_1}{W_2}\right] \text{x}100 \tag{3.3}$$

3.2.7 Swelling test

The UV-cured free films were dipped into 10 mL solvent (ethanol, toluene, distilled water) at room temperature for one week in order to obtain the degree of swelling (DS %) values. The films were dried on a filter paper until the weight becomes constant. The DS % was then calculated using the equation 3.4 where *W1* and *W2* are the weights of films before and after swelling [17].

$$DS\ (\%) = \left[\frac{W_2 - W_1}{W_1}\right] \text{x}100 \tag{3.4}$$

3.2.8 Chemical resistance

Chemical resistance of the UV-cured free films was evaluated in terms of the weight loss after the two weeks of chemical exposure at room temperature. 10 % NaOH and 10 % HCl solutions were used as chemical solvents. After that samples were washed with distilled water, dried on a filter paper at 55 ^oC. The weight loss (%) after the chemical exposure was calculated by using the equation 3.5 where *W1* and *W2* show the weights of films before and after the chemical exposure [148].

$$Weight\ Loss\ (\%) = \left[\frac{W_1 - W_2}{W_1}\right] \text{x}100 \tag{3.5}$$

3.2.9 Contact angle and surface energy measurements

Contact angle and surface energy measurements were performed from the dip-coated UV cured cord fabric surfaces with 3 μL water droplets by using a Gardco PGX+ goniometer equipped with a camera. The measurement is performed according to Young's equation as can be seen in equation 3.6, and Figure 3.6. γSV, γSL, and γLV refer to the interfacial surface free energies of vapor (V), solid (S), and liquid (L), ΘY corresponds to the Young's contact angle, respectively [149].

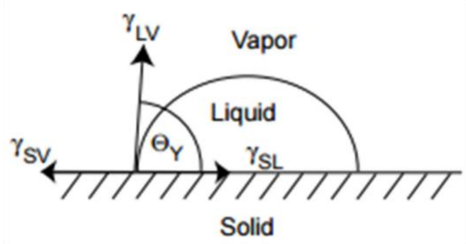

Figure 3.6 : Water droplet on a surface with the graphical vector parameters [149].

$$cos\Theta Y = (\gamma SV - \gamma SL)/\gamma LV \tag{3.6}$$

3.2.10 Hardness test

The Shore D hardness of the UV-cured free films was determined by Zwick Shore D Durometer by using 5 kg loading according to ASTM D2240 standard.

3.2.11 Tensile testing

Instron 4411 tensile testing machine was used to measure the mechanical properties of the UV-cured free films. Tensile testing was performed at room temperature with a constant extension rate of 5 mm/min. The tensile strength (MPa), elongation at break (%), and modulus (MPa) values were all recorded.

3.2.12 Peel test

T-peel test [150] was applied to measure the adhesion strength between the cord fabric and rubber surfaces in Instron 4411 tensile testing machine.

3.2.13 Scanning electron microscopy (SEM) and energy dispersive X-ray spectroscopy (EDS)

Scanning electron microscopy (SEM; JEOL Ltd, JSM-5910LV) was used for topological characterization. Energy dispersive spectrometry (EDS; INCAx-sight, 7274 Oxford Industries) was used to determine the SBR residue content on the fabric surface after peel test.

3.2.14 Light microscopy

Light microscopy images from the cord fabric surface were taken by Olympus CH-2 microscope by using a software (Digital Microscopy) in order to see the rubber residue on fiber surface after peel testing. By using the light microscopy images, the fiber thickness values were recorded from different points of fibers in longitutinal direction.

3.2.15 Limiting oxygen index (LOI) measurement

The vertical burning test [151] was used to determine the LOI values of the coated cord fabrics after UV curing, in 60x120 mm dimensions in a Fire Testing Technology type instrument. The LOI value means the total oxygen amount that is required to keep the sample in flame during a three-minute time [152].

3.3 Synthesis of the Oligomers, Preparation and Application Methods of Adhesive Formulations

3.3.1 Synthesis of epoxy vinyl ester oligomers

EA oligomers were synthesized by the following method; 300 ppm HQ, 1000 ppm TPP (out of the total weight of DGEBA and AA) were all dissolved in AA in an ultrasonic bath for 3 minutes. Then the AA solution was included slowly onto the DGEBA in the three-necked round bottom flask equipped with a magnetic stirrer, a condenser and an air inlet. DPGDA (in the amount of 10% of total weight) was used as reactive diluent to lower the viscosity of the oligomer and to increase the crosslinking density of the structure. The reaction was carried out 4 hours (2 h at 100 ^{o}C, 2 h at 120 ^{o}C) for various ratios of AA and DGEBA. Vinylphosphonic acid (VPA) was also included in some formulations in order to increase the adhesion strength between cord/rubber surfaces and to obtain a flame resist property.

3.3.2 Synthesis of acrylated epoxidized tung oil (AETO) oligomers

Epoxidation of TO was carried out in a round bottom flask equipped with a magnetic stirrer and a condenser. At first, certain amounts of TO and acetic acid, considering the carboxylic acid to ethylenic unsaturation molar ratio as 0.5:1, were added to the flask. Toluene (10 % in weight) was used as diluent medium. The amount of catalyst was weighted as 22 % of TO. 1.5 moles of H_2O_2 per mole of ethylenic unsaturation were added dropwise to the reaction mixture after ½ h to start in situ peracetic acid formation. The epoxidation reaction was carried out at 65 ^{o}C, during 3, 12, and 20 hours, respectively. Samples were coded as ETO-3, ETO-12 and ETO-20 regarding their epoxidation reaction times. At the end of the reactions, the obtained ETO were extracted with diethyl ether, then washed with distilled water and then $NaHCO_3$ (10 %) solution several times to remove free acid for neutralization. Vacuum drying was applied at 50 ^{o}C for 48 h for the removal of toluene, diethyl ether and water. All the mentioned reaction conditions were determined considering the optimum process parameters of previous studies [131, 153].

Considering the yield of the epoxidation reaction, the ETO-12 was chosen as the optimum result and acrylation reaction was performed by using this ETO. Only partial acrylation of epoxy group in TO was performed purposefully, to achieve the subsequent thermal curing process of the remaining epoxy groups. Thus only 70 % of the epoxide groups were acrylated and the rest left intentionally as epoxide. Firstly, 300 ppm HQ, 1000 ppm TPP (considering the total AA and ETO mass), were dissolved in AA in an ultrasonic bath for 3 minutes and then was inluded dropwise onto the ETO in the three-necked round bottom flask equipped with a magnetic stirrer, a condenser and an air inlet. The acrylation reaction involves the consumption of the carboxylic groups of the AA and the epoxy rings. The reaction was carried out 3 h at 110 ^{o}C and was ended when the viscosity was very high wherein the magnetic stirrer was forced. At that point, the flask was cooled to 60 ^{o}C and in order to adjust the viscosity to a reasonable level, NVP was added as reactive diluent in the amount of 50 % of the total weight.

The obtained ETO oligomer was also reacted with vinylphosphonic acid (VPA) in order to add the UV-functional groups in the oligomer structure and to enhance the adhesion strength between cord/rubber surfaces. The molar ratio of ETO/VPA was set as 1/0.5. For thermal curing stage, some of the epoxide groups in the oligomer structure were intentionally left unreacted. For the VPA modification reaction, at first, TPP (1000 ppm) and HQ (300 ppm) considering the total weight of VPA+ETO amount were dissolved in VPA in an ultrasonic bath. Reactive diluent (NVP) was included into the reaction in the amount of 25 % out of the total weight. The reaction was carried out 3 h at 110 ^{o}C and the obtained vinylphosphonic acid modified epoxidized tung oil (VPAMETO) oligomer was used in adhesive formulations.

3.3.3 Synthesis of polyurethane acrylate (PUA) oligomers

The synthesis of the oligomer was performed in a round-bottom flask equipped with a magnetic stirrer, a nitrogen gas inlet and a condenser. The oligomer was prepared by a two-step reaction by changing the TDI:HEMA molar ratio. First, TDI was charged into the flask containing THF (60 wt.%), and T12 catalyst (0.03 wt.%). Then HEMA was added dropwise to the flask in 0.5h in an ice bath. The reaction was continued for

0.5h at 30 ^{o}C and 1h at 70 ^{o}C. In the second step, PVB (in various percentages of the TDI amount) was dissolved in THF in an ultrasonic bath and added dropwise to the main flask. The reactive diluents (TMPTMA or TCDDA) also were added at this stage. The reaction was proceeded in 1h at 90 ^{o}C to eliminate the HEMA residue and to obtain the final PVB modified TDI-HEMA adduct.

3.3.4 Preparation and application of the adhesive formulations

Application of the adhesive formulations and curing stages can be seen in Figure 3.7. The obtained oligomers were used in the preparation of adhesive formulations containing photo- and thermal initiators (3 wt.%), and THF or MEK. Additional THF or MEK was used to lower the viscosity of the oligomer for better wettability on the fabric surface. The amount of oligomer in the adhesive formulation was set in such a way to have a 30 % weight increment in the fabric mass. Cord fabrics were prepared in 2.5x7.5 cm dimensions allowing to make the T-peel test and then dipped into the adhesive formulation for 3 min. A squeezing roller helped to dissipate the excess solution from the fabric. Dip-coated fabrics were dried in an oven at 70 ^{o}C for 10 min for evaporation of THF/MEK, and then the samples were put into a transparent zip-lock polyethylene bag in order to prevent oxygen inhibition during the UV-curing process. Fabrics were exposed to UV-light for 2 min from both sides of the fabric in Cole-Parmer UVP Longwave UV Crosslinker (115 VAC model) cabinet (Figure 3.8). Each dip-coated UV-cured fabric was put between two SBR layers and then thermally cured in a heated press (Carver, Inc. CH 4386 model) (Figure 3.9) at 200 ^{o}C under 700 MPa pressure for 10 min.

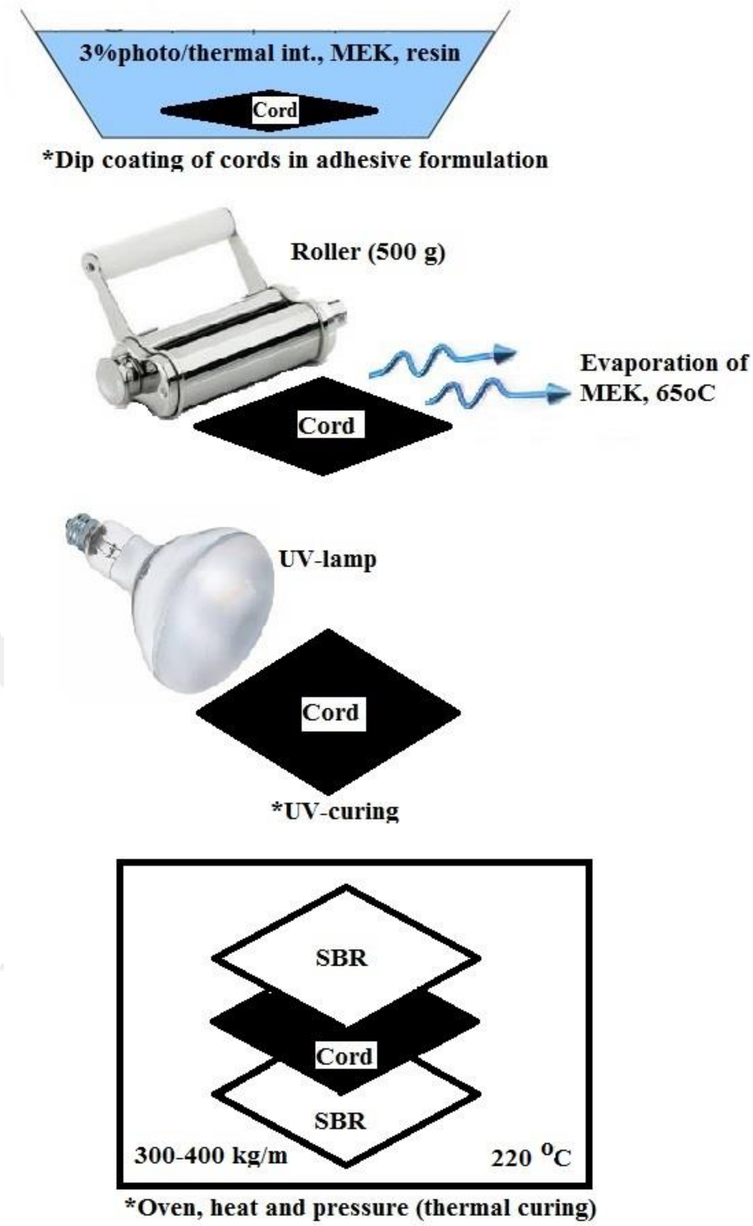

Figure 3.7 : Application and curing processes of adhesive formulations.

Figure 3.8 : Cole-Parmer UVP Longwave UV Crosslinker.

Figure 3.9 : Carver heated press.

4. RESULTS AND DISCUSSION

4.1 Synthesis and Application of Epoxyacrylates for Cord/Rubber Applications

In this study, epoxyacrylate (EA) oligomers were synthesized by using bisphenol-A based epoxy and acrylic acid in the presence of 300 ppm HQ and 1000 ppm TPP. For this purpose, HQ and TPP were dissolved in AA in an ultrasonic bath and then the AA solution was included slowly onto the round bottom three-necked flask with a magnetic stirrer, air inlet, condenser, and DGEBA. 10 % reactive diluent (DPGDA) out of the total weight was added to the reaction in order to increase the crosslinking density of the oligomer by decreasing the viscosity of the formulation [61]. By changing the molar ratio of AA and DGEBA (Table 4.1), the reaction was completed in 4 hours (2 h at 100 ^{o}C, 2 h at 120 ^{o}C). The reaction process can be seen in Figure 4.1.

Table 4.1 : Compositions of EA oligomers [154].

Sample Codes	AA (mol)	DGEBA (mol)	[COOH]/[Epoxide]
EA 25	0.5	1	0.25
EA 50	1	1	0.50
EA 75	1.5	1	0.75
EA 100	2	1	1.00

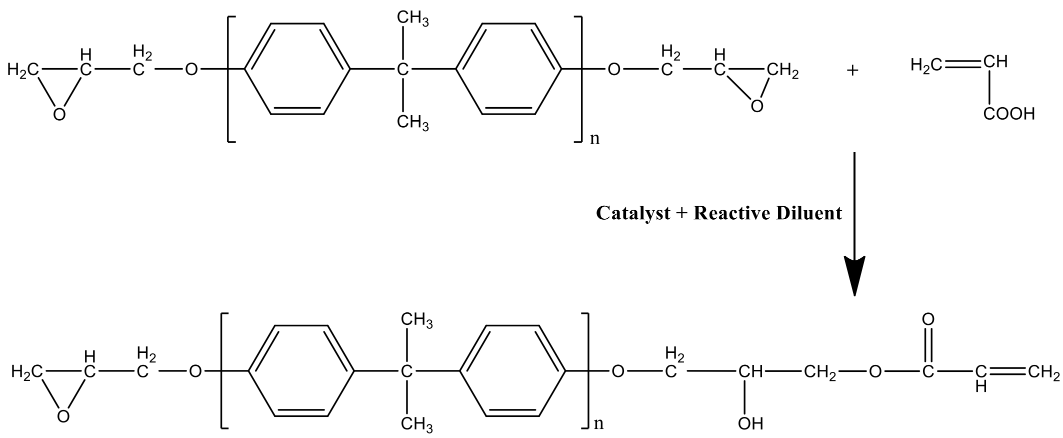

Figure 4.1 : The reaction process of EA oligomer [154].

During the reaction, at first, phosphonium betaine is formed after the epoxide ring opening reaction that is initiated by the nucleophilic attach of the catalyst. In the second step, a proton of AA is captured by the betaine, and the ester linkage is formed after the effect of carboxylate anion on the electrophilic carbon attached to the phosphorus [11]. The obtained oligomer was characterized by FTIR spectroscopy, and ^{1}H NMR analysis. Epoxy equivalent weight (EEW) and the acid value of the oligomers were determined.

Esterification reaction can be investigated by observing the acid value and EEW as shown in Table 4.2. EA oligomers with desired properties can be synthesized by controlling the stoichiometry and reaction conditions. The epoxide groups of DGEBA in both ends show the same reactivity towards saturated/unsaturated groups of acid. Thus theoretically in EA 50 oligomer, the end groups should be epoxide and one double bond of acrylate group. In other words, it should be monoacrylate-terminated EA. It is also possible that bisacrylate-terminated EA oligomers can be formed by the reaction of two AA molecules with two epoxide groups in one DGEBA molecule. In such case, one DGEBA molecule left unreacted in the reaction [11]. Almost all AA molecules were reacted with epoxy groups in the case of EA 25 and EA 50 samples. However, in the samples of EA 75 and EA 100, the excess AA cannot be totally consumed in the reaction. In the sample of EA 100, the initial carboxyl and epoxide groups are in stoichiometric amounts. It can be observed that the AA cannot be reacted completely with the epoxy groups in EA 100 system. The acid value and EEW values are 43.4 mg KOH/g and 1040.4 g equiv.$^{-1}$ respectively. At the end of the reaction, the carboxyl and epoxide concentrations decrease due to the EA formation thus the highest acid value and EEW were obtained in the case of EA 100.

Table 4.2 : Acid value and EEW of EA oligomers [154].

Sample Codes	AA (mol)	DGEBA (mol)	Acid Value (mg KOH/g)	EEW (g equiv.$^{-1}$)
EA 25	0.5	1	0.35	460.9
EA 50	1	1	5.40	675.7
EA 75	1.5	1	29.10	814.1
EA 100	2	1	43.40	1040.4

The formation of ester bonds during the EA oligomer synthesis was confirmed by FTIR spectroscopy. According to the Figure 4.2, the epoxy ring openning reaction can be followed by the broad peak at 3460 cm^{-1} that shows the secondary hydroxyl groups, and decrease in the absorption epoxide ring peaks at 1230 cm^{-1} and 880 cm^{-1}, respectively. The characteristic carbonyl peak of ester at 1720 cm^{-1} appears during the reaction. It can be seen that the carboxyl/epoxide ratio increases with increasing esterification reaction.

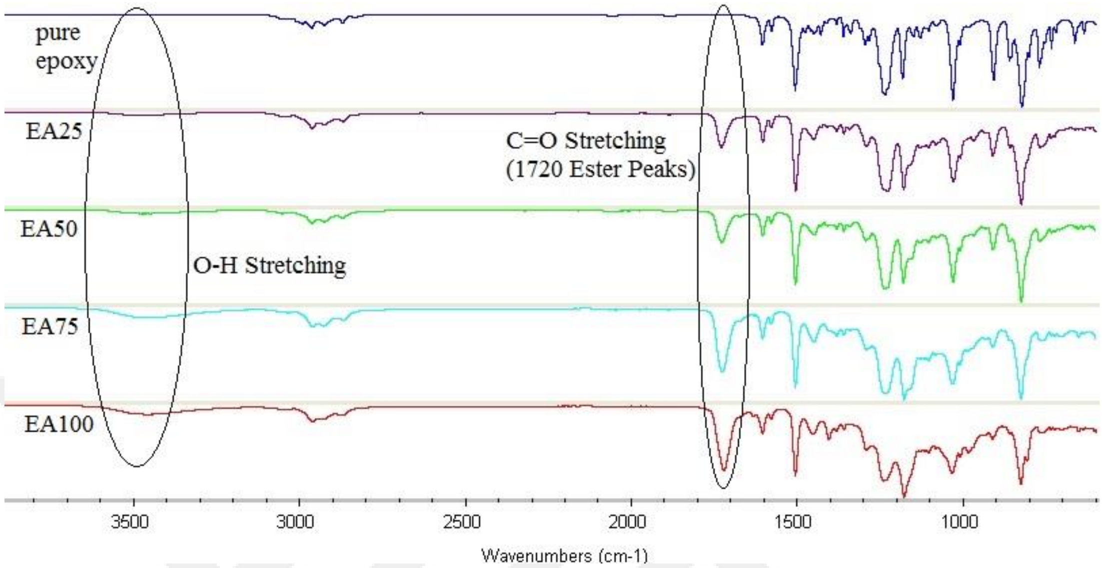

Figure 4.2 : FTIR spectra of epoxy and EA oligomers in various carboxyl/epoxide molar ratios [154].

The FTIR spectra of untreated polyester fabric, EA 100 coated fabrics before and after UV-curing process can be seen in Figure 4.3. According to the figure, acrylate peak around 1636 cm^{-1} associated with the EA 100 oligomer appeared after dip-coating process [155]. After exposure to UV light, the double bond cleavage was occurred resulting the disappearance of the unsaturated acrylate peak. Thus photo-polymerization can be performed with 2 minutes UV-light exposure on each side of fabric surfaces. Due to the increased crosslinking density and viscosity, the mobility of the monomeric and polymeric radicals becomes difficult consequently some of the unsaturated acrylate groups can remain as it is at the end of the reaction. In this case tackiness on the surface can be observed. In order to investigate the crosslinking density quantitatively, acetone extraction method was performed by using the weight loss of EA 100 coated UV-cured fabric sample before and after the extraction. Results showed that 0.02% weight loss was recorded with the acetone extraction for 4 h. This result confirms that 2 minutes UV-light exposure for photo-polymerization is adequate for EA based coatings.

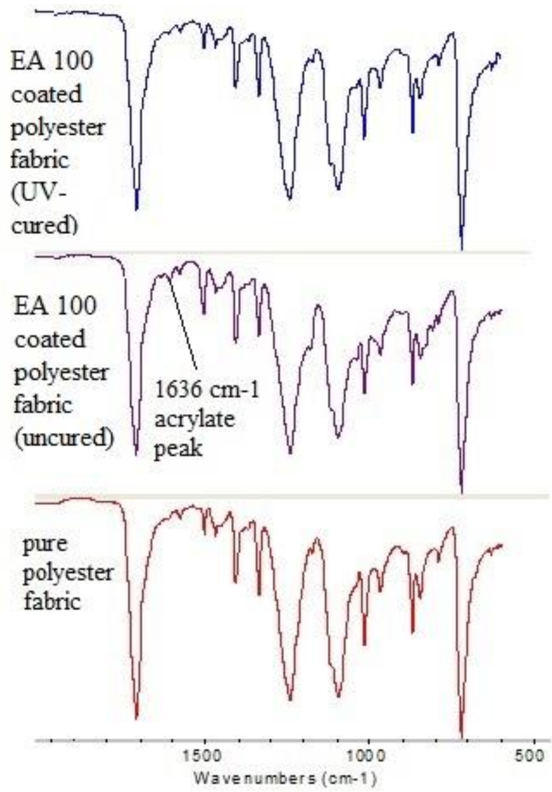

Figure 4.3 : FTIR spectra of polyester fabrics (pure, EA coated before and after UV-curing) [154].

^{1}H NMR spectra of EA 100 oligomer in $CDCl_3$ can be seen in Figure 4.4. The existence of acrylic group (CH_2=CH-) can be followed by the peaks at 5.9-6.5 ppm. The peaks at 3.9-4.3 ppm show the -CH_2 protons that are attached to the ester group oxygen atoms. The peaks at 2.6-2.8 ppm and 3.3 ppm illustrate the methylene and methine protons in the oxirane ring, respectively. The peaks at 6.7-7.2 ppm belong to the aromatic protons of phenyl rings. The–CH_3 protons in the cyclic ring appear at 1.65 ppm [156, 157].

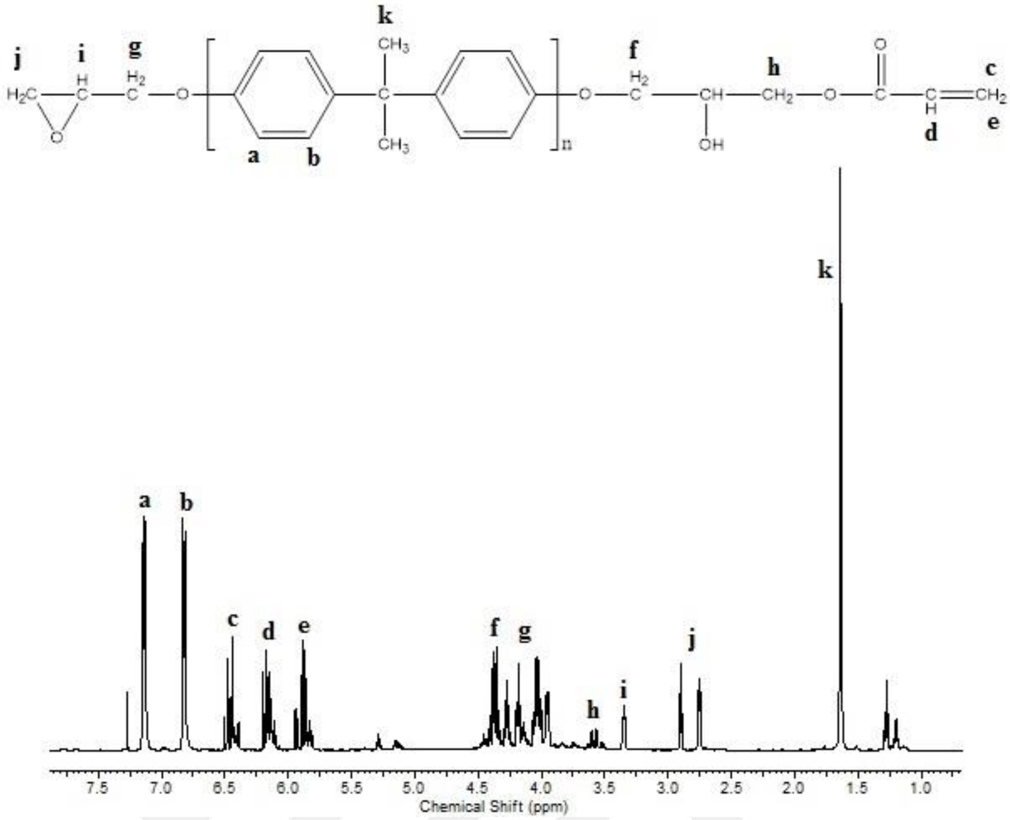

Figure 4.4 : ^{1}H NMR spectra of EA oligomer [154].

Figure 4.5 shows the TGA thermograms of untreated polyester fabric and EA 100 coated UV-cured polyester fabrics. A one-step decomposition was recorded for both sample. In untreated polyester fabric spectra, there was no decomposition till 400 ^oC whilst around 450 ^oC initial and rapid decomposition was observed. It can be seen that the TGA curve in the range of 500-550 ^oC followed a horizontal line. No weight loss was recorded above 700 ^oC. A char residue around 15 % was recorded due to the pyrolysis under nitrogen gas, that causes carbonization step. After EA 100 coating process, thermal stability increased due to the aromatic structure of the oligomer, increase in carbon amount on the surface, and performing the analysis in inert atmosphere.

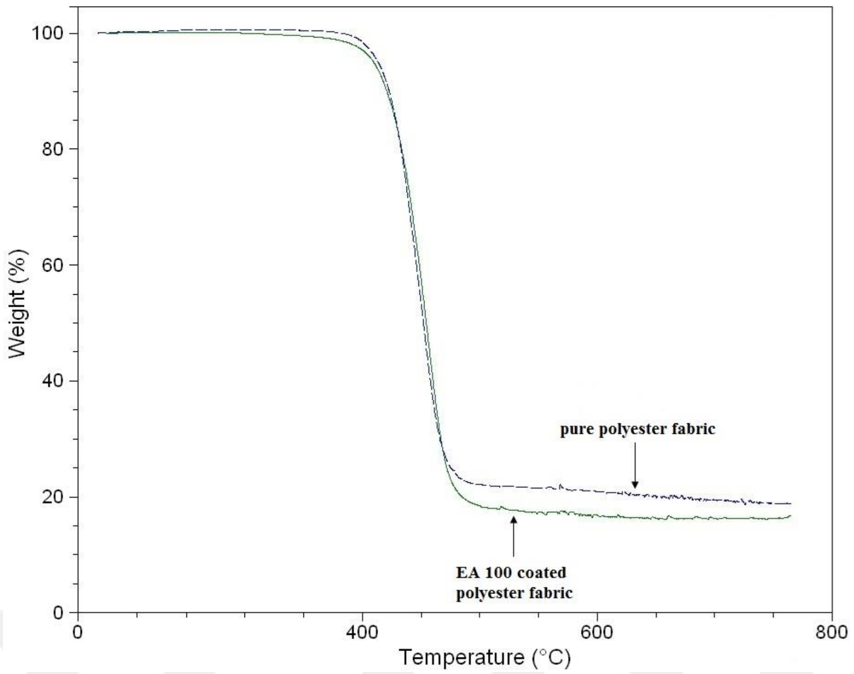

Figure 4.5 : TGA curves of polyester fabrics (pure, EA coated UV-cured) [154].

Table 4.3 shows the thermogravimetric data of the untreated polyester and EA 100 coated UV-cured polyester fabrics. Accordingly, as mentioned before, due to the increase in carbon amount on the surface after coating, thermal stability increased. Thus the 50 % weight loss temperature slightly increased to 455 ^oC from 450 ^oC after coating.

Table 4.3 : Thermogravimetric data of pure polyester fabric and EA 100 coated UV-cured polyester fabric [154].

Samples	T_1 (°C) (5% Weight Loss)	T_2 (°C) (50% Weight Loss)
Pure polyester fabric	413	450
EA 100 coated polyester fabric	409	455

The DSC thermograms of the untreated polyester and EA 100 coated UV-cured polyester fabrics can be seen in Figure 4.6. Accordingly, the characteristic sharp polyester crystals melting peak at around 260^o was observed. The melting peak of polyester slighly shifted to 250 ^oC after the EA 100 coating process. This result can be explained by the partially diffusion of EA amorf regions inside the cord fabric surface resulting a mixture with the crystalline structure of polyester.

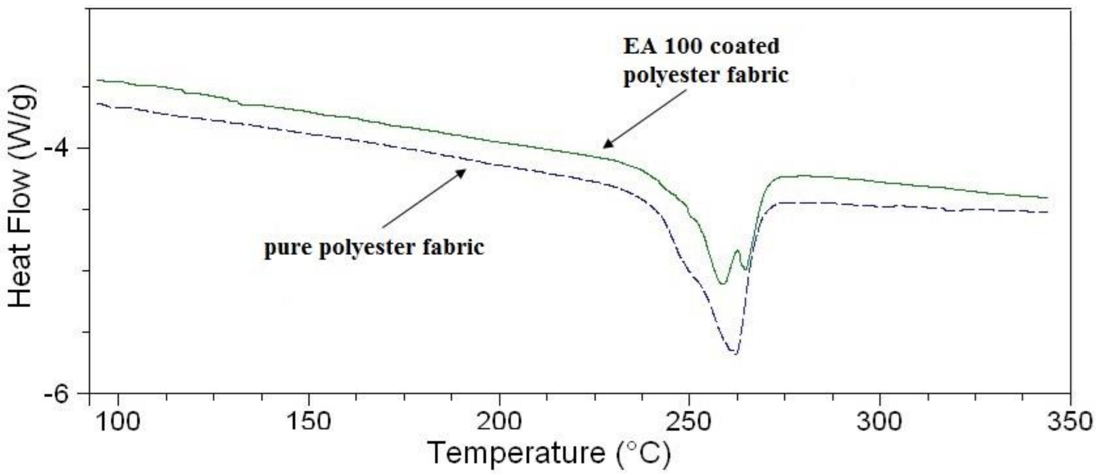

Figure 4.6 : DSC curves of pure polyester fabric and EA 100 coated UV-cured polyester fabric [154].

The SEM images of untreated polyester fiber and EA 100 coated UV-cured polyester fiber can be seen in Figure 4.7. Images illustrated that after coating process, about 0.5 μ coating layer was obtained on the single fiber surface. According to the Figure 4.7d and f, with the EA coating layer, a smooth fiber surface was obtained without any agglomeration. This result proves that a uniform, and well-dispersed EA layer on the fiber surface was formed resulting a uniform coating of each fiber within the fabric layer.

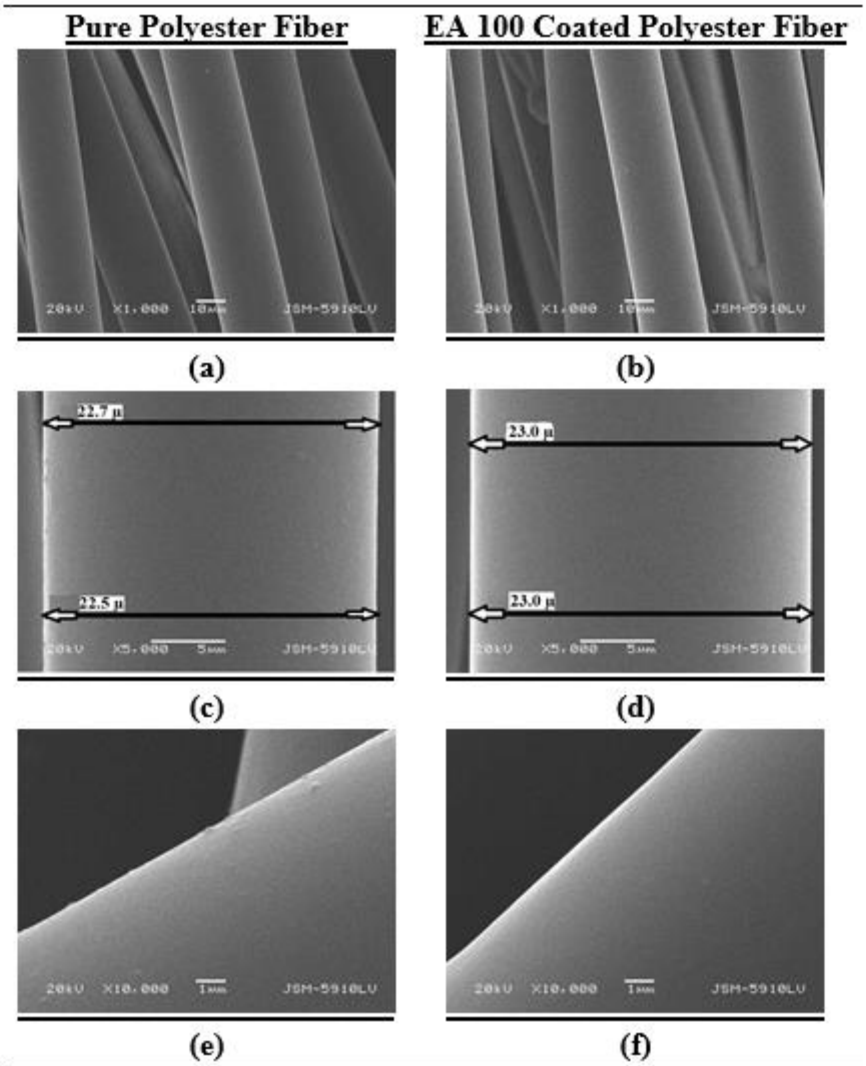

Figure 4.7 : SEM images of polyester fabrics (pure and EA 100 coated UV-cured) in various magnifications [154].

The surface energy and contact angle values of EA coated polyester cord fabrics after UV-curing stage and the images of 3 µL water droplets on fabric surface for each carboxyl/epoxide ratios can be seen in Table 4.4 and Figure 4.8, respectively. The water droplet was immediately disappeared on the polyester fabric thus the measurement cannot be made on the raw fabric. Accordingly, contact angle values were varied in the range of 52.1^{o} - 67.3^{o} for various AA molar ratio in the oligomer. AA modification of epoxy resin produces hydroxyl groups on the structure resulting increase polarity of the oligomer [13]. Results showed that polarity of the coating layer increases with increasing AA molar ratio due to the increase in hydrophilic character. The hydroxyl groups of the AA form hydrogen bonding with the oxygen atom of the polyester cord. So there were no hydroxyl group remains causing a hydrophilic behavior. In EA 100 coated UV-cured sample, the highest contact angle with 67.3^{o}

was obtained due to the highest AA amount. Whilst in EA 25 coated UV-cured sample, the least contact angle value of 52.1^{o} was observed as AA was almost consumed in that reaction that means less hyroxyl groups are existing on the surface.

Table 4.4 : Surface energy and contact angle values of coated cord fabrics after UV-curing [154].

	Contact Angle (^{o})	Surface Energy (mJ/m^2)
EA 25	52.1	62
EA 50	59.3	59.2
EA 75	65.1	56.4
EA 100	67.3	49.9

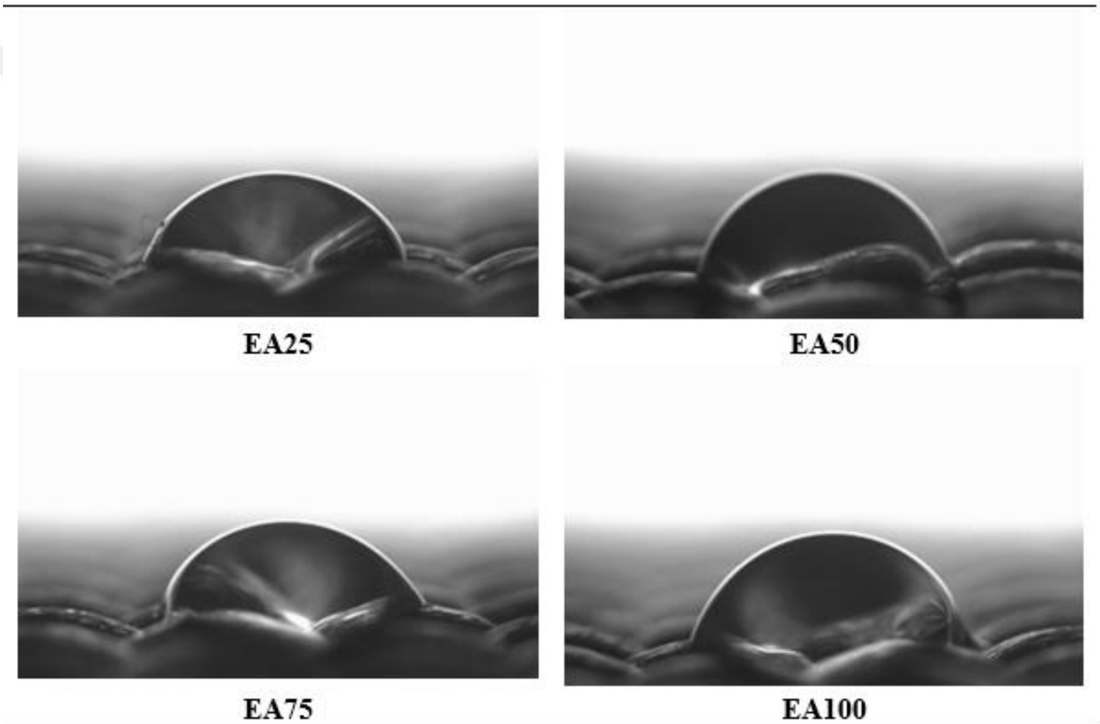

Figure 4.8 : Contact angles of water droplets on coated UV-cured polyester cord fabrics [154].

The adhesion strength values between cord/rubber surfaces for each formulation can be seen in Table 4.5. The adhesion strength value of 12.3 N/cm was recorded upon the adherence of the untreated polyester cord fabric on rubber surface. In order to increase the adhesion strength between cord/rubber surfaces, adhesive formulations containing EA oligomer were applied on cord fabrics. EA oligomers were synthesized by adjusting the carboxyl/epoxide molar ratio. Results showed that the best adhesion strength value of 18.0 N/cm was observed in EA 100 coating formulation due to having the highest acrylate functionality which give reaction with the unsaturated double bonds of SBR during the thermal curing stage. Additionally, acrylate groups are responsible for the flexibility of the oligomer which cause increase in adhesion strength.

Table 4.5 : Adhesion strength values of cord/rubber surfaces for each formulation [154].

Sample Codes	Peel Testing Results (N/cm)		
	F_{max}	$F_{ave.}$	F_{min}
Polyester Fabric	12.3	8.0	5.9
EA 25	12.4	11.0	9.6
EA 50	13.9	11.4	10.2
EA 75	16.7	15.1	12.3
EA 100	18.0	15.3	12.8

Coating formulations were also prepared by using EA oligomer and vinylphosphonic acid (VPA) in different percentages. Before the coating process, cord fabrics were washed with a non-ionic detergent, and then treated with NaOH solution in order to improve the adhesion strength between cord/rubber surfaces. The non-ionic washing process of PA/PES cord fabrics was performed by using 4 g/L ECE detergent solution at 40 ^{o}C for ½ h. The detergent residue remains on fiber surface was removed by several washings [158]. Then fabrics were immersed in alkali solution (4 mol/L NaOH) at 70 ^{o}C for 1 h and then several washings were applied by 1 M HCl solution, ethanol, and distilled water, respectively [40]. Cord fabrics were dried at room temperature. The weight loss was recorded as 6.5 % after alkali treatment. The compositions of the adhesive formulations can be seen in Table 4.6.

Table 4.6 : Compositions of flame retardant adhesive formulations [159].

Sample Compositions	Sample Codes	Phosphorous (%)	VPA (mol %)
Untreated fabric	S1	0	0
ECE+NaOH treated fabric	S2	0	0
EA coated fabric	S3	0	0
EA+2.5% VPA coated fabric	S4	0.68	10.29
EA+5% VPA coated fabric	S5	1.32	18.67
EA+7.5% VPA coated fabric	S6	1.94	25.64
EA+10% VPA coated fabric	S7	2.52	31.46

Figure 4.9, 4.10, and Table 4.7 show the FTIR spectra of the raw polyester and polyamide fibers, and alkali treated/coated fibers with the related band assignments,

respectively. Considering the FTIR spectra of raw fibers and alkali treated polyester and polyamide fibers, it can be seen that peak intensities were changed after alkali treatment due to the conformational rearrangement of crystalline and amorphous regions, and chemical changes [36]. The changes in peak intensities of C-H aromatic ring vibrations at 1342 and 1410 cm^{-1} correspond to the changes in bulk crystallinity caused by the alkali treatment. Moreover, conformational changes of ethylene units between the aromatic groups can be observed from the peaks at 973-1042 cm^{-1} [160, 161]. The characteristic polyester peak of C=O at 1709 cm^{-1} can be observed for all samples in Figure 4.9. After EA coating and UV-curing processes, newly formed peaks of C=C at 1636 cm^{-1}, CH_2 bending at 1200 cm^{-1}, and C-O stretching at 810 cm^{-1} appeared due to the acrylate functionality. Additionally, the existence of VPA in the formulation can be observed from the characteristic peaks at 1000 and 1043 cm^{-1} in Figure 4.9 [162]. The crosslinking density of the coating layer on cord fabric surface after UV-curing was investigated by acetone extraction for 4h. Accordingly, the weight loss after extraction was found as 0.08%. That means photo-polymerization was completed in 2 minutes UV-light exposure.

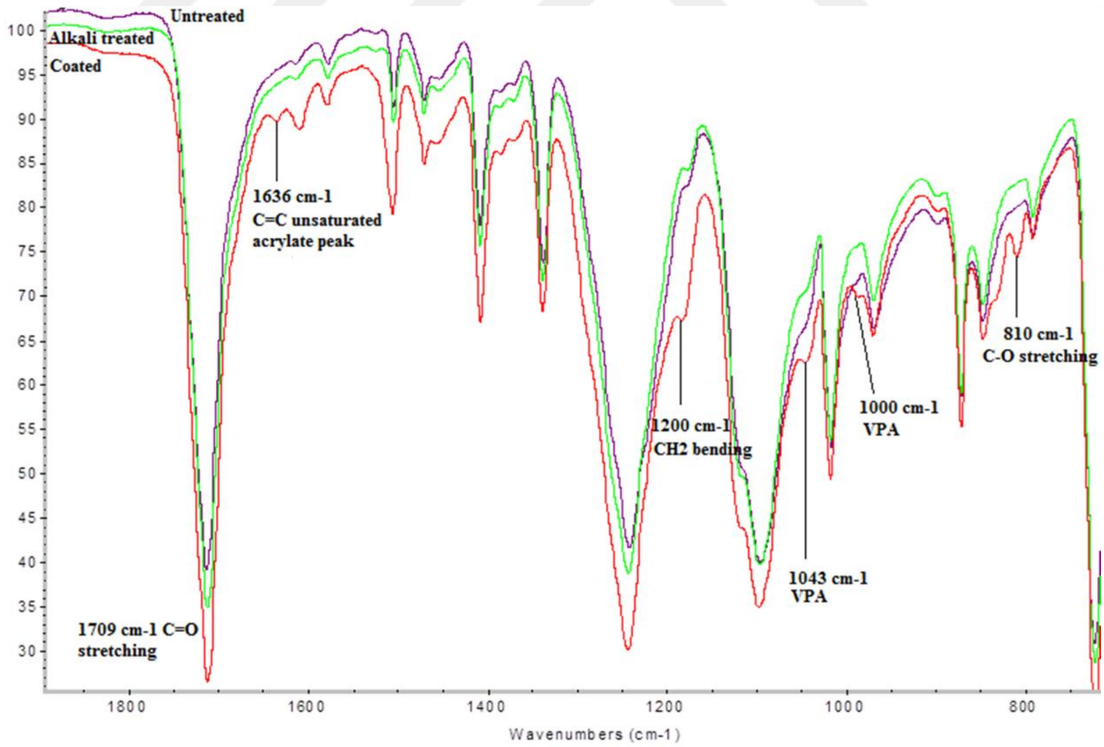

Figure 4.9 : FTIR spectra of polyester fibers (raw, alkali treated, coated) [159].

The FTIR spectra of PA fibers (raw, alkali treated, coated) were given in Figure 4.10. Accordingly, the peak intensities changed after alkali treatment due to the rearrangement of amorphous and crystalline regions. Characteristic PA peaks of amide can be seen in the range of 1493-1631 cm^{-1}. The N-H bending vibration peak at 675 cm^{-1} and the aliphatic C-C and C-H rocking peaks in the range of 900-1200 cm^{-1} can be seen in Figure 4.10, respectively [163]. The ester carbonyl stretching peak of C=O at 1720 cm^{-1}, characteristic VPA peaks at 1000 and 1043 cm^{-1}, CH_2 bending peak at 1200 cm^{-1} and C-O stretching peak at 810 cm^{-1} were all recorded after the application of adhesive formulations.

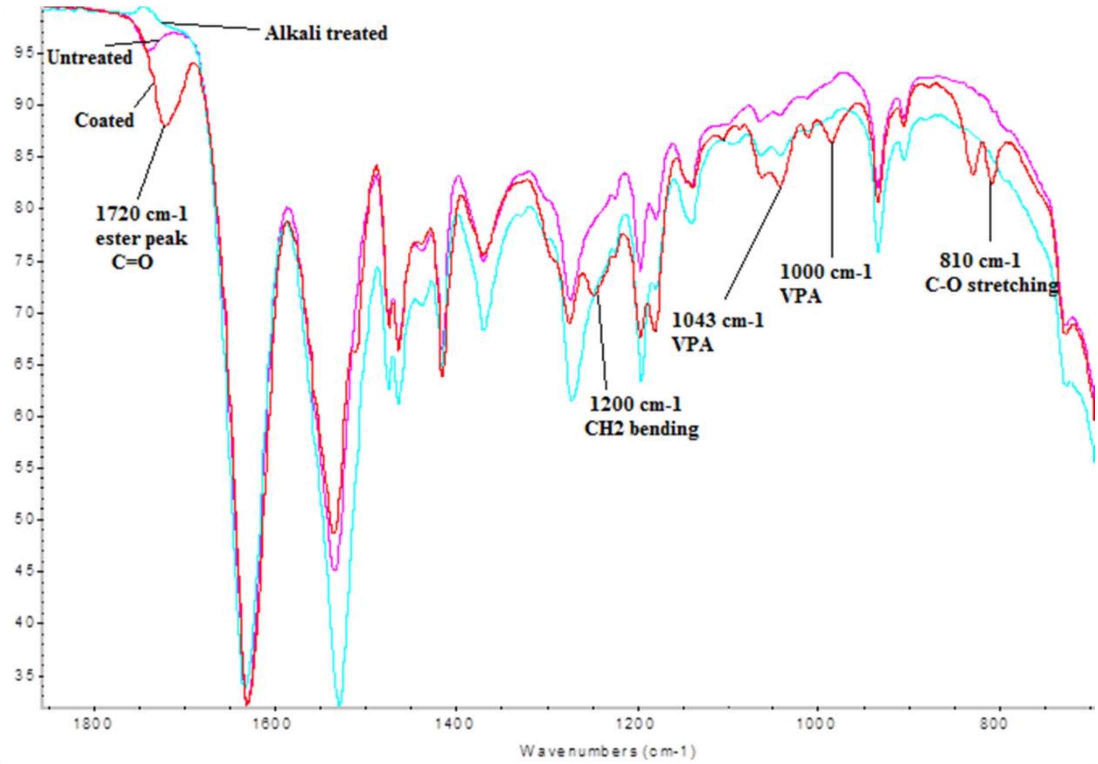

Figure 4.10 : FTIR spectra of polyamide fibers (raw, alkali treated, coated) [159].

Table 4.7 : Band assingnments of polyester, polyamide fiber FTIR spectra [159].

	Wavenumbers (cm^{-1})	Band Assignment	
PES	795	C=O rocking vibration	**Untreated and Alkali Treated**
	848	Rocking vibration of methyl units	
	973-1042	Stretching vibrations of ether units	
	1342, 1410	C-H aromatic ring vibration	
	1709	C=O ester stretching	
	810	C-O stretching	**Peaks After Coating**
	1000, 1043	VPA peaks	
	1200	CH_2 bending	
	1636	C=C unsaturated acrylate peak	
PA	675	N-H bending vibration	**Untreated and Alkali Treated**
	900-1200	Aliphatic C-C and C-H rocking	
	1493	Amide, N-H+C-C+C=O bending	
	1533	Amide, C-N+N-H	
	1631	Amide, C=O+C-N	
	810	C-O stretching	**Peaks After Coating**
	1000, 1043	VPA peaks	
	1200	CH_2 bending	
	1720	C=O ester peak	

Figure 4.11 and 4.12 illustrate the optical microscopy images of polyamide and polyester fibers (raw, alkali treated, coated) and the fiber thickness values after all stages, respectively. During the alkali treatment, hydrolytic scission of ester bonds in polyester and amide bonds in polyamide, caused by the hydroxyl anions of NaOH, was occurred. This deformation and abrasion on fiber surface cause weight loss and conformational re-arrangements. Due to the abrasion on fiber surface, new surfaces are formed resulting a better coating process [36].

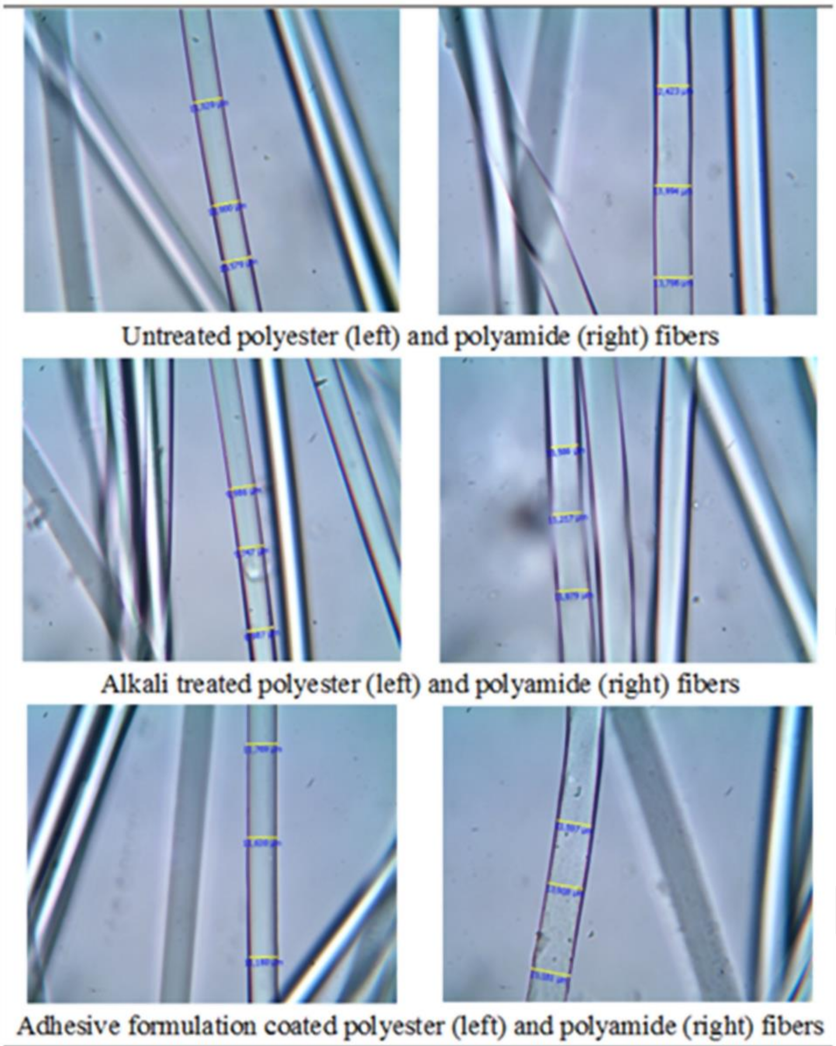

Figure 4.11 : Optical microscopy images of fibers [159].

According to the Figure 4.12, the polyamide and polyester fibers showed 16.1 % and 12.3 % loss in thickness values with alkali treatment, respectively. Due to the non-polar structure of polyester fiber, alkali solution cannot diffuse deeply within the fiber surface, thus the thickness loss of polyester fiber is less than polyamide fiber [36]. Having a non-polar property also affects the thickness increment after coating process. Thus, after adhesive formulation coating stage, 20.5 % and 26.5 % thickness increment values were recorded for polyester and polyamide fibers, respectively.

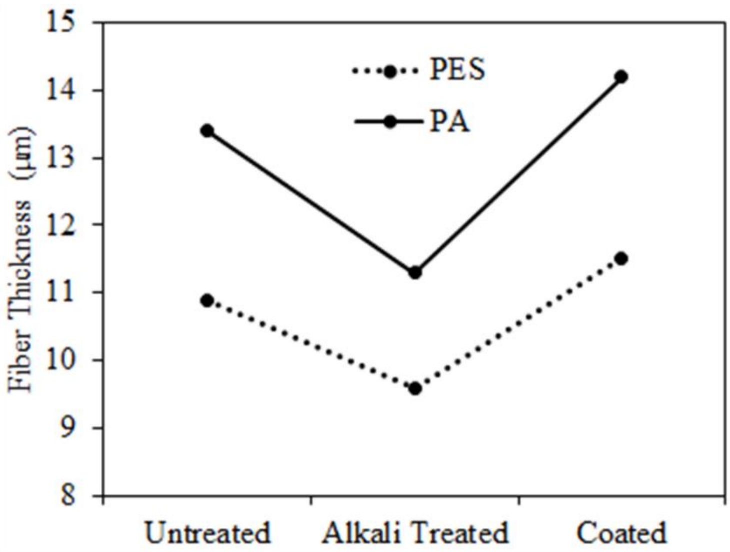

Figure 4.12 : Fiber thickness values of fibers (raw, alkali treated, coated) [159].

Figure 4.13 and Table 4.8 show the TGA thermograms and the thermogravimetric data of UV-cured free films with and without VPA addition. According to the TGA curves, decomposition of the films occurred in one-step. A rapid decomposition was observed in the range of 390-430 ^oC for all films. Due to the flame resist property of phosphorous, whenever VPA amount increases in the formulation, the char yield and the weight loss temperatures increase [92]. In other words, whenever VPA amount increases, thermal stability also increases. Considering the sample of S3 that is not containing any VPA, the char yield was recorded as just 7 % whilst in the sample of S4, after the addition of 2.5 % VPA to the formulation, the char yield increased up to 15 %. T_1 and T_2 correspond to the temperatures which 5 % and 50 % weight loss values were obtained after decomposition. According to the Table 4.8, T_1 increases when VPA ratio increases in the formulation. T_2 values were obtained in the range of 370-430 ^oC for all samples.

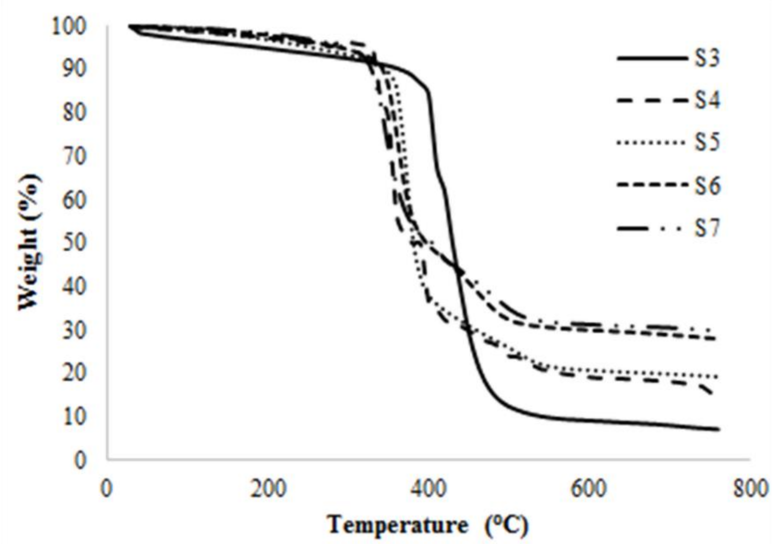

Figure 4.13 : TGA thermograms of UV-cured free films [159].

Table 4.8 : TGA data of UV-cured free films [159].

Sample Codes	T_1 (°C) (5% Weight Loss)	T_2 (°C) (50% Weight Loss)	Char Yield (%)
S3	190	430	7
S4	240	370	15
S5	255	380	19
S6	290	390	28
S7	300	400	30

In order to investigate the flame retardancy property of the adhesive formulations, the LOI test was applied on coated UV-cured cord fabrics. The LOI values of the samples are given in Figure 4.14. The LOI values in S1 and S2 samples are almost the same, that means non-ionic washing process and alkali treatment do not affect the flame retardancy property. The LOI value of S3 sample (EA coated) is lower than S1 (untreated fabric) and S2 (washed, alkali treated) samples. This result can be explained by the lower LOI value of EA layer by itself comparing to the polyester/polyamide cord fabrics. The LOI value of EA oligomer is 21, whereas the LOI values of polyester and polyamide polymers are 23 and 24, respectively [164, 165]. As the VPA amount increases in the formulation, the LOI values also increase. The sample of S7 having 10 % VPA, showed the highest LOI value of 25.5. The S3 and S7 sample images after LOI test can be seen in Figure 4.15. Accordingly, the higher char residue is characteristic property of a material with flame retardant property. The sample images and the thermogravimetric data show consistancy in terms of the char residue. As mentioned before, higher char amounts lead to flame resist property by preventing the heat transfer through the sample due to the VPA inclusion to the formulations [166].

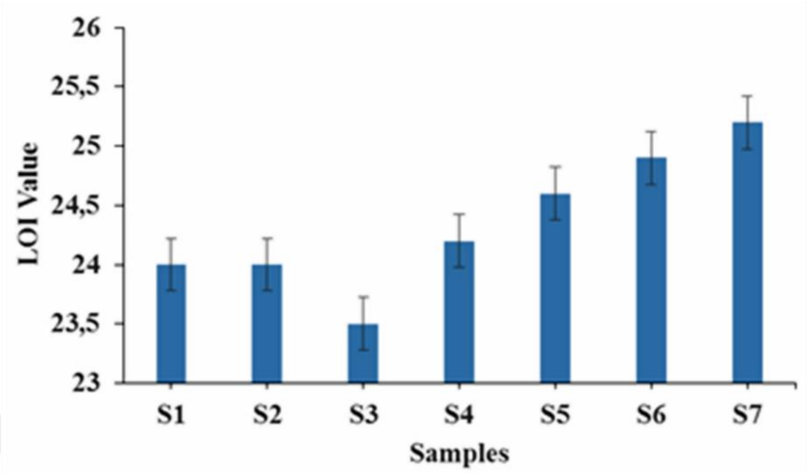

Figure 4.14 : Flame retardancy testing results of coated UV-cured fabric samples [159].

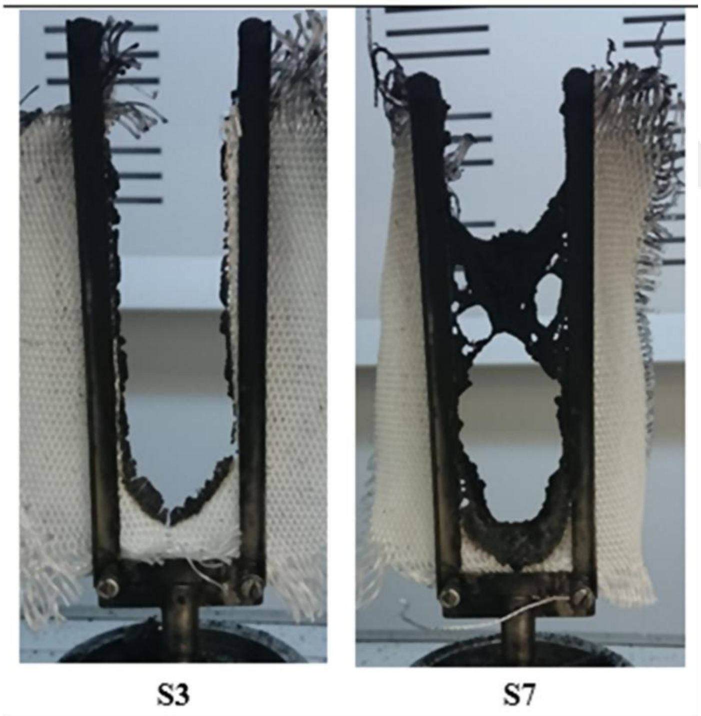

Figure 4.15 : Photographs of coated UV-cured fabric samples after flame retardancy test [159].

Table 4.9 shows the surface energy and contact angle values of coated UV-cured fabrics for each VPA content. Wettability of a surface can be evaluated by measuring the contact angle of a liquid droplet on the surface. In general contact angle values less than 90^o correspond to a surface with high wettability character, whilst contact angles higher than 90^o refer to the hydrophobic surfaces. Surface energy is related to the degree of attraction that is shown against to the different surfaces (liquid etc.) and can be indirectly measured by contact angle testing [167, 168]. According to the Table 4.9, the contact angle testing cannot be applied on S1 (untreated) and S2 (ECE+NaOH treated) samples due to immediate absorption of water droplets on the surfaces. Considering the samples of S3 and S4, when the VPA was introduced to the formulation, contact angle value decreased due to the polarized functional groups. VPA addition into the formulation caused a more polarized structure thus the contact angle values decrease whenever VPA ratio increases in the formulation by giving a hydrophilic character to the surface [118, 169]. The highest hydrophilic behavior so the lowest contact angle value (45^o) was observed in S7 sample with 10 % VPA inclusion to the formulation.

Table 4.9 : Surface energy and contact angle values of coated UV-cured polyester/polyamide cord fabrics [159].

Sample Codes	Contact Angle (^{o})	Surface Energy (mJ/m^2)
S1	--	--
S2	--	--
S3	75	40
S4	72	43
S5	62	45
S6	54	46
S7	45	49

Figure 4.16 shows the peel strength values between the cord/rubber surfaces for each formulation. When the untreated cord fabric was adhered on rubber by means of heat and pressure (thermal curing occurs), the peel strength value was recorded as 24.1 N/cm. The peel strength value was increased to 26.6 N/cm after the ECE washing and NaOH treatments (sample S2, without any adhesive formulation) on cord fabric, due to the formation of polar hydroxyl groups on the fiber surface. In the sample of S7 with 10 % VPA inclusion, the best adhesion strength value of 50.8 N/cm was observed due to the low contact angle value and high wettability character of the surface. This result supports the idea of usage VPA in adhesive formulations as adhesion promoter.

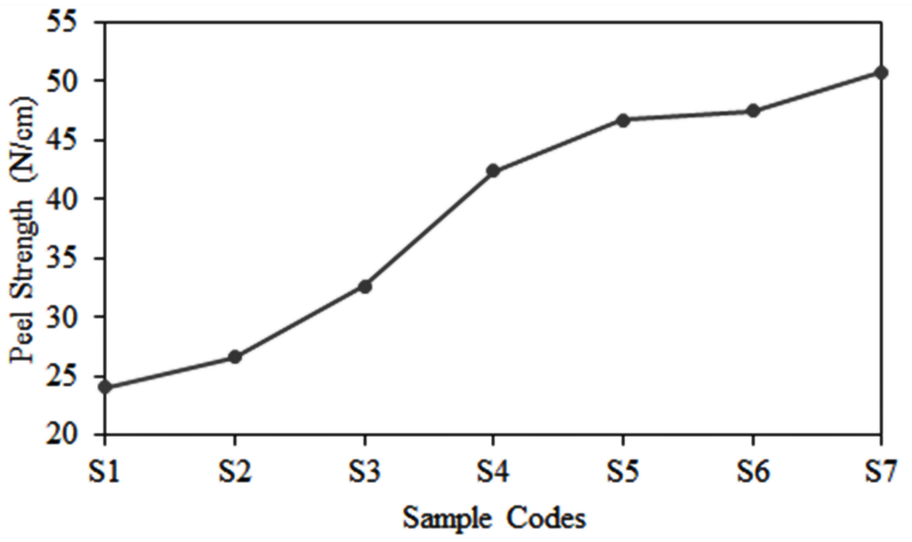

Figure 4.16 : Peel strength values between coated UV-cured cord fabric and rubber surfaces [159].

4.2 Synthesis and Application of UV-Curable Tung Oil Based Adhesive Formulations for Cord/Rubber Applications

In this study, bio-based adhesive formulations were prepared by using tung oil (TO) as bio source. Due to the high unsaturation amount, TO is a good candidate to design oligomers with desired functional properties. At first, TO was epoxidized and then acrylated by AA. The obtained acrylated epoxidized tung oil (AETO) oligomers were used in adhesive formulations in order to adhere cord/rubber surfaces. The synthesis steps of oligomer can be seen in Figure 4.17.

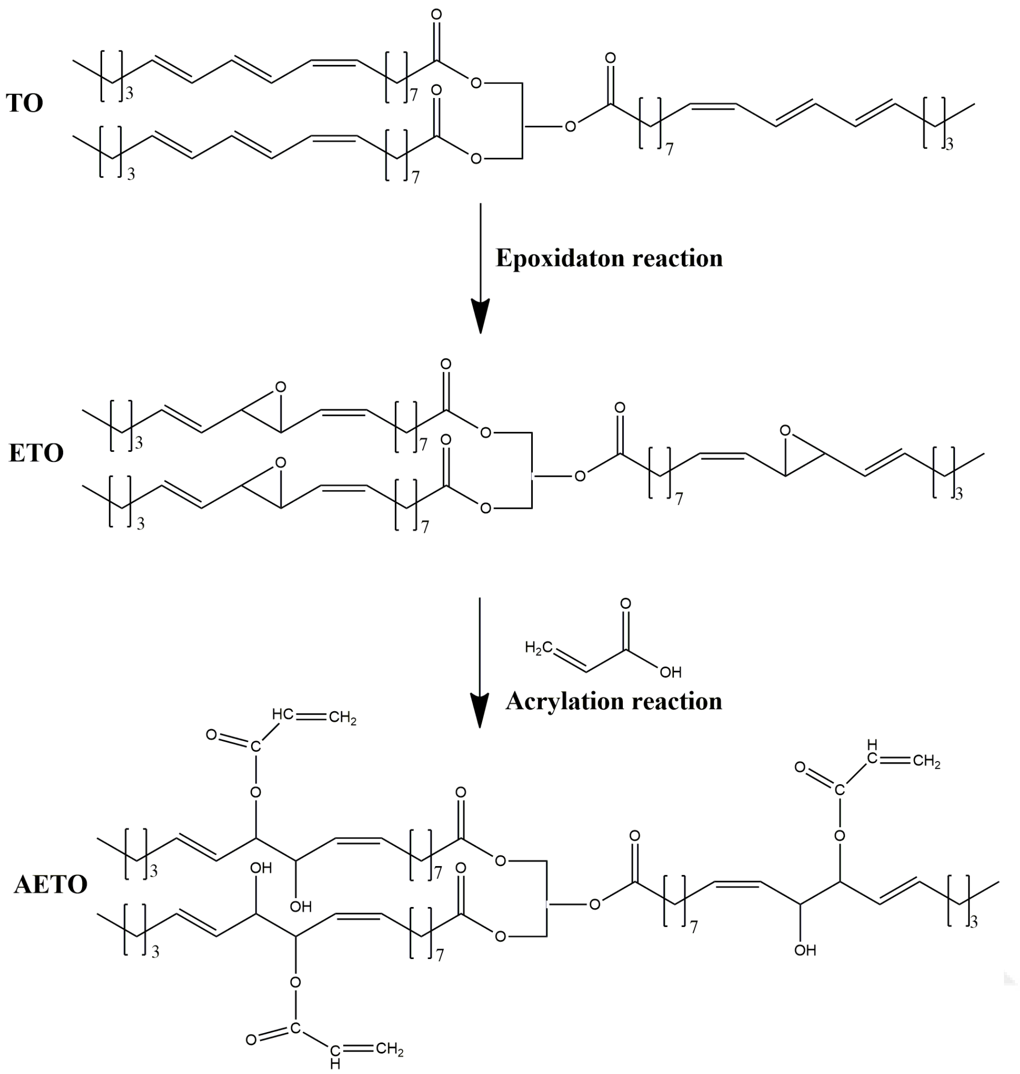

Figure 4.17 : Synthesis steps of AETO oligomer.

In this study, TO was epoxidized by using three different time periods; 3 h, 12 h, and 20 h according to the yield values and previous studies in literature [170]. During the reaction, the acid value, epoxide content, degree of epoxidation (DOE), and the yields of the ETO for different reaction times were observed. The completion of the epoxidation reaction can be followed from the formation of epoxide groups by depleting the acetic acid in the reaction. According to the Table 4.10, the highest acetic acid depletion and yield value, epoxide content, and epoxidation degree were all observed in the sample of ETO-12. Thus this oligomer was used in further testing and characterization stages.

Table 4.10 : Properties of ETO oligomers for each reaction time.

Sample Codes	Reaction Time (h)	Acid Value (mgKOH/g)	Epoxide Content (%)	DOE (%)	Yield (%)
ETO-3	3	44.3	3.2	53.8	62.1
ETO-12	12	24.5	4.9	82.8	70.6
ETO-20	20	36.3	3.2	53.7	65.3

Figure 4.18 shows the FTIR spectra of TO and ETO oligomers in various epoxidation times. The epoxidation and acrylation reactions can be followed by the newly formed peaks, changes in peak intensities or shapes, and shifts of the existing peaks. The ester peak of C=O, belongs to the triglycerides, at 1740 cm^{-1} can be seen in all spectra [171]. The characteristic TO peaks at 2924-2854 cm^{-1} of aliphatic CH_2 groups, C=C puckering peak at 1665 cm^{-1}, -CH_2- deformation peak at 1458 cm^{-1}, CH_3 peak at 1377 cm^{-1}, O-C=O-C peak at 1236 cm^{-1}, -CH-O-C- peak at 1158 cm^{-1}, CH_2O stretching peaks at 1115 and 1097 cm^{-1}, CH_2 wagging peak at 726 cm^{-1} were all observed [172]. According to the FTIR spectra of TO, the disappearance of unsaturation can be followed by the peak at 3015 cm^{-1}. After the 12 h and 20 h epoxidation reactions, this peak disappears as can be seen in the FTIR spectra of ETO oligomers [173]. The depletion of the double bonds can also be followed from the decrease in peak intensity at 1665 cm^{-1}. Additionally, newly formed peaks at 903-808 cm^{-1} and 901-817 cm^{-1} in ETO-12 and ETO-20 spectra were attributed to the epoxide stretching peak of C-O-C proving the success of the epoxidation reaction [11, 172]. In the FTIR spectra of ETO-3, the unsaturation peak around 3010 cm^{-1} is still existing whilst newly formed peaks at 3463, 3421, and 3432 cm^{-1} in ETO-3 and ETO-20 spectra, show the O-H stretching that supports the epoxy ring opening reaction [153].

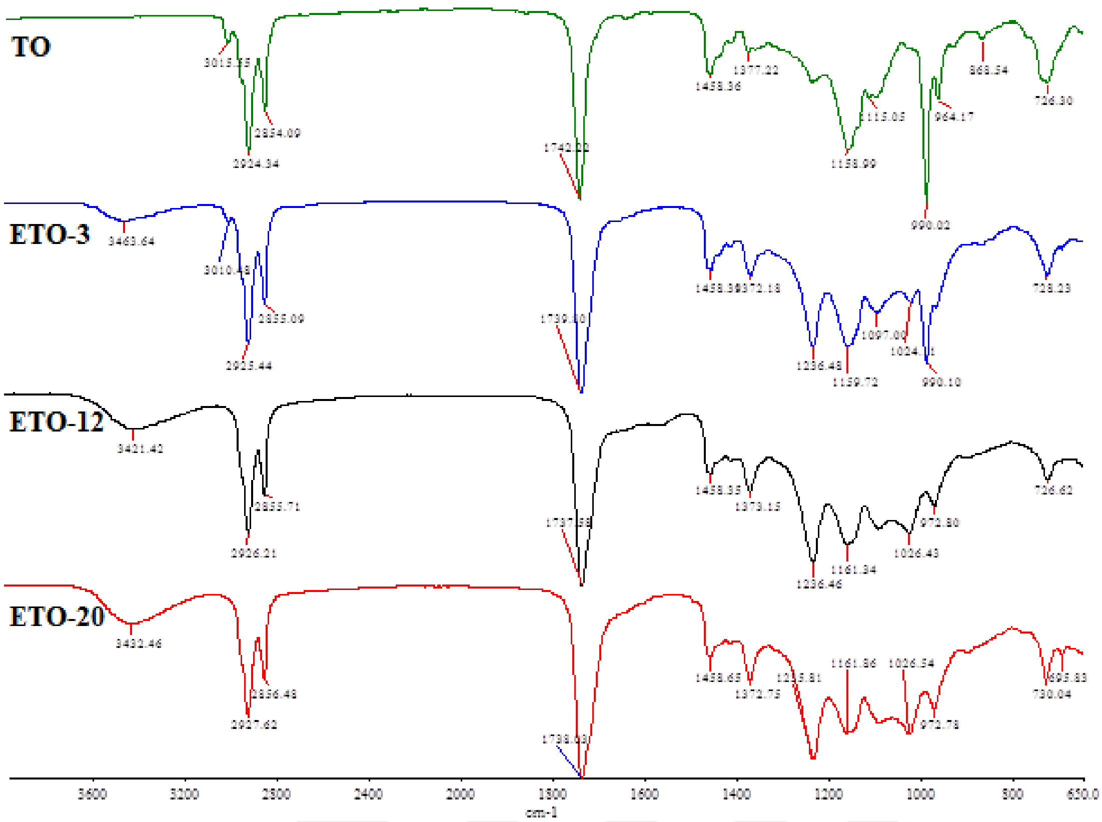

Figure 4.18 : FTIR spectra of TO and ETO in various reaction times.

Figure 4.19 shows the FTIR spectra of TO, ETO-12, and AETO oligomers. The acrylation reaction can be confirmed by the newly formed acrylate peaks of $CH=CH_2$ at 843, 930, and 1421 cm^{-1} [174]. Additionally, the carboxyl group absorption C=O peak at 1696 cm^{-1}, and the C=C stretching peak at 1626 cm^{-1} were observed. The residual epoxy peak at 905 cm^{-1} after the acrylation process can be observed [11].

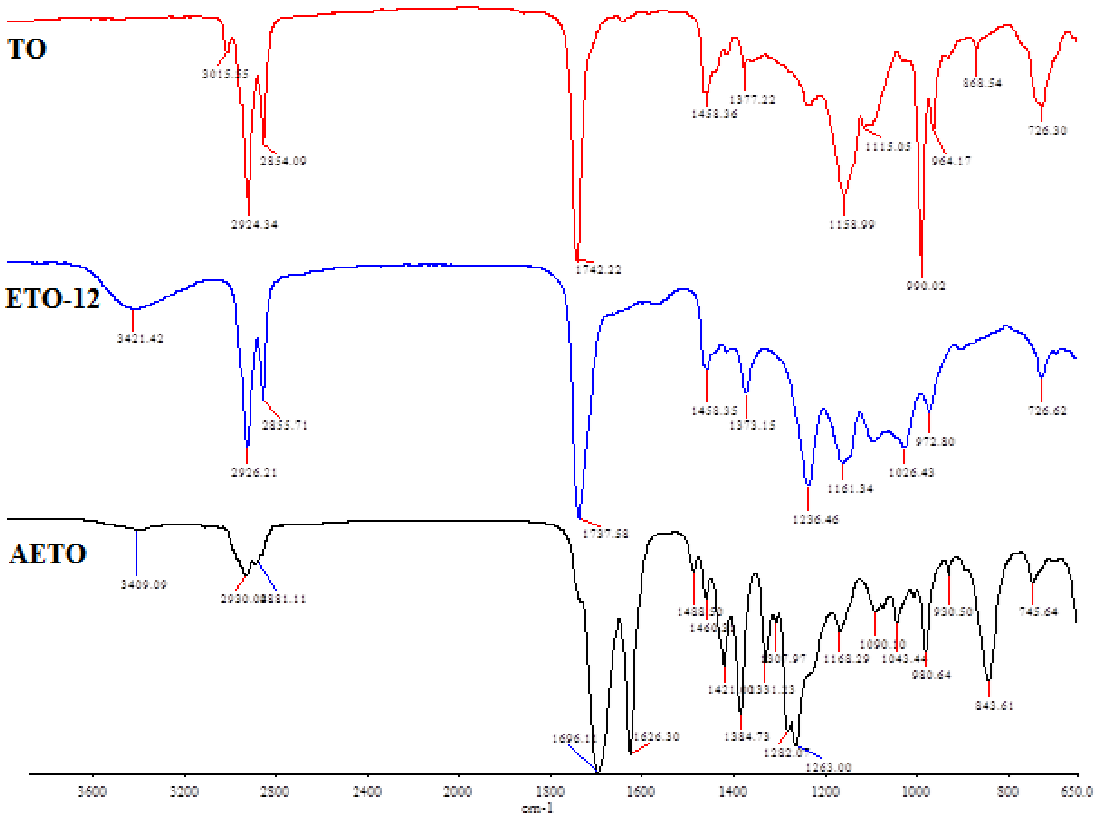

Figure 4.19 : FTIR spectra of TO, ETO-12, and AETO oligomers.

Figure 4.20 illustrates the ^1H NMR spectra of TO, ETO-12, and AETO, respectively. The terminal methyl (-CH_3) protons of fatty acids of TO can be seen at around 0.9 ppm in all spectra. TO has fatty acid side chains with unsaturated groups (-CH=CH-CH_2-CH=CH-) which can be observed with the minor peak at 2.8 ppm coming from the protons in methylene groups between two unsaturated groups [175]. The peaks at 1.3 and 1.5 ppm in TO spectra, correspond to the hydrogens of –CH_2- in fatty acid groups. The peaks around 4.1-4.4 ppm and 5.2-5.3 ppm prove the glyceride structure of TO, by illustrating the protons of the glycerol backbone in a glyceride unit. The protons of conjugated trienes of triglyceride are presented in 5.3-6.5 ppm region with multiple peaks. The peak around 5.4 ppm belongs to the unsaturated cis –CH=CH_2 groups. The –CH2- peaks beside the double bond can be seen at 2.1-2.2 ppm [127, 176].

Regarding the ^1H NMR spectra of ETO-12, the formation of epoxy ring can be proved by the epoxy proton peak at 2.8-3.2 ppm. The methylene protons attached to the C=C unsaturation groups of TO, are represented at 5.2-5.6 ppm region [171]. Moreover, fatty acid ester bonding is presented by the chemical shift at 4.0-4.4 ppm region, and at 5.3 ppm -CH- protons of C=C group, at 2.9-3.1 ppm region -CH- protons of epoxy group can be observed.

In the ^{1}H NMR spectra of AETO, existence of the acrylate group (-CH=CH-) was proved by the minor peaks at 5.2-5.6 ppm region [171]. Protons at 3.5 ppm and 2.5 ppm correspond to the protons nearby the electron donor groups such as CH_2, CH_3, and protons in allylic positions, respectively. Protons of carbon atoms coming from the opening of epoxide groups and protons nearby the electronegative groups (carboxylic groups of acrylates, vinylic protons) can all be seen at 4.4 ppm.

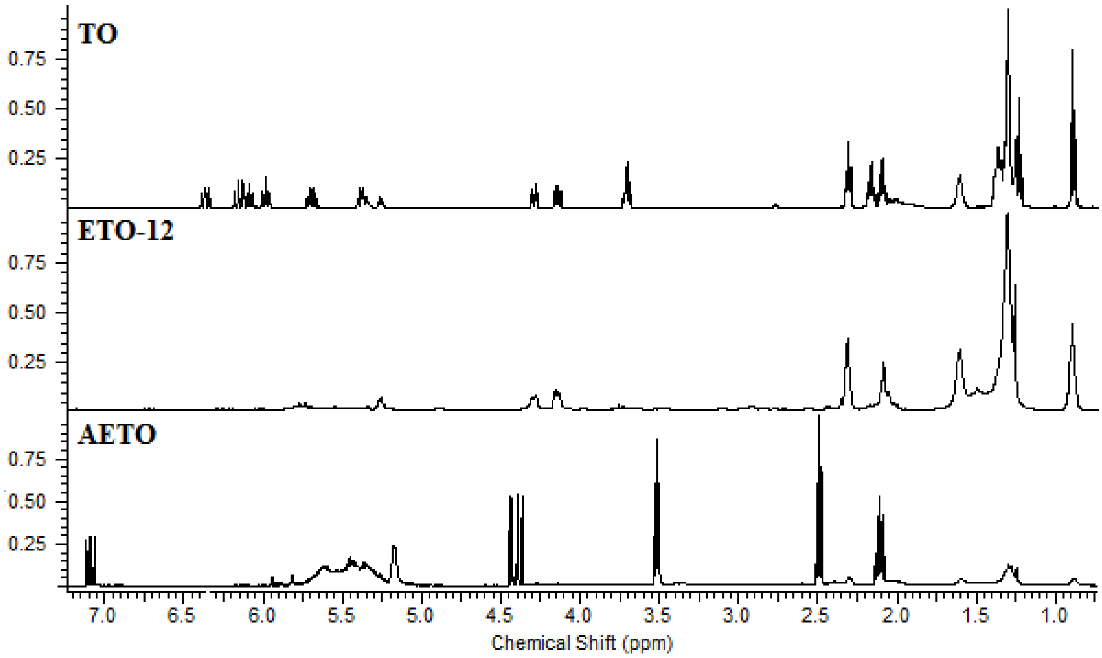

Figure 4.20 : ^{1}H NMR spectra of TO, ETO-12, and AETO oligomers.

The TGA thermograms and the thermogravimetric data of UV-cured free films under air with a 10 ^{o}C/min heating rate were given in Figure 4.21 and Table 4.11, respectively. Existence of aromatic groups in the oligomer structure, conformational re-arrangements, chain rigidity, composition and chemical structure of polar groups are all effective parameters determining the thermal oxidative stability of polymers [107, 154]. According to the TGA results, the free film samples of TO, ETO-12, and AETO showed thermal stability till 280, 250, and 150 ^{o}C, and they presented a 50 % weight loss at 400, 420, and 190 ^{o}C, respectively [177]. Epoxidation reaction caused increase in thermal oxidative stability due to the presence of aromatic structure in epoxy groups. Due to the addition of polar groups into the structure with the acrylation process and the depletion of epoxide groups, the thermal oxidative stability decreased in AETO sample.

Table 4.11 : Weight loss temperatures of UV-cured free films.

Samples	T_1 (ºC) (5% weight loss)	T_2 (ºC) (50% weight loss)
TO	150	400
ETO-12	190	420
AETO	100	190

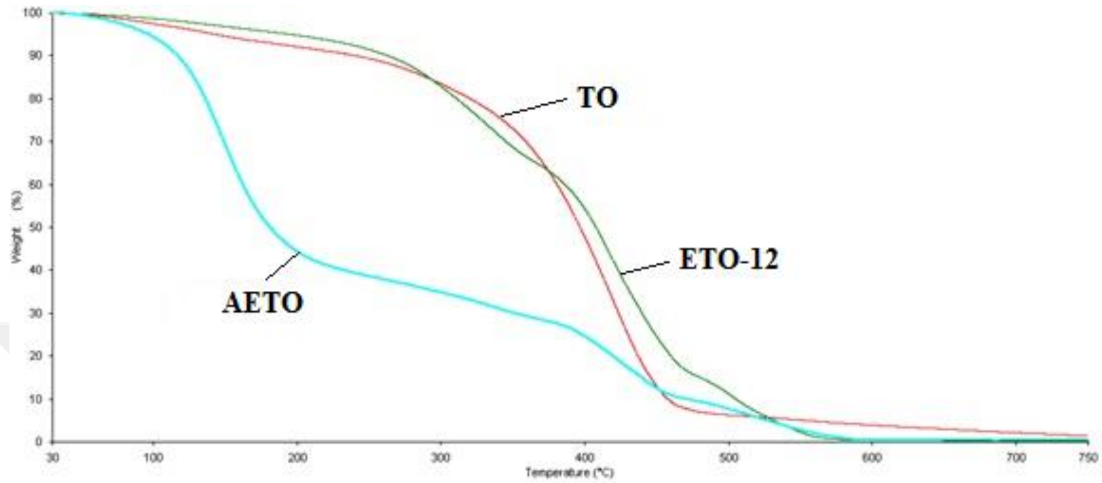

Figure 4.21 : TGA curves of UV-cured free films.

The swelling degree (%) values of UV-cured free films after the immersion in toluene can be seen in Figure 4.22. Accordingly, all films showed a good stability in the range of 1-6 % in toluene. The AETO ratio in the formulation is highly effective on swelling ratio and rate. The highest swelling degree of 6 % was recorded in the sample without PUA inclusion after 1h immersion in toluene. In the samples containing both AETO and PUA oligomers, the swelling degree increases with increasing AETO amount in the formulation due to the hydrohilic and porous nature of AETO oligomer [178].

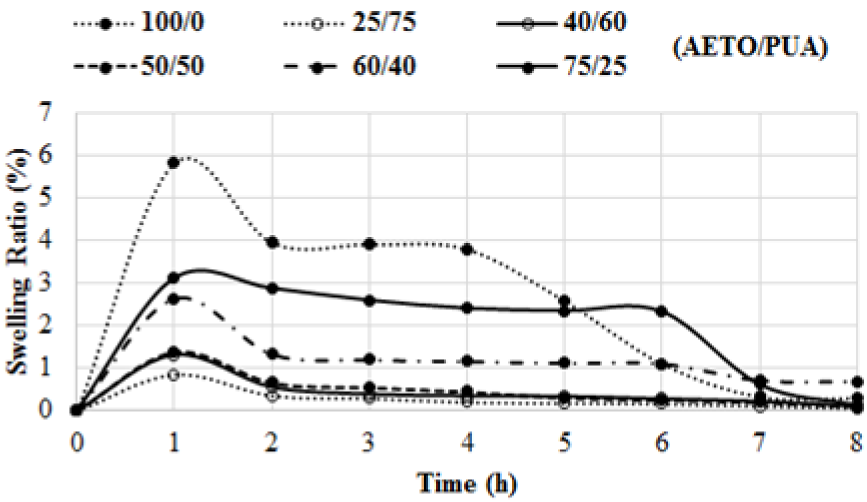

Figure 4.22 : Swelling degree of UV-cured free films in various AETO/PUA ratios.

The hydrophobic character and crosslinking density are effective parameters determining the gel content of UV-cured free films. Higher gel content means that the crosslinking density of the films is also high. In order to investigate the gel content of UV-cured free films in various AETO/PUA ratios, the Soxhlet extraction method in THF was performed for 6 h. After the extraction process, all unreacted substances and uncrosslinked ingredients were removed. Table 4.12 shows the gel content of UV-cured free films for each AETO/PUA ratio. Accordingly, the gel content values of UV-cured free films were found in the range of 70-99 % which prove the formation of a three dimensional structure within the films. The sample containing 25/75 % AETO/PUA showed the highest gel content with 98.6 % due to having the highest amount of acrylate groups representing in both AETO and PUA oligomers [171]. Higher gel content value means that almost all reactive groups in the formulation were converted into crosslinked structure with the help of UV exposure. Additionally, slightly decrease in gel content value was observed in the sample without PUA inclusion. Results showed that the gel content value decreased with increasing AETO amount in the formulation due to the existence of epoxidized free fatty acids in AETO oligomer which is related to the acrylation degree of the oligomer consequently affects the crosslinking density.

Table 4.12 : Gel content values of UV-cured free films in various AETO/PUA ratios.

AETO/PUA (%)	Gel Content (%)
25/75	98.6
40/60	98.5
50/50	96.2
60/40	83.1
75/25	69.9
100/0	91.3

Adhesive formulations were applied on cord fabrics and then cured by UV-light according to the process in Figure 3.7. The completion of photo-polymerization on cord fabric surface was investigated by acetone extraction method for 4h and then a 0.22% weight loss was observed after extraction. This result confirms the formation of UV-curing process. The wettability character of the coated UV-cured surfaces was investigated by contact angle measurement. The images of water droplets on coated UV-cured fabric surfaces in terms of the AETO/PUA ratios can be seen in Figure 4.23.

The contact angle and surface energy values for each formulation were presented in Table 4.13. Results showed that whenever AETO ratio increases up to 50 % in the formulation, contact angle value also increases to 87.9°. After that point, contact angle values decrease with increasing AETO amount in the formulation. This result can be explained by the hydrophilic nature of epoxidized free fatty acids in AETO structure.

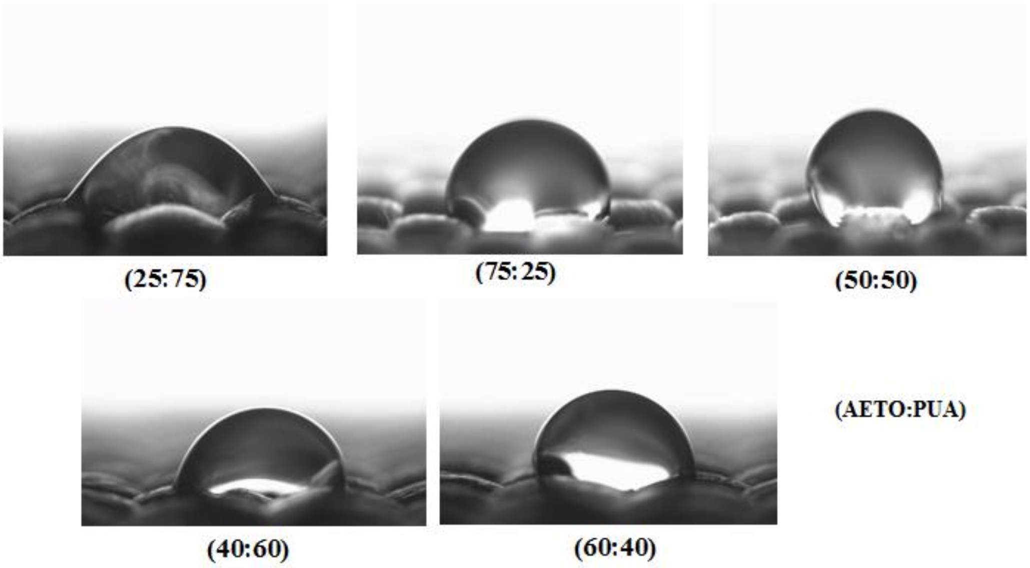

Figure 4.23 : Images of water droplets on coated UV-cured cord fabrics.

Table 4.13 shows the adhesion strength values of cord fabric/rubber composites in various AETO/PUA ratios. Accordingly, the highest adhesion strength value of 26.0 N/cm was recorded when the AETO/PUA ratio was set as 50/50 %. In theory, whenever contact angle increases the surface shows a hydrophobic behavior resulting a poor adhesion property. But in this study, the adherence should be considered after the thermal curing stage of the adhesive between cord fabric/rubber surfaces, not only from the hydrophilicity of the cord fabrics.

Table 4.13 : Peel strength values of fabric/rubber composites. Surface energy, and contact angle values of coated fabrics after UV-curing.

AETO/PUA (%)	Contact Angle (°)	Surface Energy (mJ/m^2)	Peel Strength (N/cm)
25/75	54.8	54.2	16.8
40/60	61.2	52.5	17.1
50/50	87.9	42.2	26.0
60/40	77.7	47.1	20.2
75/25	69.7	50.8	19.6
Pure fabric	--	--	12.3

ETO was also modified by vinylphosphonic acid (VPA) and the obtained vinylphosphonic acid modified epoxidized tung oil (VPAETO) oligomer was included in adhesive formulations. The adhesion strength between cord/rubber surfaces was investigated. Synthesis steps of the oligomer can be seen in Figure 4.24.

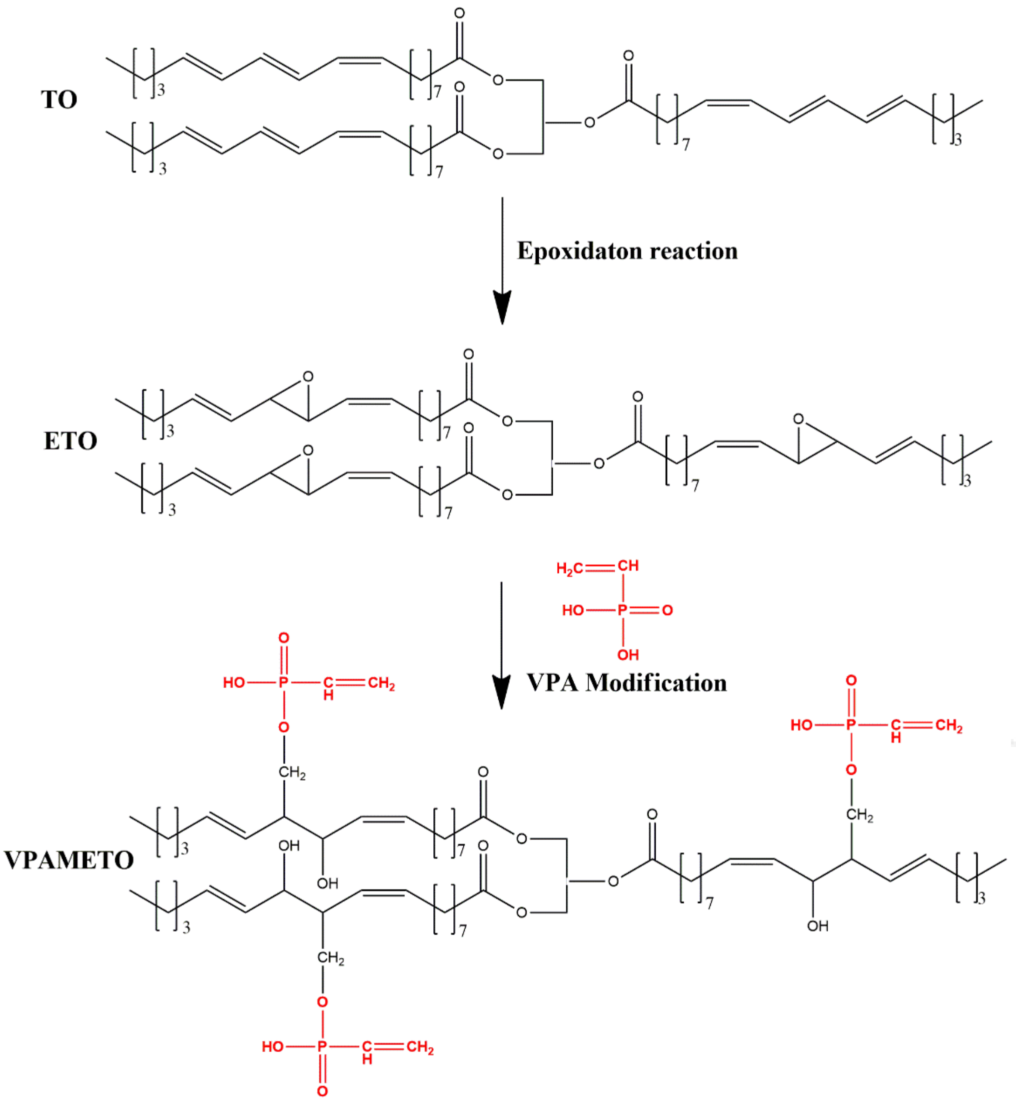

Figure 4.24 : Synthesis of VPAMETO oligomer.

EEW of the synthesized oligomer was determined by using $HClO_4$ titration method after the epoxidation stage [11] and recorded as 858.8 g/equivalent. The epoxidation and VPA modification reactions were followed by FTIR spectroscopy. As can be seen in Figure 4.25, the ester peak of triglyceride (C=O) and the unsaturated groups of TO can be observed at 1740 cm^{-1} and 3015 cm^{-1}, respectively. The peaks due to unsaturation were all disappeared after the epoxidation stage [131]. The O-H stretching peak at 3421 cm^{-1} in ETO FTIR spectra, illustrated that the epoxide group might be opened via side reactions [132]. Considering the FTIR spectra of VPAMETO oligomer, the characteristic oxirane peak at 825 cm^{-1} in ETO oligomer was completely disappeared with the VPA modification reaction. Furthermore, the vibration peak of phosphate ester at 1002 cm^{-1} supported the existence of VPA in the oligomer structure [92].

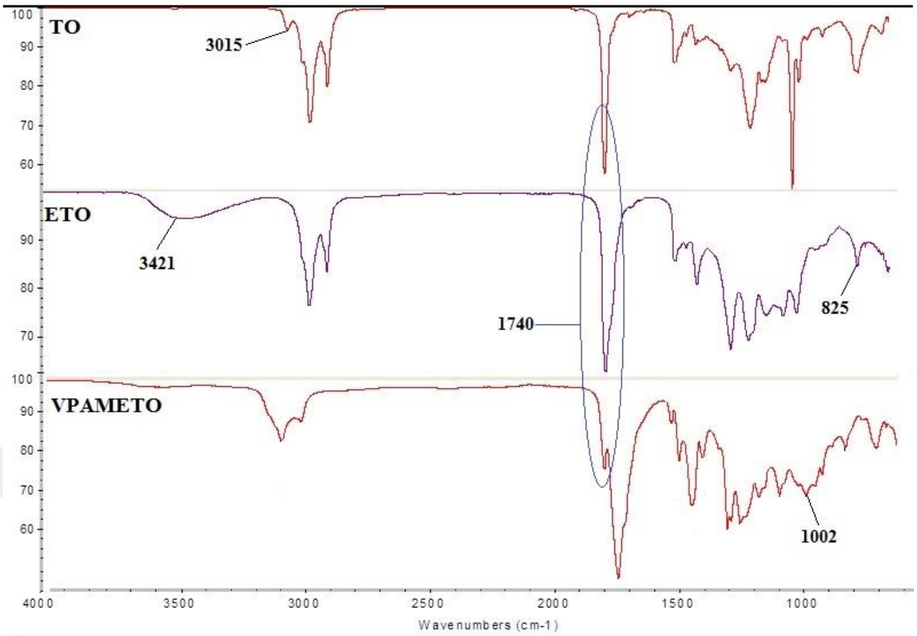

Figure 4.25 : FTIR spectra of TO and modified TO oligomers [179].

The ^{1}H NMR spectra of TO, ETO, and VPAMETO oligomers were given in Figure 4.26, respectively. Regarding the ^{1}H NMR spectra of TO, in 6-6.5 ppm region, the CH and CH_2 protons between the unsaturated groups in fatty acids of TO were observed. The epoxidation reaction caused the formation of epoxide group peaks at around 2.8-3.1 ppm region associated with the CH protons linked to the oxygen of the epoxide groups. The CH and CH_2 protons of vinyl group in VPA can be observed at 6.3 ppm and 5.6 ppm, respectively [130].

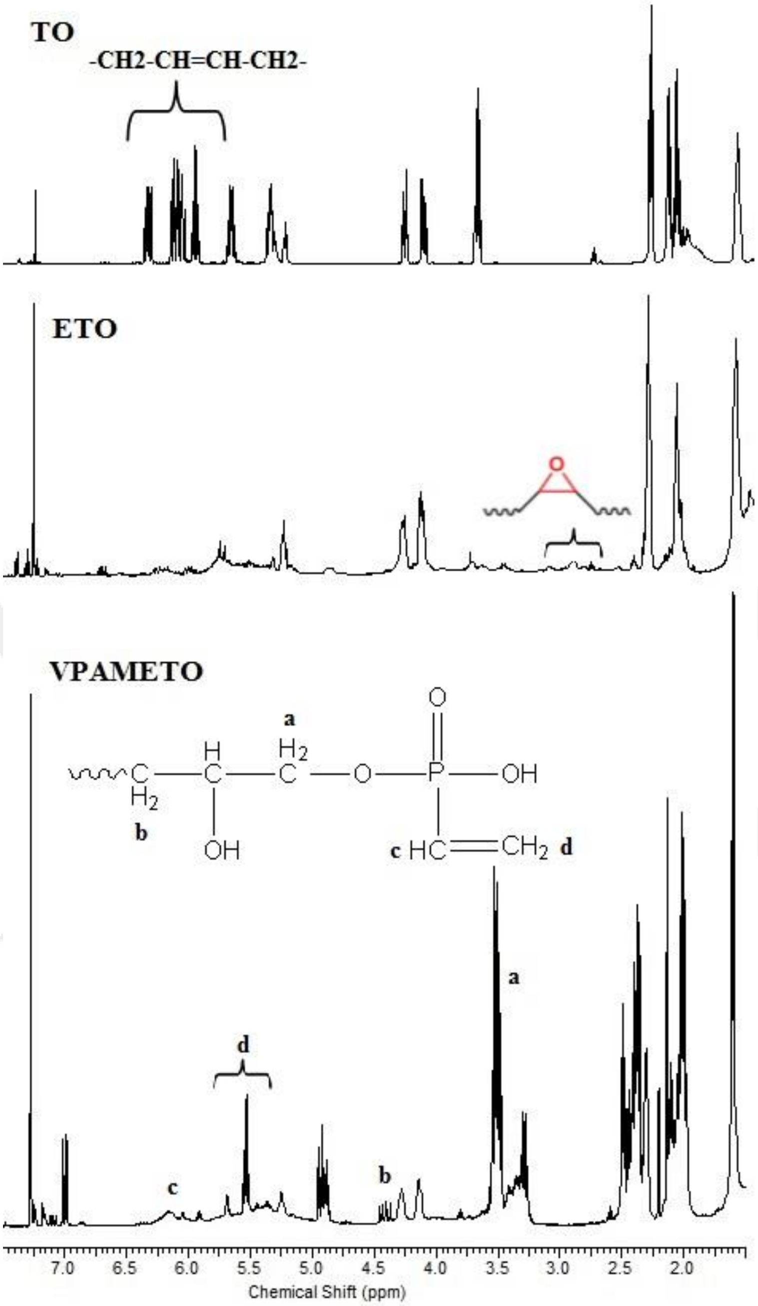

Figure 4.26 : ^{1}H NMR spectra of TO and modified TO oligomers [179].

Adhesive formulations were applied on cord fabrics by dip-coating and then cured by UV-light. The completion of UV-curing was followed in coated UV-cured fabric by ursing acetone extraction method for 4h. Accordingly, the weight loss after extraction was recorded as 0.06% which confirms the formation of a crosslinked structure on fabric surface after UV-curing. The images of water droplets on coated UV-cured cord fabrics in various VPAMETO/PUA ratios can be seen in Figure 4.27. According to the images, it can be seen that the hydrophilicity of the fabric increased, thus contact angle value decreased with increasing VPAMETO amount in the adhesive formulation. This result can be explained by the increasing number of hydroxyl groups due to the existence of VPA in the oligomer structure associated with the VPAMETO.

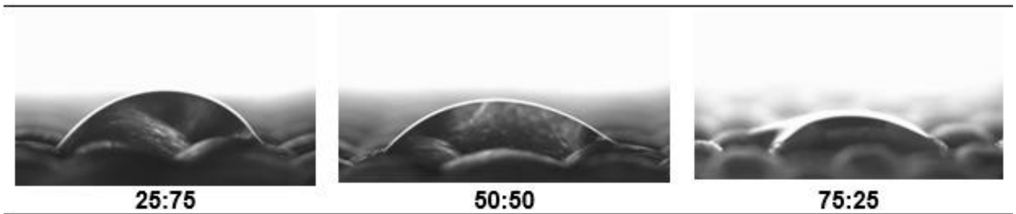

Figure 4.27 : Images of water droplets on VPAMETO:PUA coated UV-cured cord fabrics [179].

The contact angle and surface energy values from the coated UV-cured cord fabric surfaces, and the peel strength of cord fabric/rubber composites were all illustrated in Table 4.14. Accordingly, a consistent behavior was observed among all results. In other words, whenever VPAMETO increases in adhesive formulation contact angle value decreases, surface energy value increases, so the peel strength value increases. Due to the hydroxyl functional groups of VPA, the hydrophilic character of the fabric increased after dip-coating, thus the best adhesion strength value of 20.5 N/cm was recorded when the VPAMETO/PUA ratio was set as 75/25 in the adhesive formulation.

Table 4.14 : Peel strength, contact angle, and surface energy values of the samples in various VPAMETO/PUA ratios [179].

VPAMETO (%)	PUA (%)	Contact Angle (°)	Surface Energy (mJ/m^2)	Peel Strength (N/cm)
25	75	56.7	57.7	13.2
50	50	44.3	60.7	18.6
75	25	40.2	63.2	20.5
Pure fabric		--	--	12.3

4.3 Synthesis and Application of Polyurethane Methacrylates for Cord/Rubber Applications

In this study, formaldehyde-free dual-curable adhesives were synthesized with the reaction of TDI and HEMA. Possible mechanisms for TDI-HEMA reaction can be seen in Figure 4.28. The obtained polyurethane methacrylate based oligomers were evaluated in terms of the adhesion strength for cord/rubber surfaces, by changing the NCO:OH ratio and reactive diluent compositions. The sample codes and compositions of adhesive formulations were presented in Table 4.15.

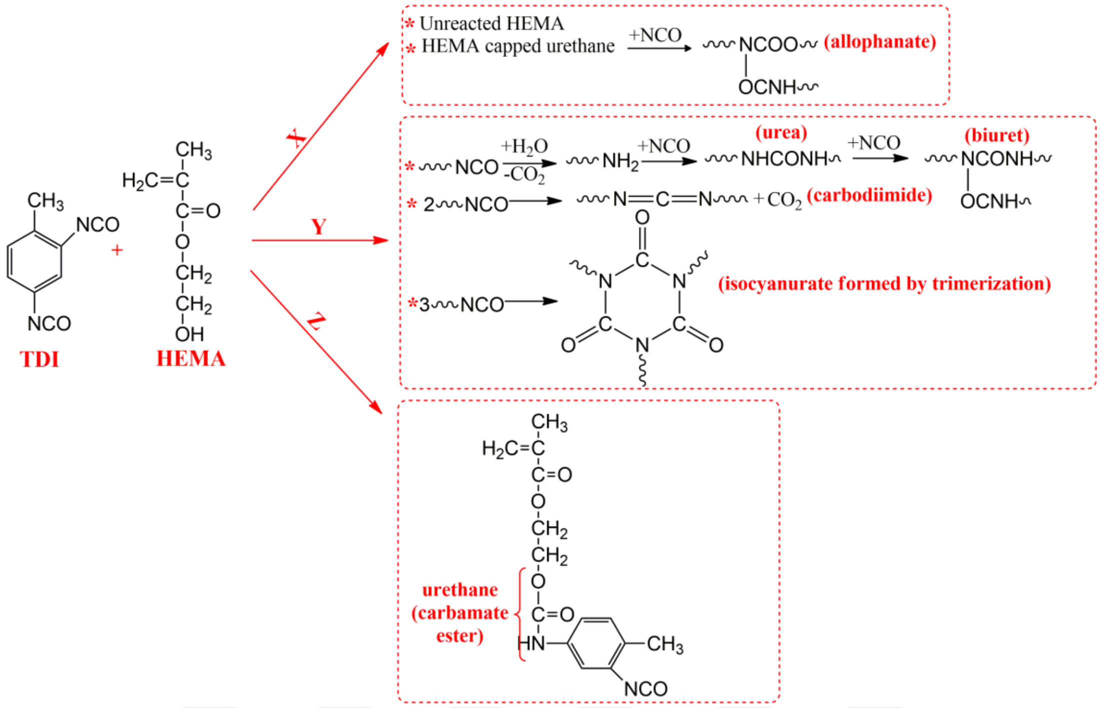

Figure 4.28 : Possible reaction mechanisms for TDI-HEMA reaction.

Table 4.15 : Compositions of adhesive formulations.

Sample Code	TDI (mol)	HEMA (mol)	NCO:OH Ratio	Reactive Diluent (50%)
X	0.5	1	1:1	--
X-1	0.5	1	1:1	TCDDA
X-2	0.5	1	1:1	TMPTMA
Y	1	0.5	4:1	--
Y-1	1	0.5	4:1	TCDDA
Y-2	1	0.5	4:1	TMPTMA
Z	1	1	2:1	--
Z-1	1	1	2:1	TCDDA
Z-2	1	1	2:1	TMPTMA

Figure 4.29 shows the ^{1}H NMR spectra of the samples of X, Y, and Z. According to the spectra, the existence of HEMA in the oligomer structure can be proved by the peaks at 4.27-4.39 ppm (-O-CH_2-CH_2-O-), at 5.59-5.60 ppm ($C(CH_3)=CH_2$ trans), and at 6.10-6.18 ppm ($C(CH_3)=CH_2$ cis), respectively. The methyl groups of TDI and HEMA can be observed at 2.14-2.17 ppm and 1.94-1.95 ppm. When the NCO:OH ratio increased in the formulation, the peak intensities of methyl groups of TDI increased whilst methyl and methylene groups of HEMA decreased. The confirmation of the reaction between the isocyanate and hydroxyl group can be made by the peak at 4.85 ppm refering to the –NH- peak of urethane (carbamate) group. The peaks at 7.10-7.92 ppm region correspond to the phenyl ring protons of TDI. The existence of urea

linkage (-NHCONH-) due to the some side reactions between the trace amount of water and excess isocyanate, can be followed by the peak at 6.7. ppm. The possible side reactions are given in Figure 4.24. The formation of urea can be seen only in the spectra of Y and Z samples due to having excess isocyanate groups in the formulation. In the spectra of X sample, the peaks at 3.44-3.85 ppm region illustrate the methylene protons existing on the hydroxyl groups of HEMA. [17, 89, 180-182].

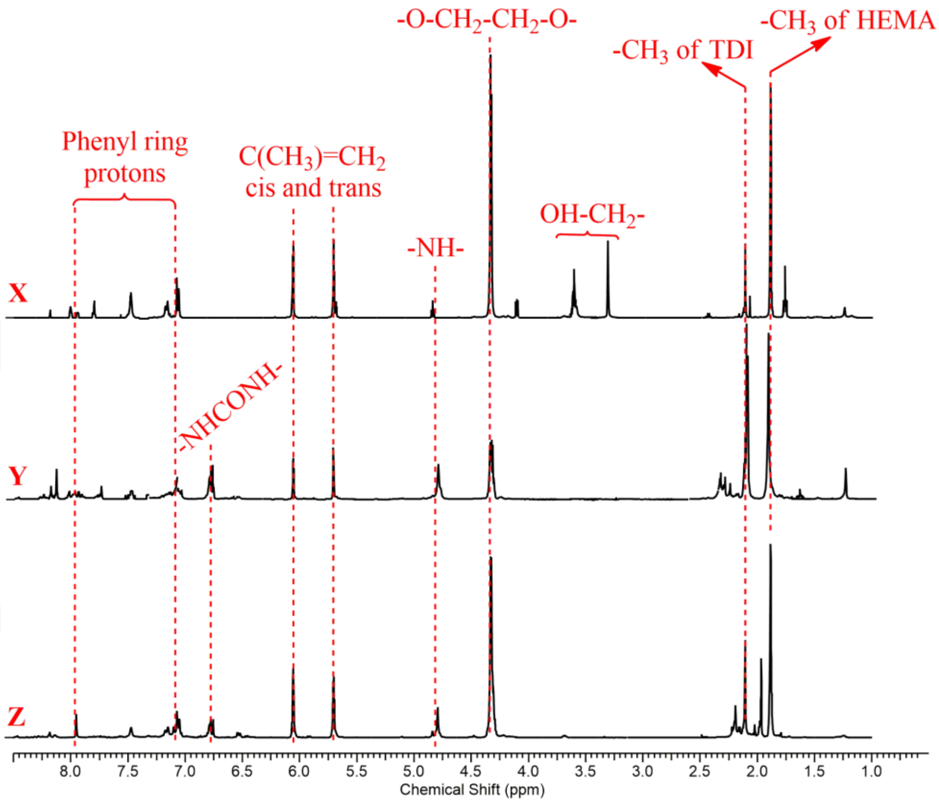

Figure 4.29 : ^{1}H NMR spectra of polyurethane methacrylate oligomers in various NCO:OH ratios.

The swelling degree (DS %), the gel fraction (GF %), and the chemical resistance values of UV-cured free films were all given in Table 4.16. The chemical resistance of films were measured based on the weight loss (%) values after immersion into the solutions. A high GF (%) value corresponds to the high crosslinking densities whilst DS (%) and weight loss (%) after exposure to chemicals decrease whenever crosslinking density increases. Results showed that the increasing NCO:OH ratio in the formulation, increased the GF (%) value from 80 % to 99 % considering the X and Y-1 samples. Reactive diluent inclusion to the formulations increased the GF (%) values for all samples. With the inclusion of reactive diluent to the oligomer structure and increasing NCO:OH ratio, the DS (%) values decrease in all solvents. This result is stemming from the highly crosslinked structure of the samples. Due to the existence of strong intermolecular interactions and secondary bondings such as hydrogen bonding, and bonding of rigid phenyl groups, all samples presented a good chemical resistance property in both NaOH and HCl solutions. Eventually, the weight loss (%) after exposing to chemicals decreased whenever the reactive diluents exist and the NCO:OH ratio increases in the formulation [6, 17].

Table 4.16 : Physicochemical characteristics of UV-cured film samples.

Sample Codes	DS (%)			GF (%)	Chemical Resistance Weight Loss (%)	
	Toluene	Ethanol	Water		NaOH (10%)	HCl (10%)
X	9.96	12.26	8.72	80.78	3.23	1.98
X-1	9.02	10.06	7.58	86.21	1.48	0.74
X-2	9.46	10.92	7.83	83.75	1.99	1.01
Y	1.82	1.94	1.74	98.65	2.51	1.84
Y-1	0.37	0.89	0.26	99.97	0.98	0.59
Y-2	1.58	1.62	1.49	99.41	1.71	0.75
Z	4.27	5.69	3.91	88.75	2.61	1.89
Z-1	3.09	4.74	2.54	93.33	1.28	0.61
Z-2	3.54	5.02	2.76	92.13	1.86	1.17

Figure 4.30 shows the TGA curves of UV-cured free films for each sample composition. Accordingly, all samples thermally decomposed similarly in two-step. The urea and urethane bonds depolymerized into TDI and HEMA at around 240-260 ^{o}C. In 350-385 ^{o}C region, the chain scission of HEMA and the decomposition of the aromatic group of TDI were recorded. In the first step, a 20-40 % weight loss was observed in 300-385 ^{o}C region for each sample due to the decomposition of urethane linkages. In the second step, in 400-500 ^{o}C region, the carbodiimide and isocyanurate groups decomposed resulting the main weight loss (60-90 %) of the films. Figure 4.30.a shows the thermal decomposition character of the films in terms of the NCO:OH ratio. Increase in NCO:OH ratio caused increase in thermal stability of the films due to the formation of isocyanurate units (trimerization) (Figure 4.28), that is formed by the excess isocyanate groups, resulting increase in crosslinking density [6, 183]. When the reactive diluents are included into the formulations as in Figure 4.30.b, c, and d, thermal stabilities of the films all increased because of the increasing crosslinking density. The increase in thermal stability is more significant in the samples of X-1, Y-1 and Z-1, comparing to the X-2, Y-2, and Z-2, because of the cycloaliphatic, bulky character of TCDDA, that is effective on crosslinking density and thermal stability, by decreasing the chain mobility in the structure [184].

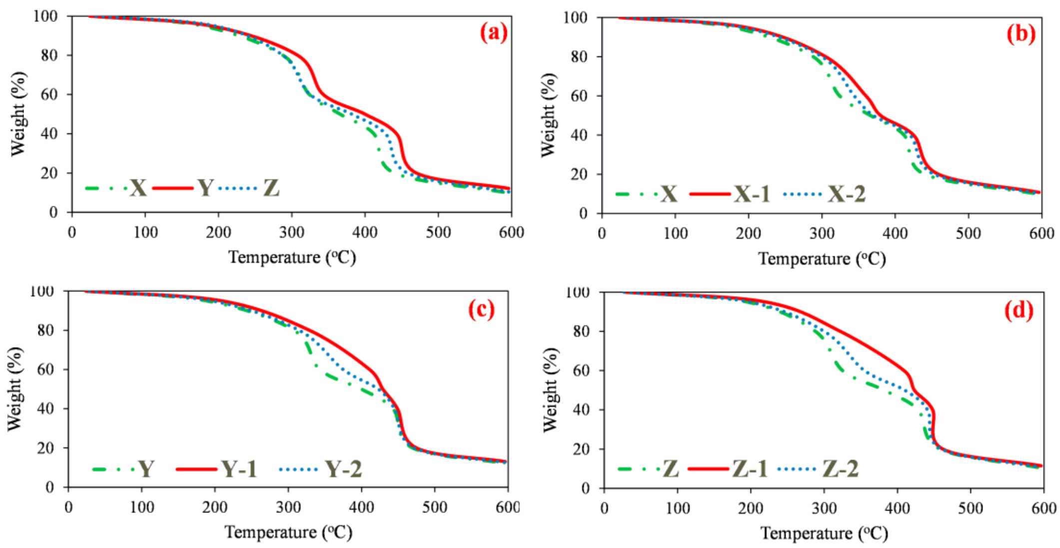

Figure 4.30 : TGA curves of UV-cured free films in terms of NCO:OH ratio (a), and reactive diluent types (b, c, d).

The thermogravimetric data and the thermal transitions of the UV-cured free films can be seen in Table 4.17. Due to the decomposition of carbodiimide and isocyanurate groups and performing the thermal analysis under nitrogen atmosphere, carbonization, also known as pyrolysis, occurs. Thus char formation was observed after testing [183]. The 5 %, 50 %, and 80 % weight loss values during thermal exposure were given in order to evaluate the thermal behavior of free films in detailed. According to the results, when the NCO:OH ratio increases, the decomposition temperatures also increase. Due to the existence of cyclic, bulky groups in TCDDA, films having TCDDA as reactive diluent showed higher thermal stabilities and high char yields, comparing to the films with TMPTMA. As mentioned before, TCDDA increases thermal stability by increasing the crosslinking density of the structure.

Table 4.17 : Thermogravimetric and thermal transitions data of UV-cured free films.

Sample Code	T_g (°C)	^1T_d (°C)	^2T_d (°C)	Weight Loss (%), Temperature (°C)			Char Yield (%)
				5%	50%	80%	
X	-49	45	262	178	366	440	9.8
X-1	45	123	303	196	380	459	10.8
X-2	22	109	296	192	370	453	10.3
Y	24	132	305	190	400	470	12.2
Y-1	95	196	326	210	429	475	13.1
Y-2	58	144	312	197	423	472	12.5
Z	-20	101	294	195	382	458	10.4
Z-1	61	156	318	220	423	462	11.5
Z-2	32	140	303	198	410	460	10.8

T_g glass transition temperature, ^1T_d first decomposition temperature, ^2T_d second decomposition temperature

The DSC curves and data of UV-cured free films can be seen in Figure 4.31 and Table 4.17, respectively. Accordingly, all films showed mainly three different termal transitions (T_g, ^1T_d, and ^2T_d). Due to the existence of soft and hard segments in the oligomer structure, two different decomposition temperatures were recorded. The first one (^{1}Td) was observed in 45-196 °C region and corresponds to the microdomains of the structure. The second one (^{2}Td) refers to the hard segments of urethane/isocyanurate groups in high crosslinking density. The second decomposition temperature (^{2}Td) is related to the hard segment domains formed by the urethane/isocyanurate groups with high crosslinking densities. According to the Figure 4.31.a, increasing NCO:OH ratio in the formulation, caused increase in Tg and decomposition points. Due to the trimerization reaction (Figure 4.28) of excess isocyanate groups, the highest decomposition temperatures (132 °C, 305 °C), and the highest Tg (24 °C) value were all obtained in Y sample. All transitions jumped to the higher temperatures considering the Figure 4.31.b, c, and d, due to the inclusion of reactive diluents to the formulations. Tg of TCDDA (186 °C) is higher than the Tg of TMPTMA (80 °C), because of the cyclic, bulky structure of TCDDA. Thus the highest decomposition temperatures (196 °C, 326 °C) with the highest T_g (95 °C) value were recorded in Y-1 sample which has the highest NCO:OH ratio and TCDDA [17, 180, 185, 186].

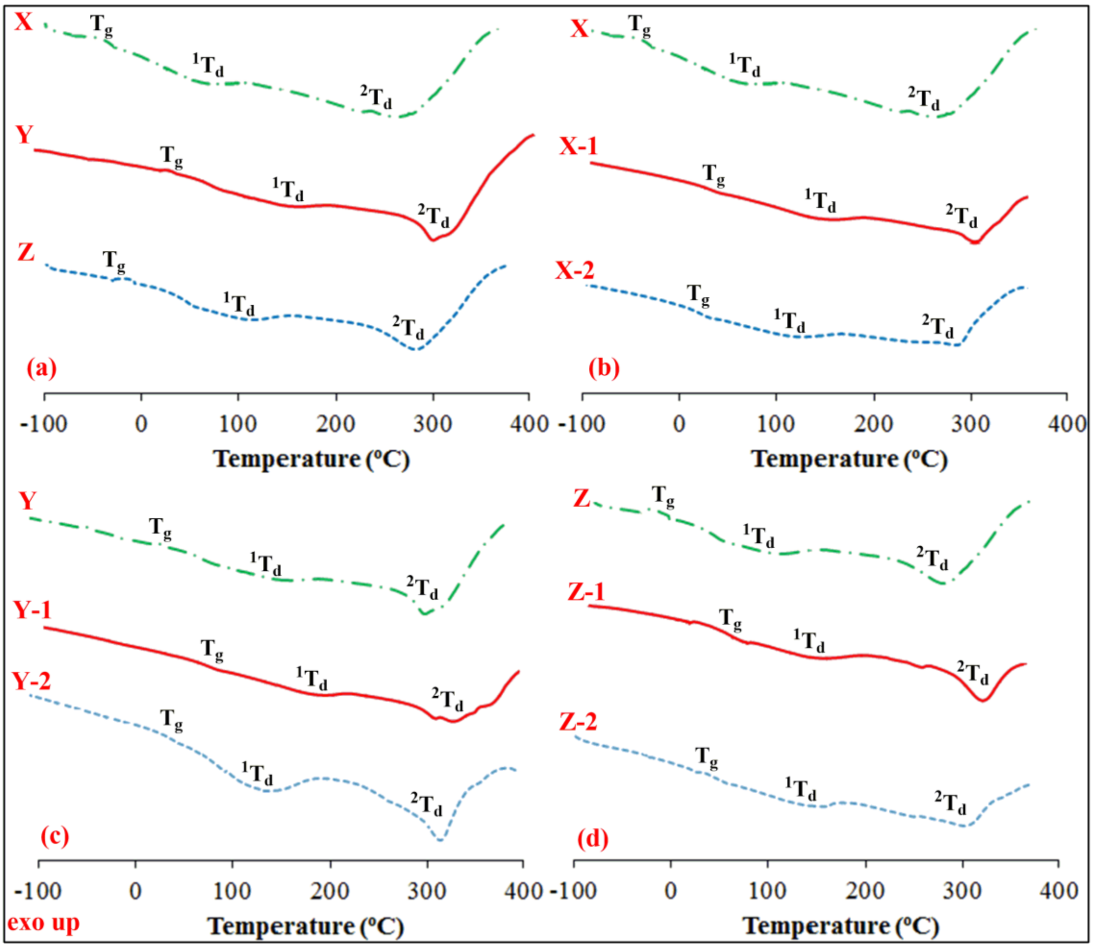

Figure 4.31 : Thermal transitions of UV-cured free films in terms of NCO:OH ratio (a), and the reactive diluent type (b, c, d).

FTIR spectra of untreated cord fabric and the fabrics coated with X, Y, Z formulations and then cured by UV light can be seen in Figure 4.32. The characteristic polyester peaks of C=O stretching at 1732 cm^{-1}, C-C-O asymmetric stretching peak involving the carbon in aromatic unit at 1267 cm^{-1}, O-C-C asymmetric stretching peak of ethylene glycol unit at 1099 cm^{-1}, and C-H bending peak at 722 cm^{-1} were observed in all spectra. The acrylate absorption peaks of C=C at 1635 cm^{-1}, $=CH_2$ at 1450 cm^{-1}, and =CH at 810 cm^{-1} supported the inclusion of HEMA into the structure. The broad peak at 3328 cm^{-1} corresponds to the OH group of unreacted HEMA in Figure 4.28.b. The N-H stretching peak of carbamate ester unit at 1529 cm^{-1} and the C=O stretching vibration peak at 1732 cm^{-1}, which is overlapping with the polyester peak, illustrate the existence of polyurethane acrylates in the oligomer structure [187-189]. The photo-polymerization was also followed by acetone extraction method for 4h in Y-1 coated UV-cured cord fabric. This sample is chosen due to having the highest GF value in the free-film form. Accordingly, weight loss value was found as 0.03% after extraction. Thus, photo-polymerization was completed in 2 minutes UV-light exposure.

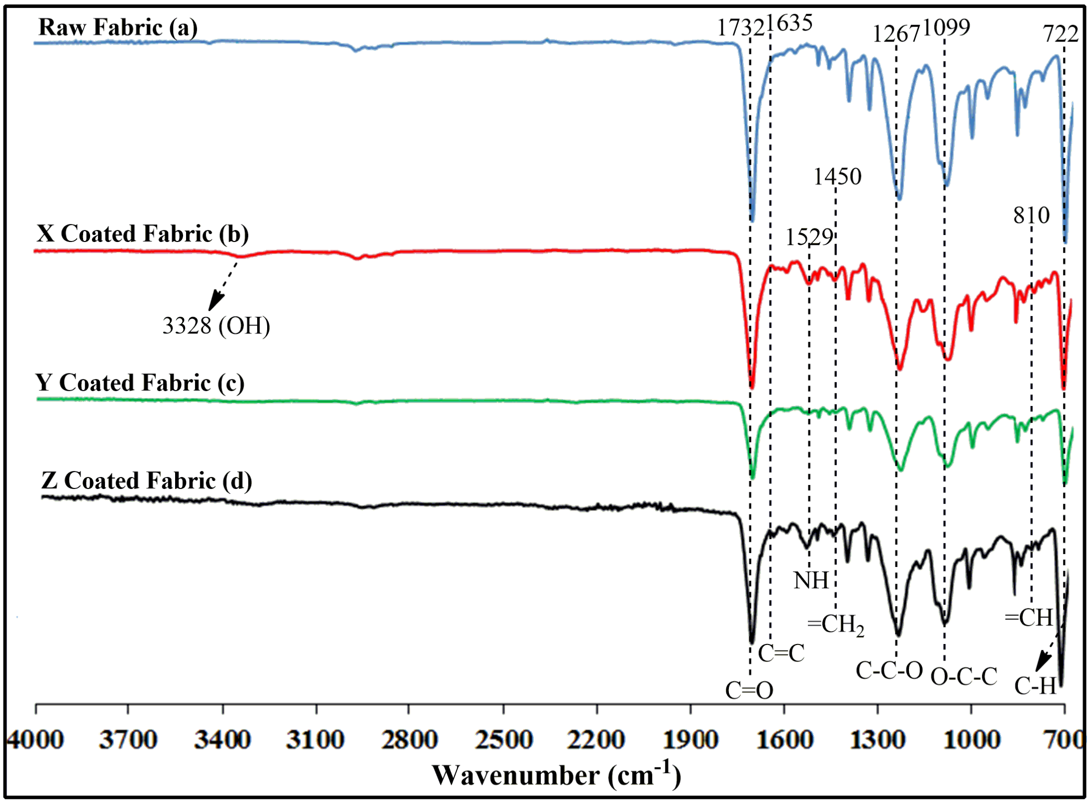

Figure 4.32 : FTIR spectra of untreated and coated UV-cured cord fabrics.

Figure 4.33 shows the contact angle values and the images of water droplets on coated UV-cured cord fabric surfaces. The surface functionality is highly effective on surface energy values. According to the images of X, Y, and Z samples, when the NCO:OH ratio increases, contact angle values decrease thus the wettability character of the fabrics are improved. Surface functionality and the crosslinking density increase with the addition of the reactive diluents to the oligomer structure. Thus surface energies are high and contact angles are low in reactive diluent included samples [190]. The best wettability property with the lowest contact angle value (57.1^{o}) was obtained in Y-1 sample, due to the highest NCO:OH ratio and TCDDA usage in the structure. The bulky and cyclic nature of tricyclodecane units of TCDDA and the side reactions of excess isocyanate increase the surface functionality so improves the surface wettability. Excess isocyanate cause the formation of some side groups (Figure 4.28) such as urea, biuret, allophanate, and urethane groups, which is capable of making hydrogen bonding with water droplets.

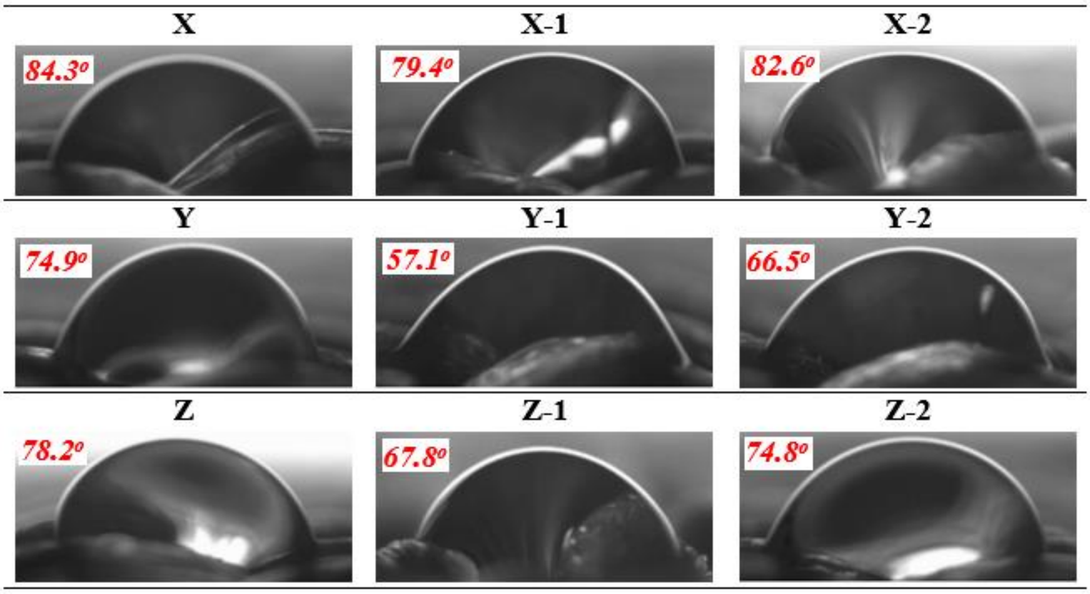

Figure 4.33 : Contact angle values and images of water droplets on coated UV-cured fabric samples.

The T-peel test was performed in cord/rubber composites after thermal curing stage between the coated UV-cured cord fabrics and rubber layers as given in Figure 3.7. The peel strength values between the cord/rubber surfaces can be seen in Figure 4.34. According to the figure, the adhesion strength value increases to 64 N/cm from 34 N/cm with increasing NCO:OH ratio from 1 to 4 when there is no reactive diluent existing in the formulation. Increasing NCO:OH ratio leads to the better adhesion strength values because of the higher crosslinking densities of the structure that is formed by the excess isocyanate groups in the reaction [6]. The acrylate groups in the oligomer structure can be reacted with the double bonds of SBR during the thermal curing stage. The other binding mechanism between cord/rubber surfaces is the strong hydrogen bonding between the carbonyl groups of polyester cord fabric and the NH groups in urea, urethane, allophanate, and biuret units [154]. The adhesion strength value increased up to 103 N/cm with the inclusion of TCDDA to the formulation as reactive diluent, due to the bulky, and cyclic structure of tricyclodecane units [191].

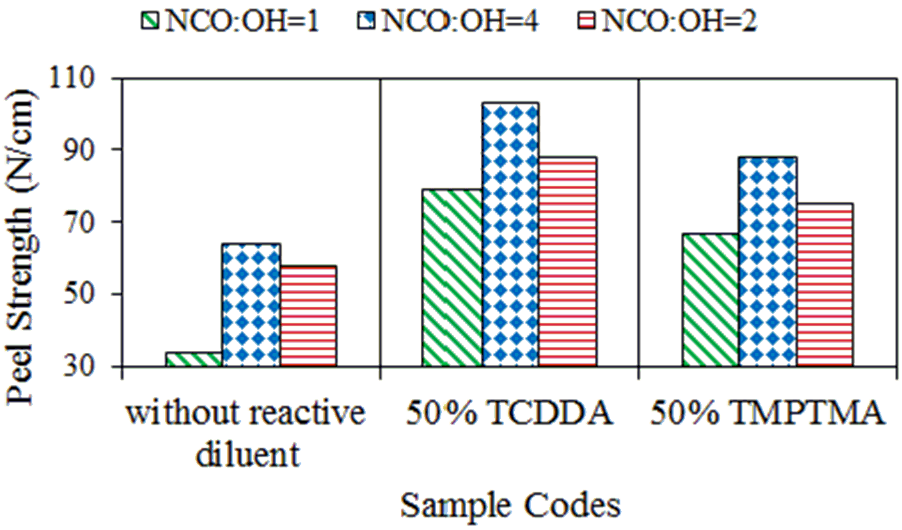

Figure 4.34 : Adhesion strength values for each compositions.

Table 4.18 shows the peel strength value, the optical microscopy images of cord fabrics after T-peel test, and the rubber residue (%) amount in 1 cm^2 fabric region. According to the images, the black regions refer to the rubber residue remained adherent on fiber surface after T-peel test. The amount of the rubber residue (%) on fabric was determined by measuring the weight uptake (%) of dip coated UV-cured cord fabric after peel test. Considering the images, the black regions on fabric surface are greater in Y-1 and Z-1 samples comparing to the other samples due to the usage of TCDDA as reactive diluent in the formulation. The best adhesion strength value of 103 N/cm with the highest rubber residue (40.99 %) were obtained in the sample of Y-1, when the NCO:OH ratio was adjusted to 4. This result can be explained by the side reactions of excess isocyanate groups in the reaction (Figure 4.28) and the cyclic, fused nature of TCDDA. Thus, the crosslinking density and the surface functionality is high in Y-1 sample resulting enhancement in peel strength value.

Table 4.18 : Adhesion strength and the rubber residue values with the fabric images after peel testing.

Sample Code	Peel Strength (N/cm)	Rubber Residue (%)	Light Microscopy Images
X	34	1.42	
X-1	64	9.82	
X-2	58	7.11	
Y	79	14.48	
Y-1	103	40.99	
Y-2	88	27.94	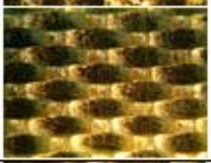
Z	67	10.85	
Z-1	88	29.81	
Z-2	75	11.14	

4.4 Synthesis and Application of PVB Based Adhesive Formulations for Cord/Rubber Applications

In this study, dual-curable formaldehyde-free polyurethane acrylate based adhesive formulations were prepared by using the TDI-HEMA-PVB reaction (Figure 4.35). The adhesive strength between the cord/rubber surfaces were investigated by changing the PVB ratio and the reactive diluent types in the oligomer structure. The dip-coating, UV- and thermal-curing stages can be seen in Figure 4.36. Table 4.19 shows the sample codes with the compositions.

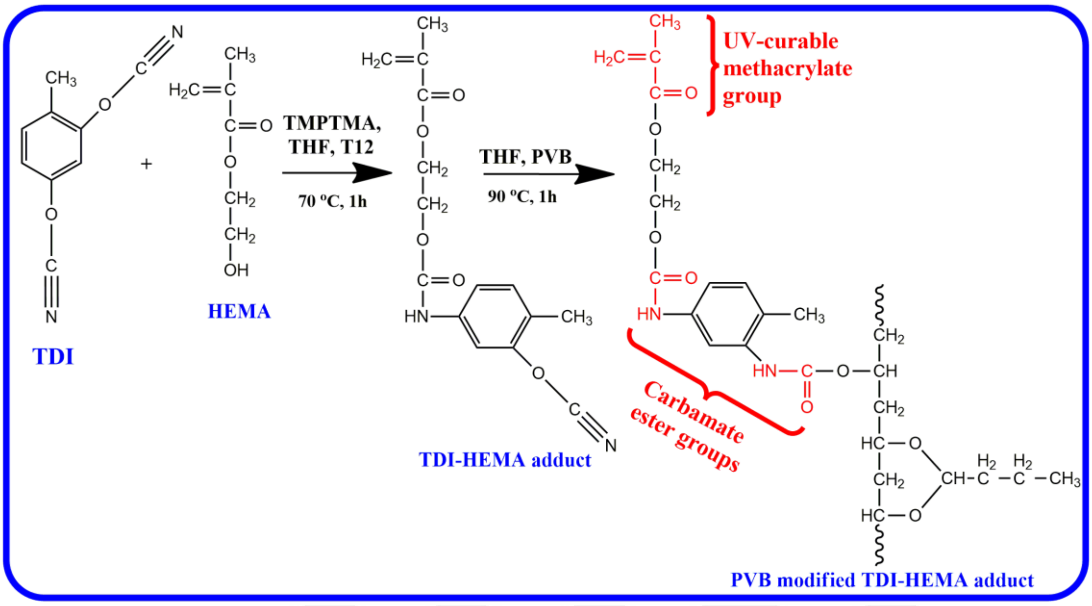

Figure 4.35 : Reaction scheme of the oligomer.

Table 4.19 : Sample compositions in various PVB amounts.

Sample Codes	Sample Compositions
S1	Untreated polyester fabric
S2	TDI-HEMA-PVB (0%) coated fabric
S3	TDI-HEMA-PVB (1%) coated fabric
S4	TDI-HEMA-PVB (3%) coated fabric
S5	TDI-HEMA-PVB (5%) coated fabric

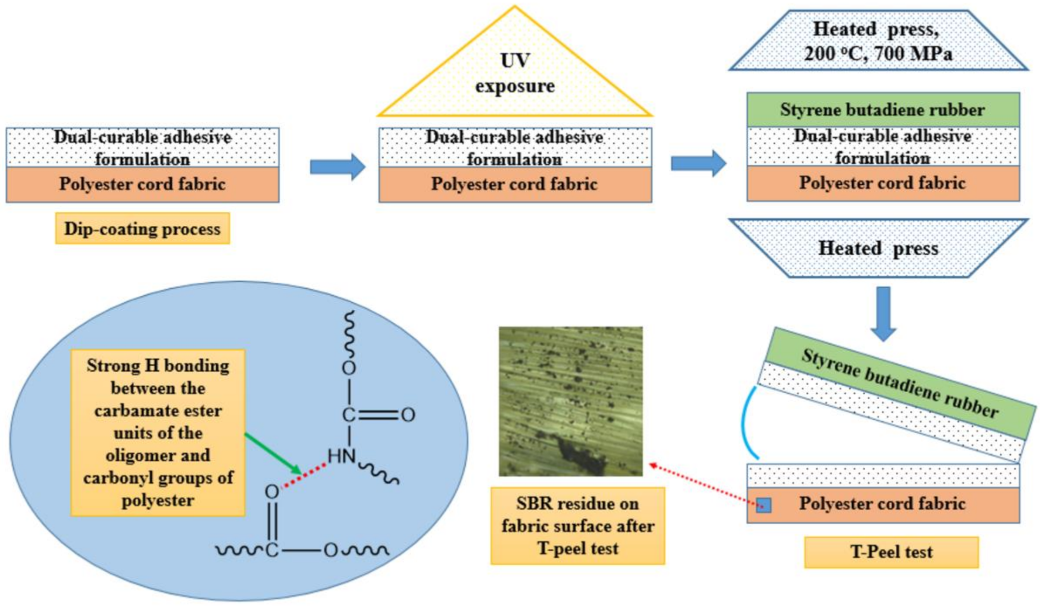

Figure 4.36 : Application, and curing of adhesive formulations, and T-peel test process for cord/rubber composites.

Figure 4.37 shows the ^{1}H NMR spectra of PVB-modified TDI-HEMA adduct. The methacrylic groups of HEMA in the oligomer structure can be observed from the characteristic peaks of (-O-CH_2-CH_2-O) at 4.27-4.39 ppm, (C(CH_3)=CH_2 trans) peak at 5.59-5.60 ppm, and (C(CH_3)=CH_2 cis) peak at 6.10-6.18 ppm. The –CH_3 groups of TDI can be seen at 2.14-2.17 ppm. The inclusion of PVB into the oligomer structure can be proved by the broad peak of –O-CH-CH_2- unit at 3.39-3.87 ppm. The reaction between the hydroxyl and isocyanate groups can be supported by the existence of the carbamate groups (-NH-COO) peak at 4.99 ppm. The phenyl ring proton peaks can be seen at 7.10-7.92 ppm region [89, 187, 192]. The characteristic PVB proton peaks of methyl, methylene, and methine were appeared at 0.95 ppm, 1.2-1.8 ppm, and 3.4-4.1 ppm region, respectively. The peak at 4.4 ppm refers to the dioxymethine (O-CH-O) proton in the acetal vinyl butyral ring in the oligomer structure [193].

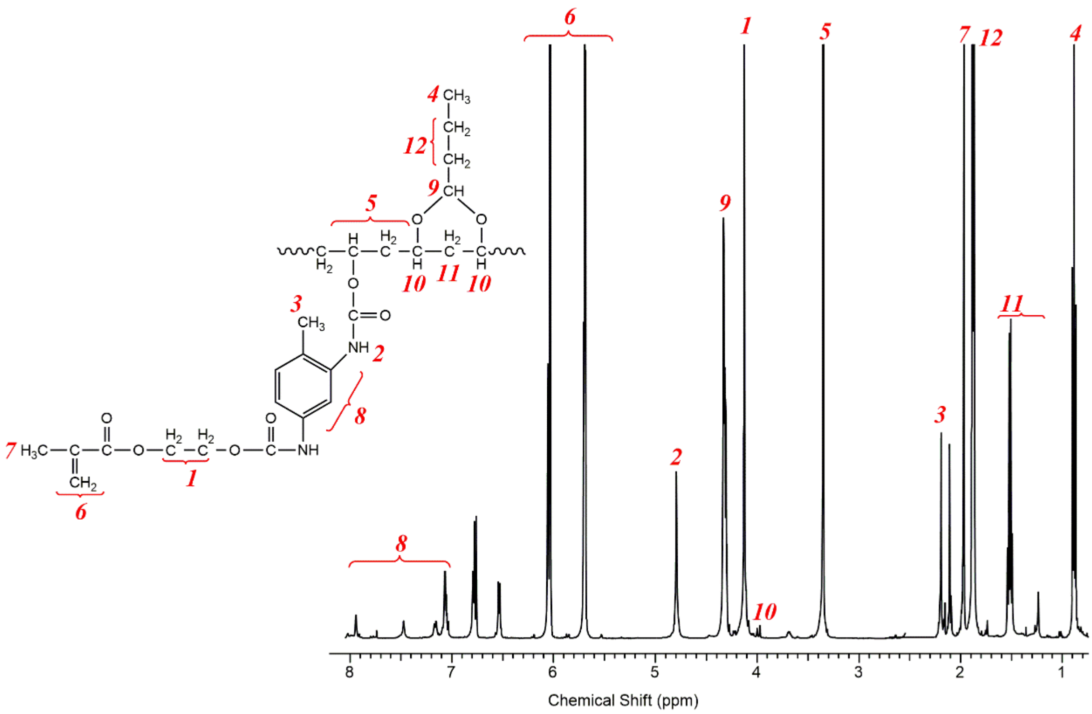

Figure 4.37 : ^{1}H NMR spectra of the sample of S5.

The FTIR spectra of untreated polyester fabric (S1) and S5 formulation applied UV-cured fabric can be seen in Figure 4.38. Considering the FTIR spectra of S5, no unreacted isocyanate group (2270 cm^{-1}) was observed in the reaction. A complete reaction between the isocyanate group and the hydroxyl groups of HEMA and PVB was supported by the existence of N-H stretching peak at 3300 cm^{-1} and N-H bending peaks at 1596 and 1639 cm^{-1}. The methacrylate group inclusion to the structure can be indicated by the peak of C=CH_2 at 812 cm^{-1}. Moreover, the characteristic small PVB peaks of C-O-C in butyral ring unit at 1132 cm^{-1} can be observed [146, 189, 194, 195]. Acetone extraction method was employed to investigate the formation of crosslinked structure of coating layer. Accordingly, the weight loss value on coated UV-cured fabric (S5) after extraction was found as 0.08%. This result confirms the existence of a crosslinked coating layer on fabric surface.

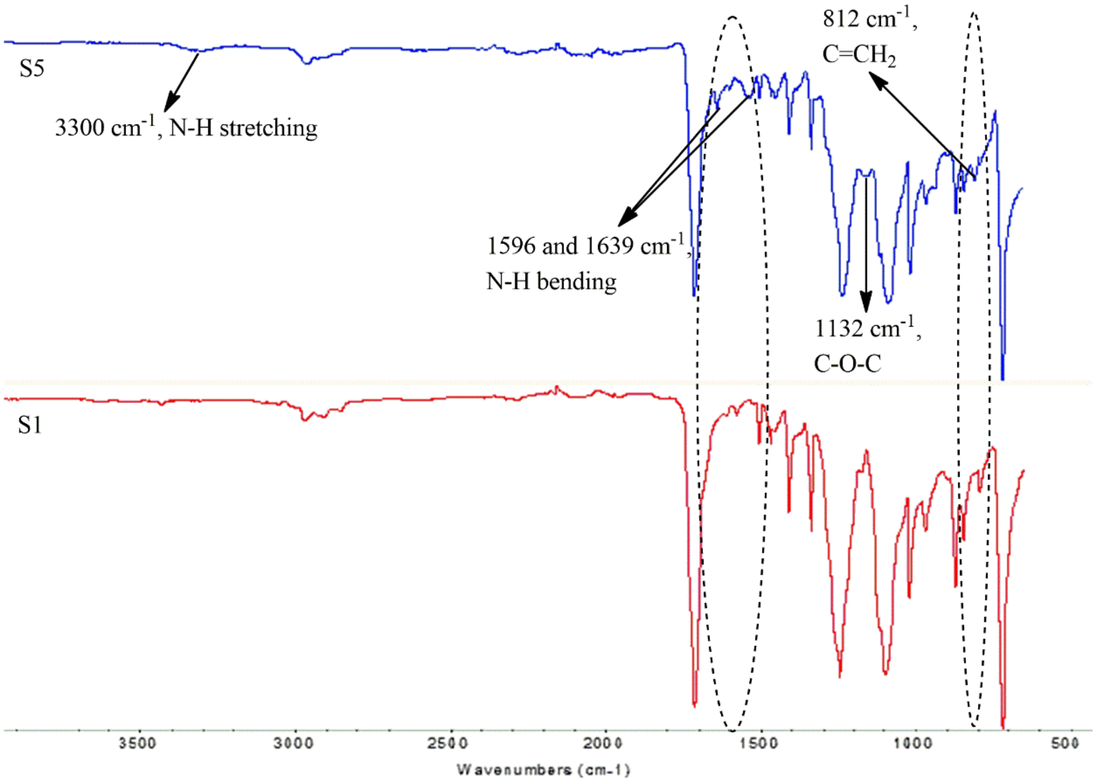

Figure 4.38 : FTIR spectra of the samples S1 and S5.

Figure 4.39 shows the TGA curves of untreated cord fabric (S1) and coated UV-cured cord fabric (S5), respectively. The usage area and performance of a coating material mainly depend on the melting temperature and the decomposition temperature of the material. As can be seen in Figure 4.39, after coating of the fabric, thermal stability decrased due to the lower thermal decomposition temperature of the coating material compared to the polyester cord. Considering the TGA curve of S5, thermal decomposition of the coating layer starts at 300 ^oC with the degradation of pendant groups. It can be observed that above 300 ^oC, PVB in the oligomer structure starts to decompose [196]. In 350-450 ^oC region, the aromatic groups of TDI-HEMA adduct in the oligomer decompose. Above 500 ^oC, the coated UV-cured cord fabric thermally decomposes completely [89]. Regarding to the TGA curve of S1, in untreated cord fabric, no decomposition was recorded till 400 ^oC, whereas in 400-500 ^oC region, a rapid and one-step decomposition was observed. Moreover, decomposition of amorphous structures is easier and faster than crystalline structures because of the chain interactions and intermolecular forces existing in crsytalline region. Thus thermal stability of cord fabric after coating stage decreased due to the amorphous structures of the coating layer [197, 198].

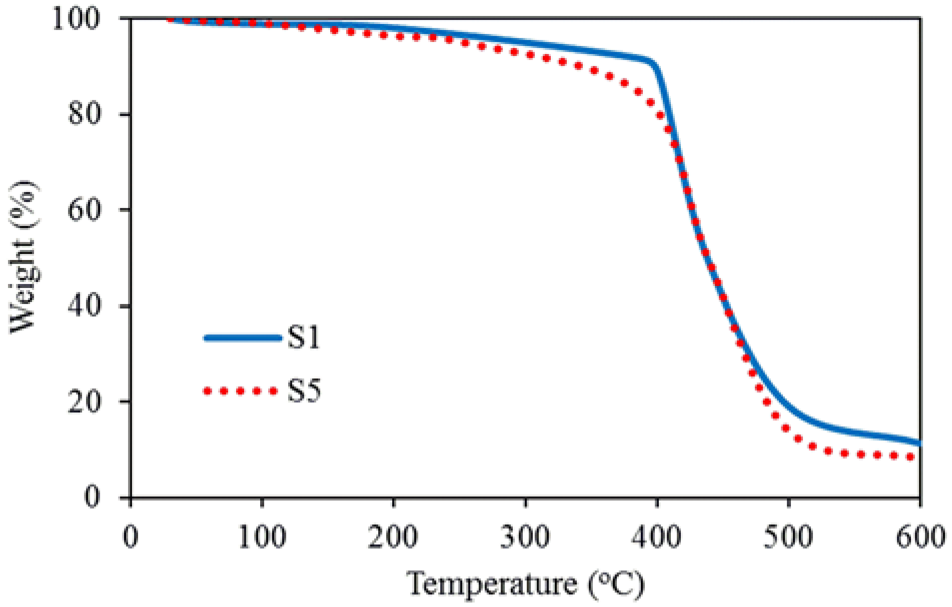

Figure 4.39 : TGA curves of the samples S1 and S5.

The thermogravimetric data of the samples of S1 and S2 were given in Table 4.20. The differences between the cord fabric and coating material in thermal decomposition temperatures and the existence of amorphous structures in coating material, caused decline in thermal stability Thus, thermal decomposition temperatures decrased after the application of PVB modified TDI-HEMA adduct onto the cord fabric surface. The thermal analysis was performed under nitrogen atmosphere, therefore pyrolysis occurs resulting the formation of the carbonization stage with the char yield. The char yield values were recorded as 11 % and 8 % for S1 and S5 samples, respectively.

Table 4.20 : Thermogravimetric data of the samples of S1 and S5.

Sample Codes	Temperature at 5% Weight Loss	Temperature at 50% Weight Loss	Residue at 400 °C (%)	Char Yield (%)
S1	396	438	90	11
S5	252	437	84	8

The DSC curves of the samples of S1 (untreated cord fabric) and S5 (coated UV-cured cord fabric) can be seen in Figure 4.40. Accordingly, melting peak of polyester associated with the crystalline regions at 265 °C with a sharp peak was observed. This peak was shifted to 255 °C after dip-coating and UV-curing processes. This result can be explained by the differences in thermal decomposition temperatures of polyester cord and the coating material. Thermal decomposition temperature of coating layer is lower than polyester cord as can be seen in Table 4.20. Besides, the amorphous coating layer partially diffused onto the crystalline regions of the polyester cord fabric resulting a lower thermal decomposition temperature [154, 197].

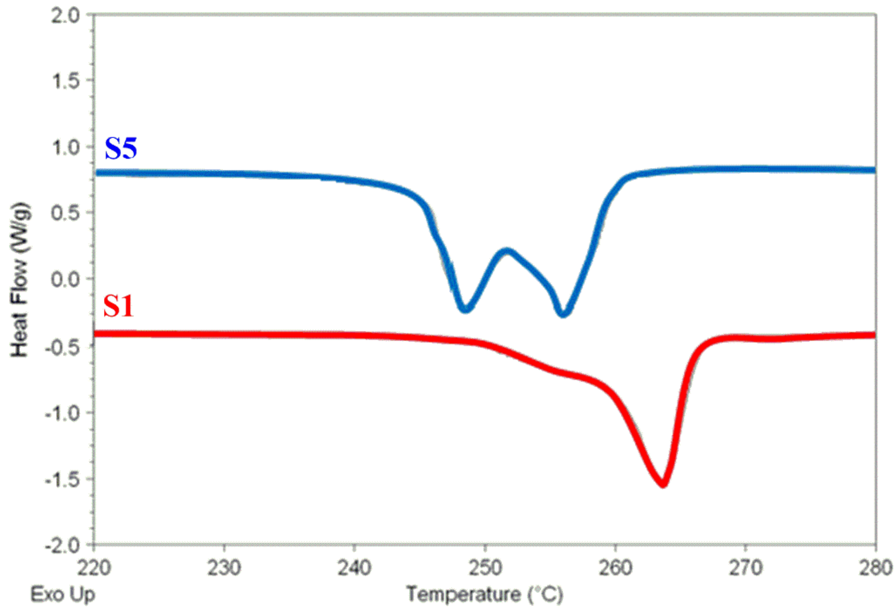

Figure 4.40 : DSC curves of the samples of S1 and S5.

The images of water droplets on coated UV-cured cord fabrics with the contact angle values were illustrated in Figure 4.41. The contact angle measurement cannot be applied on raw cord fabric surface due to the immediate absorption of water droplet. Functionality of a surface affects the wettability property of the surface by liquid [190]. Wettability property of the surfaces can be enhanced with increasing surface functionality. In other words, contact angle value decreases with increasing surface functionality. After the inclusion of PVB into the oligomer structure, surface functionality increase due to the increase of carbamate ester groups so as the urethane linkages in the structure. Additionally the hydroxyl groups of PVB enhance the hydrophilicity of the surface [199, 200]. Polarity of the surface was increased by the unreacted hydroxyl groups of PVB in the oligomer structure, resulting lower contact angle values. Because of having the highest functionality and polarity, the lowest contact angle value (59.8^{o}) was recorded in S5 sample.

Figure 4.41 also shows the adhesion strength values between cord/rubber surfaces. When the untreated cord fabric was adhered onto the rubber surface in a heated press, the adhesion strength value of 12.3 N/cm was observed. The S2 sample was coated by the adhesive formulation without any PVB inclusion. The possible bonding mechanisms between the cord/rubber surfaces are as follows: the unsaturated groups of SBR can be reacted with the methacrylate functionality of the oligomer during thermal curing stage (Figure 4.42). The peel strength values were gradually increased with increasing PVB amount in the oligomer structure. The unreacted hydroxyl groups of PVB within the oligomer increase the surface polarity. Strong H bonding was formed between the carbonyl groups of polyester and the NH groups of carbamate ester groups. Besides, flexibility of the cord/rubber composite increased with PVB functionality resulting higher peel strength values [154]. In the sample of S5, having 5 % PVB inclusion, the best peel strength value of 94.7 N/cm was recorded.

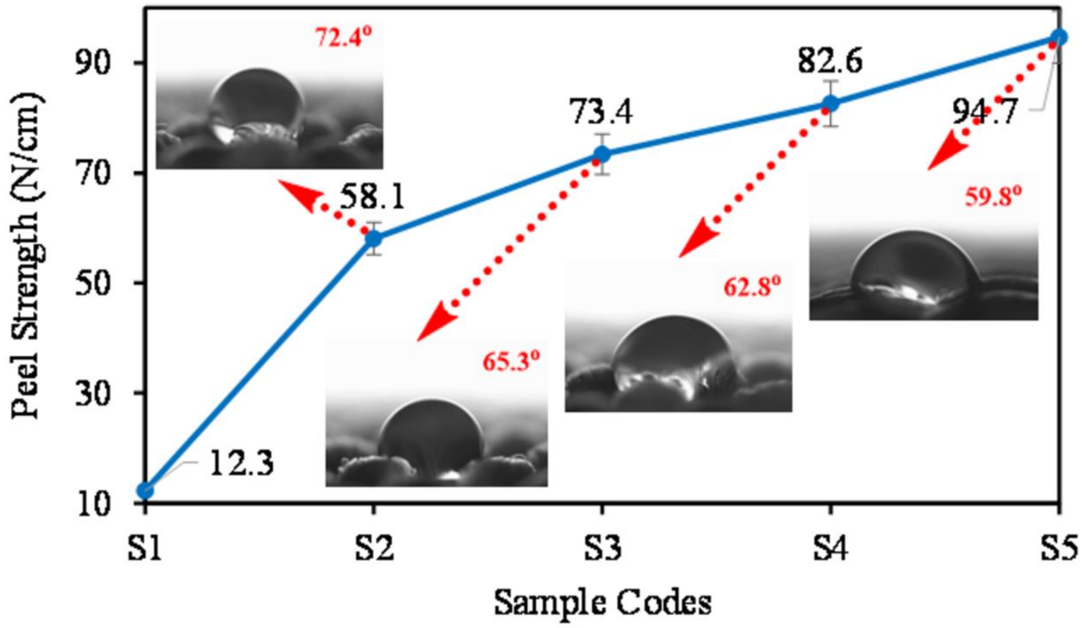

Figure 4.41 : Peel strength values between cord/rubber surfaces, and the images of water droplets with contact angle values on dip-coated UV-cured cord fabrics.

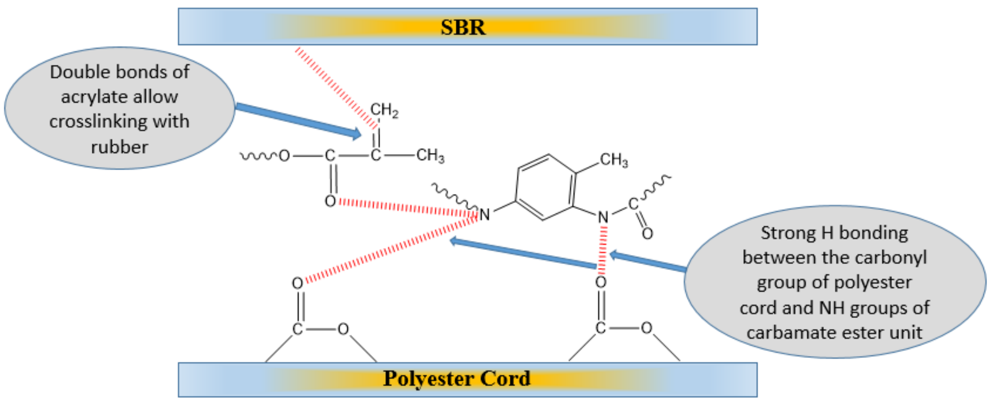

Figure 4.42 : Bonding mechanism between the SBR and polyester layers after coating and thermal curing stages.

Figure 4.43 illustrates the light microscopy images of cord fabrics with their grayscale binary images after peel test. Accordingly, the SBR residue, remained adherent after peel test, is represented by the black regions on the images. This regions are more visible in grayscale binary images. The density of the black regions is much higher in the sample of S5. In other words the cord fabric in S5 sample showed a better resistance against to peel from rubber surface due to the good adhesion, so the best peel strength value was obtained in S5 sample.

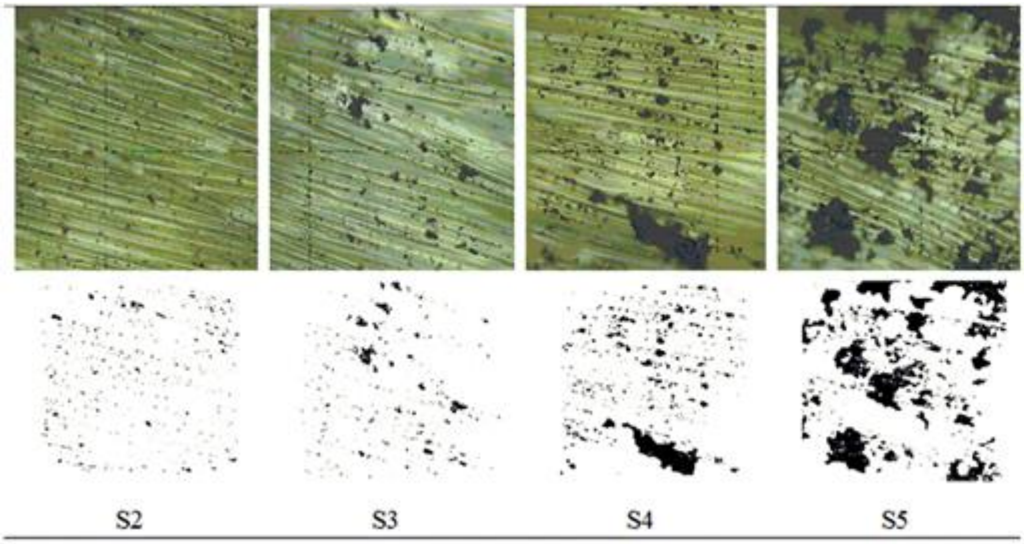

Figure 4.43 : Cord fabric optical microscopy images after peel test.

The peel strength between cord fabrics and rubber surfaces was also investigated in terms of reactive diluent types by using urethane acrylate based oligomers in the adhesive formulation. TMPTMA and TCDDA were chosen as reactive diluent types. The sample codes and compositions were illustrated in Table 4.21. The prepared adhesive formulations were applied on polyester/polyamide cord fabrics by dip-coating and the coating layer on fabric surface was cured by UV-light.

Table 4.21 : Sample codes and compositions.

Oligomer	Reactive Diluent	Sample Codes
	--	S1
	--	S2
PVB Modified TDI-HEMA Adduct	TMPTMA, 50%	S3
	TCDDA, 50%	S4

The completion of photopolymerization was investigated by acetone extraction method on S4 sample for 4h. Accordingly, about 0.06% weight loss was recorded with extraction. The FTIR spectra of raw and dip-coated UV-cured polyamide (weft) and polyester (warp) fibers can be seen in Figure 4.43 and Figure 4.44, respectively. Regarding the Figure 4.44, in all samples, characteristic peaks of polyamide such as

N-H stretching vibration peaks at 3090 and 3298 cm^{-1}, N-H bending peaks at 686 and 1560 cm^{-1}, $-CH_2-$ stretching vibration peak at 2913 cm^{-1}, C=O vibration peak at 1666 cm^{-1}, and -CH- stretching vibration peak at 2850 cm^{-1} were all obsreved. The peaks at 1560-1666 cm^{-1} region are representing the characteristic polyamide peaks of N-H and C=O groups, and are overlapping with the carbonyl peaks of carbamate group in the formulation. No displacement or shift in primary amide peaks was observed. This result supports the idea of that, the interaction between the fabric surface and coating layer was not performed by the primary amide functional groups [201, 202]. After the application of adhesive formulation and UV-curing stage, the urethane acrylate oligomer on fabric surface can be followed by the methacrylate peaks of HEMA ($C=CH_2$) at 812 cm^{-1}, the butyral ring group peak (C-O-C) at 1132 cm^{-1}, and the ester peak (C=O) at 1732 cm^{-1} [146, 189, 194, 195].

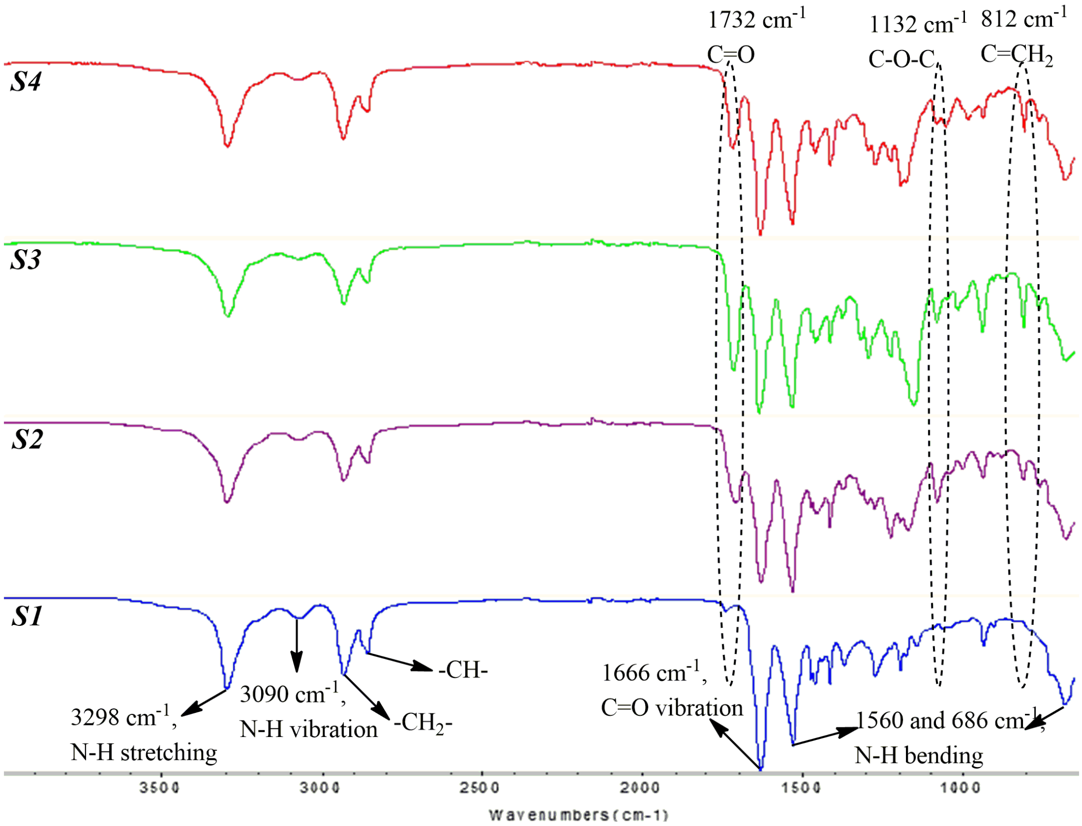

Figure 4.44 : FTIR spectra of untreated (S1) and coated UV-cured (S2, S3, S4) polyamide fibers.

The FTIR spectra of untreated polyester fiber and coated UV-cured polyester fibers were given in Figure 4.45. Accordingly, the characteristic polyester peaks of C=O stretching, C-C-O asymmetric stretching with the carbon of aromatic group, O-C-C asymmetric stretching of ethylene glycol unit, and C-H bending were all observed at

1732 cm^{-1}, 1267 cm^{-1}, 1099 cm^{-1}, and 722 cm^{-1} [188, 203-205]. After the application of adhesive formulations, new peaks were appeared such as the methacrylate groups of HEMA peak ($C=CH_2$) at 812 cm^{-1}, bending and stretching peaks of carbamate ester unit (N-H) at 1560 and 3298 cm^{-1}. Furthermore, the existence of PVB was supported by the stretching vibration peaks ($-CH_2-$, -CH-) at 2913 and 2850 cm^{-1}, and the formation of carbamate group in the oligomer was observed with the peak (C=O) at 1666 cm^{-1}, respectively [146, 189, 194, 195].

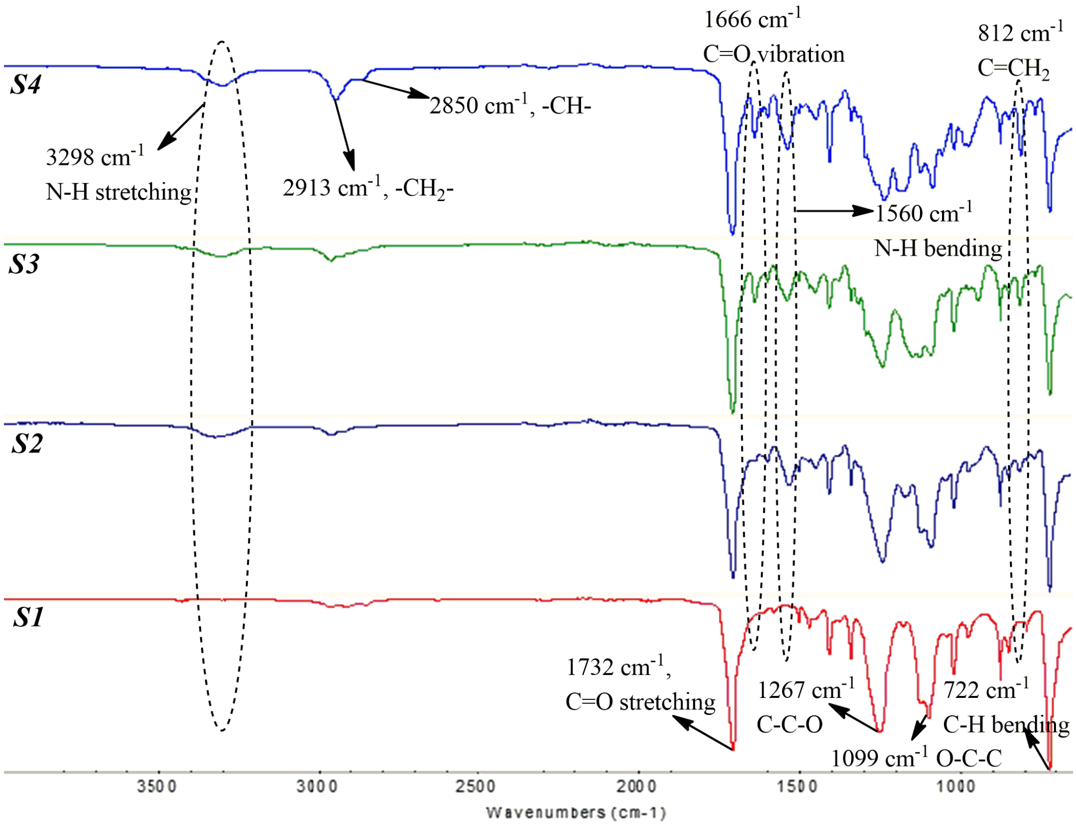

Figure 4.45 : FTIR spectra of untreated (S1) and coated UV-cured (S2, S3, S4) polyester fibers.

The ^{1}H NMR spectra of the urethane acrylate oligomer with and without PVB inclusion can be seen in Figure 4.46. Accordingly, the existence of HEMA in oligomer structure can be followed by the methacrylate group peaks in 1.79-1.83 ppm ($-O-CH_2-CH_2-O$), in 5.61-5.72 ppm ($C(CH_3)=CH_2$ trans), and in 6.10-6.18 ppm ($C(CH_3)=CH_2$ cis) regions. The TDI in the oligomer structure can be observed from the aromatic ring and methyl protons at 7.10-7.92 ppm and 2.14-2.17 ppm, respectively. The reaction between the hydroxyl and isocyanate group can be supported by the carbamate group peak (-NH-COO) at 4.83 ppm. After the inclusion of PVB to the reaction, the intensity of the carbamate peak increased. Additionally, the methyl group peak at 0.87 ppm, the methylene group peaks at 1.25-1.75 and 2.21 ppm, -O-CH-CH_2 peak at 3.32-3.71 ppm, and O-CH-O dioxymethine proton peak at 4.4 ppm were all supported the existence of PVB [89, 187, 192, 193]. The peaks at 6.51 and 6.78 ppm correspond to the aryl-alkylalkyl urea that is formed by the side reactions of secondary amine functional groups with urethane linkages [206].

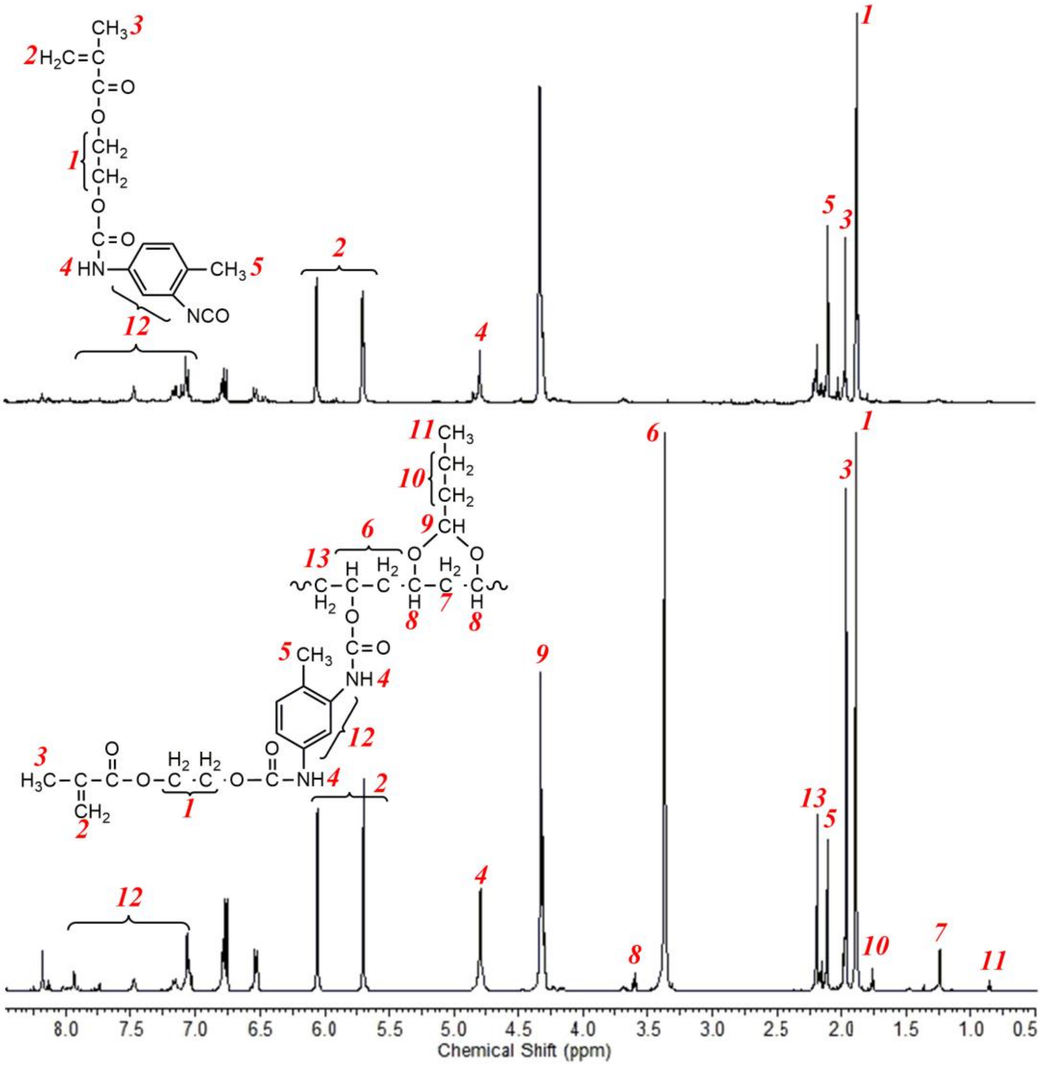

Figure 4.46 : ^{1}H NMR spectra of polyurethane methacrylate oligomer before and after PVB inclusion.

The TGA curves and the thermogravimetric data of UV-cured free films can be seen in Figure 4.47 and Table 4.22, respectively. No remarkable decomposition was observed up to 200 ^{o}C in all samples. The decomposition of urethane linkage to its structural (isocyanate and alcohol) units starts at 200 ^{o}C [207]. The aromatic structure in TDI-HEMA unit starts to decompose in the range of 350-450 ^{o}C. Thermal decomposition is completed at around 500 ^{o}C in all films. After the inclusion of reactive diluents to the formulations, as in S3 and S4, thermal stability increased.

Additionally, reactive diluent inclusion caused to formation of more thermally stable materials. More than half of the films remain stable till 400 ^{o}C. The cycloaliphatic and bulky nature of TCDDA inhibits the molecular movements comparing to the TMPTMA, thus the thermal stability increase is much greater in S4 than S3 [184]. Due to performing the thermal analysis under nitrogen atmosphere, carbonization occurs and pyrolysis with char yield is observed.

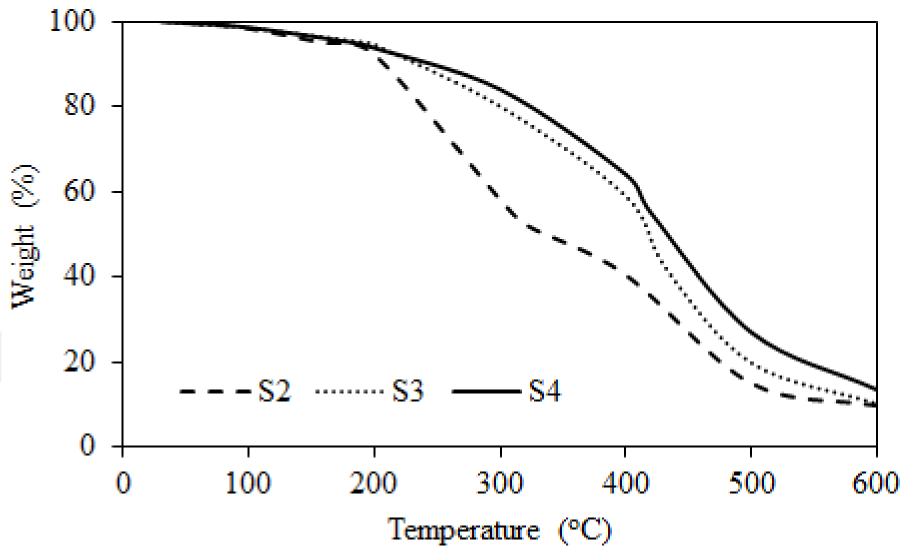

Figure 4.47 : TGA curves of UV-cured free films.

Table 4.22 : Thermogravimetric data of UV-cured free films.

Sample Codes	**Temperature at 5% Weight Loss**	**Temperature at 50% Weight Loss**	**Residue at 400 °C (%)**	**Char Yield (%)**
S2	157	339	40	9.7
S3	182	423	59	10.4
S4	191	445	64	13.5

The DSC curves of UV-cured free films can be seen in Figure 4.48. Accordingly, the glass transition temperature (T_g) of the polyurethane methacrylate oligomer was found as 65 ^{o}C. After the reactive diluent inclusion to the formulations, the glass transition temperaures were shifted to 82 ^{o}C and 175 ^{o}C for the sample of S3 and S4, respectively. This result is stemming from the higher glass transition values of reactive diluents by themselves (TCDDA, around 186 ^{o}C and TMPTMA, around 80 ^{o}C). The T_g of TCDDA is greater than the T_g of TMPTMA due to the bulky and cycloaliphatic groups in TCDDA resulting in a higher crosslinking density. The mentioned cyclic structure leads to a small free volume in polymer matrix by decreasing the oxygen diffusion inside the polymer resulting increase in thermal stability with higher glass transition temperatures as in S4 sample [208].

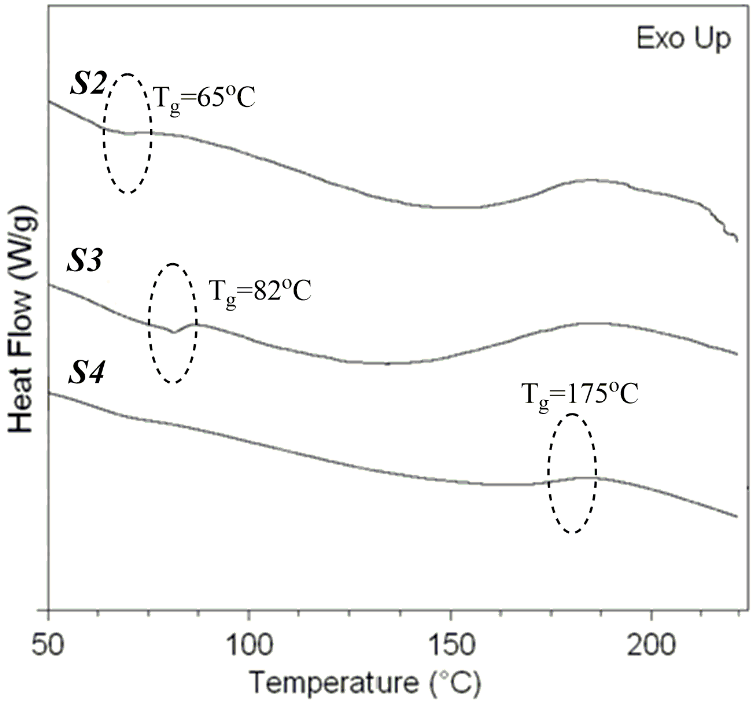

Figure 4.48 : DSC curves of UV-cured free films.

Figure 4.49 shows the contact angle values and the water droplet images on coated UV-cured cord fabric surfaces for each formulation. Surface energy increases with increasing crosslinking density so increasing functionality. It means that contact angle values decrease with increasing surface functionality [190]. The image of the water droplet on untreated fabric (S1) cannot be captured due to the immediate absorption of the water droplet by the surface. According to the images, the lowest contact angle value (70.2^{o}) was observed in S4 sample due to the higher functionality with a higher crosslinking density of TCDDA caused by the tricyclodecane unit, resulting a hydrophilic character on the surface.

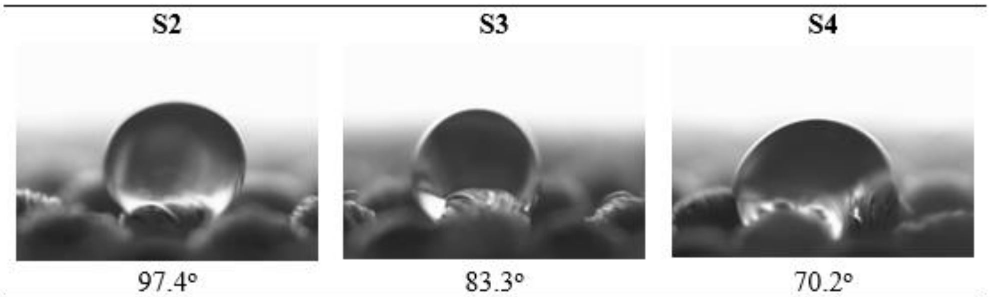

Figure 4.49 : Contact angle values and images of water droplets on coated UV-cured fabric surfaces.

Figure 4.50 illustrates the T-peel test values between polyester/polyamide cord fabrics and rubber surfaces. The adhesion strength value of 24.1 N/cm was obtained when the rubber and raw fabric were adhered together by heated press. When the urethane methacrylate oligomer was included in adhesive formulation without PVB inclusion (S2), the peel strength value was recorded as 47.3 N/cm. So the formulation in S2 sample doubles the peel strength results comparing to the untreated (S1) sample. The possible bonding mechanism between the cord and rubber layers can be occured between the unsaturated groups of SBR and the arylate groups of the oligomer during the thermal curing stage [154]. Another bonding mechanism can be observed between the carbonyl groups of polyester cord fabric and the NH groups of carbamate ester units in the oligomer. Moreover, the NH groups of polyamide fabric can be bonded with the carbonyl groups in the oligomer structure via hydrogen bonding mechanism. In the sample of S3 and S4, due to the inclusion of reactive diluents to the formulation, adhesion strength values increased. It can be seen that reactive diluents act as adhesion promoters by increasing the bonding mechanism between cord/rubber surfaces. In the sample of S4, having TCDDA as reactive diluent, showed the best adhesion strength value of 100.4 N/cm. This result can be explained by the cyclic, fused-ring structure of TCDDA which improves the bonding properties of the surfaces [191].

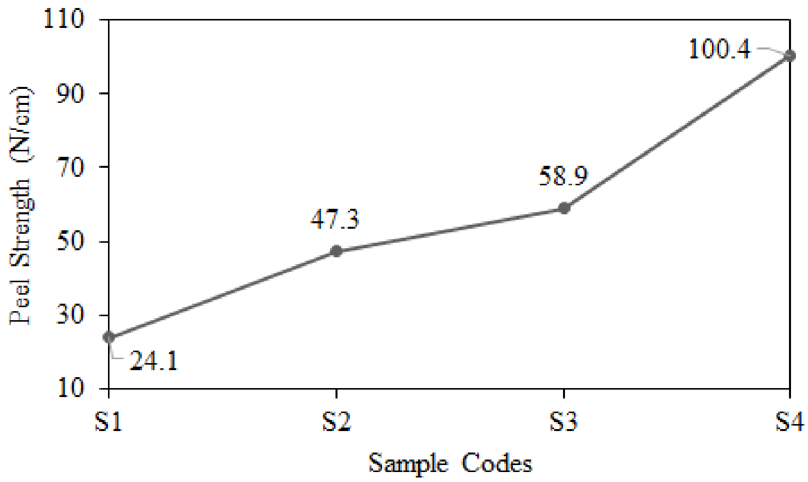

Figure 4.50 : Peel strength values of polyester/polyamide cord fabric-rubber composites.

Figure 4.51 shows the polyester/polyamide fabric surfaces after T-peel test. According to the images, the black regions correspond to the SBR which remains adherent on the surface in other words resists peeling from the fiber surface after T-peel test. Whenever peel strength increases, the black regions on fabric surface also increases. It is obvious that the sample of S4 has the highest rubber residue due to having the highest peel strength value.

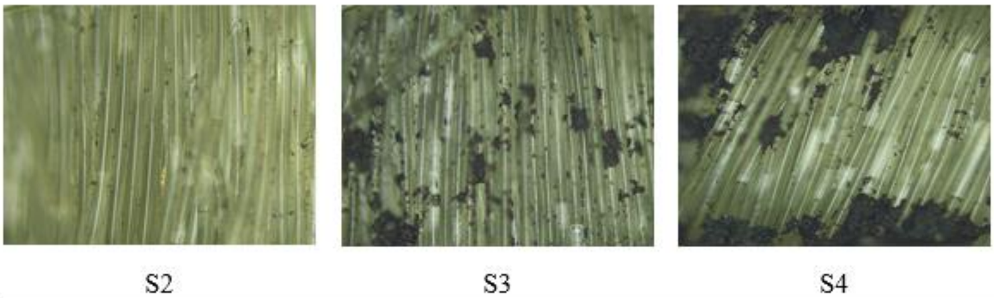

Figure 4.51 : Polyester/polyamide cord fabric images after peel testing.

Adhesive formulations were also prepared by using 5 % PVB modified TDI-HEMA adduct and different types of acrylate based reactive diluents. The effects of reactive diluent combination (TCDDA/TMPTMA) on the adhesion strength between cord/rubber surfaces were investigated. Table 4.23 shows the sample codes and the reactive diluent compositions.

Table 4.23 : Sample codes with reactive diluent compositions.

Sample Codes	Reactive Diluent Compositions (TCDDA/TMPTMA)
S1	--
S2	0/100
S3	25/75
S4	40/60
S5	50/50
S6	60/40
S7	75/25
S8	100/0

Table 4.24 illustrates the GF (%), DS (%), and weight loss (%) againist chemical exposure values for each free film sample. GF (%) value is attributed to high crosslinking densities whereas weight loss (%) with chemical exposure and DS (%) values decrease with increasing crosslinking density. Accordingly, the lowest GF (%) value with the highest DS (%) and weight loss (%) with chemical exposure were all observed in the sample of S1. After the inclusion of reactive diluents to the formulation GF (%) value increased, DS (%) and weight loss (%) value in chemical solutions decreased. This result can be explained by the increase in crosslinking desity with reactive diluent inclusion. The lowest DS (%) and weight loss (%) values after chemical exposure were observed in the sample of S8 with TCDDA inclusion. Due to

the cyclic and bulky nature of tricyclodecane units in TCDDA the crosslinking density increase is higher comparing to the TMPTMA. Whenever TCDDA ratio increases in the formulation crosslinking density increases resulting higher GF (%) value and lower DS (%), weight loss (%) values in chemical solutions.

Table 4.24 : Physicochemical characteristics of UV-cured free films for each reactive diluent compositions.

Sample Codes	**DS (%)**			**GF (%)**	**Chemical Resistance Weight Loss (%)**	
	Toluene	**Ethanol**	**Water**		**NaOH (10%)**	**HCl (10%)**
S1	10.79	20.79	18.09	82.37	3.05	13.04
S2	4.11	3.76	1.18	89.66	1.71	1.06
S3	5.18	5.26	1.98	86.79	1.83	3.95
S4	5.97	6.53	1.99	85.42	1.87	4.21
S5	7.99	6.73	9.35	85.55	2.11	7.69
S6	5.65	4.31	1.42	88.72	1.73	3.53
S7	1.55	2.61	0.31	92.34	1.41	0.69
S8	1.48	2.09	0.23	99.41	1.39	0.39

Figure 4.52 shows the water droplet images with contact angle values on coated UV-cured cord fabrics in various reactive diluent compositions. Images proved that, increase in surface functionality leads to higher surface energy values, thus wettability character of the surface was enhanced with reactive diluent inclusion. So the contact angle values decreased after the inclusion of reactive diluents. The lowest contact angle value (66.2^o) with the highest wettability property was observed in the sample of S8 when TCDDA was used as reactive diluent. The contact angle values decrase with increasing TCDDA ratio in the formulation. TCDDA leads to higher surface functionality compared to the TMPTMA, due to the cyclic, bulky character of tricyclodecane units in the formulation.

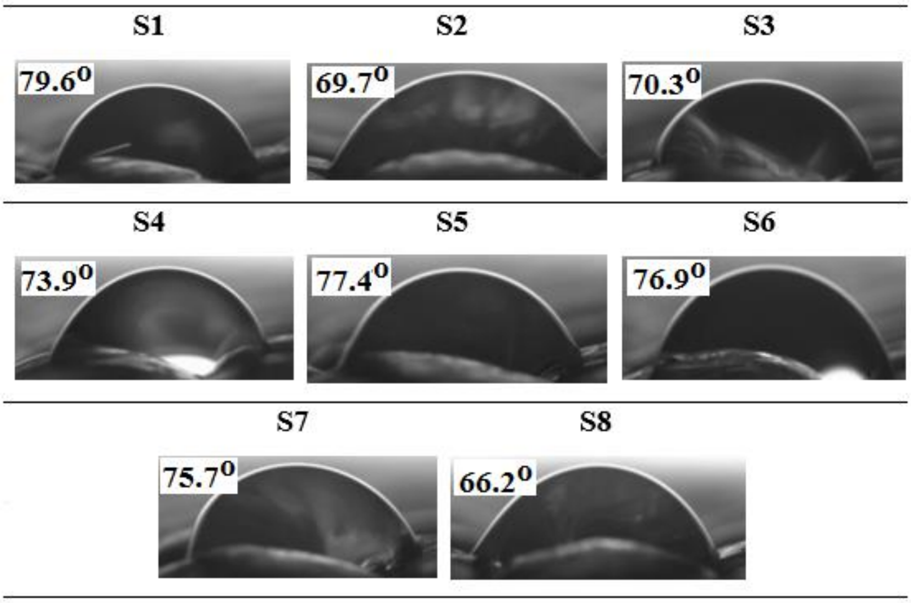

Figure 4.52 : Contact angle values and water droplet images on coated UV-cured cord fabrics in various reactive diluent compositions.

Figure 4.53 shows the adhesion strength values between the coated UV-cured cord fabric and rubber surfaces by means of reactive diluent compositions. The images were captured from the fabric surfaces after T-peel test in order to show the rubber residue remained adherent on fibers. The black resgions belong to the adherent rubber residue. Accordingly, when there is no reactive diluent exist in the formulation, the adhesion strength was recorded as 65.1 N/cm. After the inclusion of reactive diluents to the formulation the adhesion strength values were all enhanced. The adhesion strength value increased with increasing TCDDA ratio in the formulation. The highest adhesion strength value of 111.6 N/cm was obtained in the sample of S8 with TCDDA usage as reactive diluent. Considering the fabric images, the black regions are greater in the sample of S8 due to the highest peel strength value. The contribution of TCDDA to the adhesion work is greater than TMPTMA because of the cyclic bulky pendant groups of tricyclodecane units in the formulation.

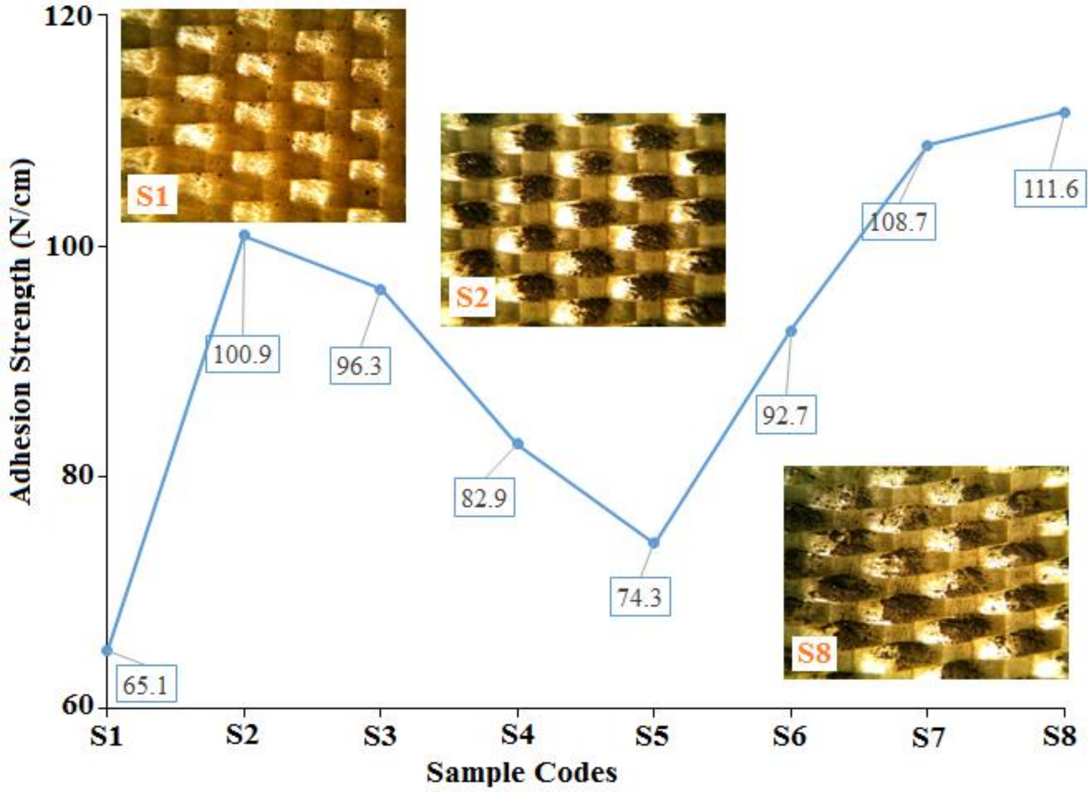

Figure 4.53 : Adhesion strength values between cord/rubber surfaces with the cord fabric images after peel test.

Table 4.25 shows the mechanical properties of the UV-cured free films for various adhesive formulations. Considering the EA adhesive formulations, tensile strength and modulus increase with increasing acrylate functionality. Acrylate functional groups are responsible for the flexibility of the films resulting increase in elongation at break value. Furthermore, hardness of the films also increases because the acrylate groups increase the crosslinking density of the structure.

VPA inclusion to the EA coating formulations caused the formation of polarized functional groups in the structure resulting in higher crosslinking densities. Thus tensile strength, modulus, and hardness values all increase with increasing VPA amount in the formulation. A slightly increase was observed in elongation at break value due to the increase of the flexibility of the structure with hydroxyl groups of VPA.

Regarding the reactive diluent combinations in polyurethane methacrylate based adhesive formulations, tensile strength, modulus, and hardness values all increased with reactive diluent inclusion due to the increase in crosslinking densitiy. The increase in elongation at break value is lower in S8 sample compared to the S2 sample.

This result can be explained by the bulky, cyclic nature of TCDDA that restricts the mobility of the chains resulting decrease in flexibility.

Table 4.25 : Mechanical properties of the UV-cured free films.

Sample Codes	Tensile Strength (MPa)	Elongation at Break (%)	Young Modulus (MPa)	Shore D Hardness
EA 25	164	0.9	3116	54
EA 50	189	1.9	3437	59
EA 75	202	2.7	3602	65
EA 100	226	3.4	3819	69
EA+2.5 % VPA	115	1.2	4213	49
EA+5 % VPA	133	1.4	4228	52
EA+7.5 % VPA	159	1.6	4278	68
EA+10 % VPA	182	1.7	4346	70
S1	58	1.5	1056	49
S2	92	2.3	1792	60
S3	88	2.2	1652	64
S4	84	2.0	1413	61
S5	82	1.9	1303	62
S6	89	1.9	1610	64
S7	96	1.8	1744	65
S8	104	1.5	1813	70

5. CONCLUSION

The presented thesis work includes synthesis, characterization, and application of three different types of formaldehyde-free dual-curable adhesive formulations. In the first part, bisphenol-A based epoxy was reacted with AA in various molar ratios. The obtained EA oligomers were characterized by FTIR and ^{1}H NMR analysis in order to observe formation/diasappearance of some chemical units in the oligomer structure. Adhesive formulations were prepared by EA oligomers and applied on polyester/polyamide cord fabric by dip-coating. The oligomer on fabric surface was cured by UV. FTIR spectroscopy was also used to observe the completion of the photopolymerization. Thermal properties of dip-coated UV-cured cord fabrics were investigated by TGA and DSC analysis. Due to the increase in carbon amount, thermal stability of the cord fabrics increased after coating stage. The melting temperature of the coated fabric is lower than the melting temperature of the untreated fabric because the coating layer provided an amorphous structure onto the fabric thus decreases the melting temperature. The smoothness of the coating layer on single fiber surface was observed by SEM. Accordingly, the oligomer covered the fiber surface completely without any agglomeration. Contact angle test form the coated UV-cured fabric surfaces illustrated that the increasing AA amount in the oligomer structure increases the contact angle values so increases the hydrophobic behavior, due to the hydrogen bonding between the OH groups of the acid and the oxygen atom of the polyester cord fabric. The coated UV-cured fabrics were put between two SBR layers and thermally cured in a heated-press. After thermal curing stage, peel test was applied on cord/rubber composites in order to evaluate the adhesion property of the formulations. The effects of the carboxyl/epoxide ratio of the oligomer structure on adhesion strength between cord/rubber surfaces were searched. The best adhesion strength value of 18.0 N/cm was recorded when the carboxyl/epoxide ratio was set as 1. Due to the highest acrylate functionality in the formulation, more connection points between cord/rubber surfaces were obtained via the double bonds of SBR and acrylate groups of the oligomer during the thermal curing stage. In order to increase the adhesion strength, VPA was included into the adhesive formulations in various percentages. Results proved that, VPA acts as adhesion promoter and better peel test values were obtained with flame resistant property due to the inherent flame-resist behavior of phosphorous in VPA. The existence of phosphorous in the structure also caused increase in thermal stability and char yield values. Non-ionic washing and alkali treatment were applied on cord fabrics prior to the dip-coating stage in order to get a more hydrophilic and functionalized fabric surfaces. The best adhesion strength value of 50.8 N/cm was observed in the sample including 10 % VPA.

In the second part of the thesis, bio-based oligomers were synthesized by using TO as bio-source due to the high unsaturation degree compared to the other vegetable oils. TO was epoxidized first, and then reacted with AA and VPA. The obtained oligomers were characterized by FTIR, ^{1}H NMR, and thermal analysis. Adhesive formulations were prepared by using various percentages of AETO and VPAMETO with PUA resin, and then applied on cord fabrics via dip-coating. Contact angle measurement was performed on coated UV-cured cord fabrics. Hydrophilicity of the surface increased with increasing AETO and VPAMETO amount in the formulation due to the inclusion of hydroxyl groups of the acids to the structure. Epoxidation reaction caused increase in thermo-oxidative stability due to the existence of epoxide groups in the oligomer. The peel strength was measured after thermal curing stage between cord/rubber surfaces. The highest peel strength values of 26.0 N/cm and 20.5 N/cm were obtained with the inclusion of 50 % AETO and 75 % VPAMETO oligomers to the formulations.

In the third part of the thesis, polyurethane methacrylate based oligomers were synthesized by the reaction of TDI and HEMA in various NCO:OH molar ratio. In order to increase the functionality of the oligomer, the obtained TDI-HEMA adduct was also reacted with PVB in various percentages. Oligomers were characterized by FTIR, ^{1}H NMR, and thermal analysis, respectively. Thermal analysis showed that thermal stability and melting temperature of coated UV-cured cord fabrics decreased compared to the untreated fabric due to the inclusion of amorphous regions into the fabric structure. Adhesive formulations were prepared by using the obtained oligomers and reactive diluents (TMPTMA and TCDDA), then applied on cord fabrics by dip-coating. Surface wettability of the coated UV-cured cord fabrics were investigated by contact angle measurement. After thermal curing stage between two SBR layers, the peel test was applied in order to investigate the adhesion properties of the formulations.

The effects of NCO:OH molar ratio, PVB percentage, and the reactive diluent type on adhesion strength were searched. Results showed that adhesion strength increased with increasing PVB amount in the formulation. PVB gives strong binding ability and acts as adhesion promoter. The highest adhesion strength value of 94.7 N/cm was recorded in 5 % PVB added formulation. Considering the reactive diluent type in the formulation, the bulky and cycloaliphatic character of TCDDA gives higher thermal stability, higher rigidity, with a better adhesion property compared to the TMPTMA. Thus, the highest adhesion strength value of 100.4 N/cm was obtained when TCDDA was used as reactive diluent. Regarding the NCO:OH molar ratio in the formulation, when the NCO:OH ratio increased, thermal stability, gel fraction, glass transition and melting temperatures, adhesion strength were all increased whereas swelling degree and weight loss with chemical exposure decreased. This result can be explained by the excess isocyanate groups in the formulation resulting in trimerization reactions, and formation of intermolecular hydrogen bondings, giving a three-dimensional highly crosslinked network. The highest adhesion strength value of 103 N/cm was recorded when the NCO:OH molar ratio was set as 4. The adhesion strength was also investigated by means of reactive diluent combinations. TCDDA and TMPTMA were used as reactive diluents in various percentages. Results proved that adhesion strength value increased with increasing TCDDA ratio in the formulation. The contribution of TCDDA to the adhesion strength is greater than TMPTMA due to the higher functionality with the cycloaliphatic units of TCDDA. The highest adhesion strength value of 111.6 N/cm was recorded in the sample having only TCDDA as reactive diluent.

It can be concluded that adhesive formulations can be prepared without using vinyl pyridine latex and formaldehyde resin. In this thesis work, it was aimed to observe the effects of both high modulus EA and low modulus PUA oligomers on the adhesion between cord/rubber surfaces. Due to the high unsaturation ratio, which allows more crosslinking sites in the molecule, TO was chosen as bio source to design a bio-based oligomer. In conclusion, adhesive formulations were all prepared by using the synthesized oligomers with various modifications, and different types of reactive diluents in various combinations, consequently the adhesion strength between cord/rubber surfaces successfully increased up to 111.6 N/cm from 18 N/cm. Regarding the conventional RFL dipping process, the adhesion strength between cord/rubber layers, can be varied in the range of 3-290 N according to the type of the cord fabric (aramid, polyester, polyamide etc.), structural properties of the cord fabric (thickness, weight, yarn count etc.), type of the peel test (T-peel test, H-pull test etc.), type of the rubber (SBR, ethylene methyl acrylic, silicon, natural rubber, ethylene-propylene-diene, nitrile etc.). Thus, the obtained adhesion strength results in this thesis are promising for the usage in industrially scale.

REFERENCES

[1] **Jamshidi, M., Afshar, F., Mohammadi, N., and Pourmahdian, S.** (2005). Study on cord/rubber interface at elevated temperatures by H-pull test method, *Applied Surface* Science, *249*, pp. 208-215.

[2] **Shi, X., Ma, M., Lian, C., and Zhu, D.** (2013). Investigation on effects of dynamic fatigue frequency, temperature and number of cycles on the adhesion of rubber to steel cord by a new testing technique, *Polymer Testing, 32*, pp. 1145-1153.

[3] **Phetphaisit, C. W., Bumee, R., Namahoot, J., Ruamcharoen, J., and Ruamcharoen, P.** (2013). Polyurethane polyester elastomer: Innovative environmental friendly wood adhesive from modified PETs and hydroxyl liquid natural rubber polyols, *International Journal of Adhesion and Adhesives, 41*, pp. 127-131.

[4] **Wu, J., Zhang, X., Liu, J., Xiong, M., Lu, X., Fan, H., Wang, X., and Zhang, X.** (2016). Medium density fiberboard production by hot pressing without adhesive using Triarrhena sacchariflora residue bio-pretreated by white-rot fungus Coriolus versicolor, *Journal of Applied Microbiology, 121*, pp. 415-421.

[5] **Aung, M. M., Yaakob, Z., Kamarudin, S., and Abdullah, L. C.** (2014). Synthesis and characterization of Jatropha (Jatropha curcas L.) oil-based polyurethane wood adhesive, *Industrial Crops and Products, 60*, pp. 177-185.

[6] **Dutta, S. and Karak, N.** (2006). Effect of the NCO/OH ratio on the properties of Mesua Ferrea L. seed oil-modified polyurethane resins, *Polymer International, 55*, pp. 49-56.

[7] **Kayaman-Apohan, N., Amanoel, A., Arsu, N., and Güngör, A.** (2004). Synthesis and characterization of UV-curable vinyl ether functionalized urethane oligomers, *Progress in Organic Coatings, 49*, pp. 23-32.

[8] **Moon, J. H., Shul, Y. G., Han, H. S., Hong, S. Y., Choi, Y. S., and Kim, H. T.** (2005). A study on UV-curable adhesives for optical pick-up: I. Photo-initiator effects, *International Journal of Adhesion and Adhesives, 25*, pp. 301-312.

[9] **Hwang, J.-S., Kim, M.-H., Seo, D.-S., Won, J.-W., and Moon, D.-K.** (2009). Effects of soft segment mixtures with different molecular weight on the properties and reliability of UV curable adhesives for electrodes protection of plasma display panel (PDP), *Microelectronics Reliability, 49*, pp. 517-522.

[10] **Haddon, M. R. and Smith, T. J.** (1991). The chemistry and applications of UV-cured adhesives, *International Journal of Adhesion and Adhesives, 11*, pp. 183-186.

[11] **Su, Y.-C., Cheng, L.-P., Cheng, K.-C., and Don, T.-M.** (2012). Synthesis and characterization of UV-and thermo-curable difunctional epoxyacrylates, *Materials Chemistry and Physics, 132*, pp. 540-549.

[12] **Tan, C., Chan, Y., Chan, H., Leung, N., and So, C.** (2004). Investigation on bondability and reliability of UV-curable adhesive joints for stable mechanical properties in photonic device packaging, *Microelectronics Reliability, 44*, pp. 823-831.

[13] **Park, Y.-J., Lim, D.-H., Kim, H.-J., Park, D.-S., and Sung, I.-K.** (2009). UV- and thermal-curing behaviors of dual-curable adhesives based on epoxy acrylate oligomers, *International Journal of Adhesion and Adhesives, 29*, pp. 710-717.

[14] **Chiang, T. H. and Hsieh, T.-E.** (2006). A study of monomer's effect on adhesion strength of UV-curable resins, *International Journal of Adhesion and Adhesives, 26*, pp. 520-531.

[15] **Wu, S., Jorgensen, J. D., Skaja, A. D., Williams, J. P., and Soucek, M. D.** (1999). Effects of sulphonic and phosphonic acrylic monomers on the crosslinking of acrylic latexes with cycloaliphatic epoxide, *Progress in Organic Coatings, 36*, pp. 21-33.

[16] **Park, C.-H., Lee, S.-W., Park, J.-W., and Kim, H.-J.** (2013). Preparation and characterization of dual curable adhesives containing epoxy and acrylate functionalities, *Reactive and Functional Polymers, 73*, pp. 641-646.

[17] **Bhusari, G. S., Umare, S. S., and Chandure, A. S.** (2015). Effects of NCO: OH ratio and HEMA on the physicochemical properties of photocurable poly (ester-urethane) methacrylates, *Journal of Coatings Technology and Research, 12*, pp. 571-585.

[18] **Suzuki, T., Shibayama, M., Hatano, K., and Ishii, M.** (2009). [NCO]/[OH] and acryl-polyol concentration dependence of the gelation process and the microstructure analysis of polyurethane resin by dynamic light scattering, *Polymer, 50*, pp. 2503-2509.

[19] **Gopakumar, S. and Nair, M. G.** (2005). Swelling characteristics of NR/PU block copolymers and the effect of NCO/OH ratio on swelling behaviour, *Polymer, 46*, pp. 10419-10430.

[20] **Somani, K. P., Kansara, S. S., Patel, N. K., and Rakshit, A. K.** (2003). Castor oil based polyurethane adhesives for wood-to-wood bonding, International *Journal of Adhesion and Adhesives, 23*, pp. 269-275.

[21] **Wennekes, W.** (2008) *Adhesion of RFL-treated cords to rubber*, ed: University of Twente Enschede.

[22] **Hamilton, S.** (2016) *A Compherensive Guide to Tyres,* Available: https://www.lifesure.co.uk/blog/2014/02/a-comprehensive-guide-to-tyres/

[23] **Isayev, A. I. and Palsule, S.** (2011). *Encyclopedia of Polymer Blends, Volume 2:* Processing vol. 2: John Wiley & Sons.

[24] **Rodgers, B. and Waddell, W.** (2005). 14 - Tire Engineering A2 - Mark, James E," in Science *and Technology of Rubber (Third Edition)*, B. Erman and F. R. Eirich, Eds., ed Burlington: Academic Press, pp. 619-661.

[25] **Naskar, A. K., Mukherjee, A., and Mukhopadhyay, R.** (2004). Studies on tyre cords: degradation of polyester due to fatigue, *Polymer Degradation and Stability, 83*, pp. 173-180.

[26] **Arul, M. A.** (2013). "Improvement Of Interface Adhesion Between Nylon Tyre Cord and Rubber Compound," APOLLO TYRES LIMITED, CHENNAI, BIRLA INSTITUTE OF TECHNOLOGY & SCIENCE PILANI, India, April.

[27] **Amornchaiyapitak, C., Taweepreda, W., and Tangboriboonrat, P.** (2008). Modification of epoxidised natural rubber film surface by polymerisation of methyl methacrylate, *European Polymer Journal, 44*, pp. 1782-1788.

[28] **Romero-Sánchez, M. D. and Martín-Martínez, J. M.** (2006). Surface modifications of vulcanized SBR rubber by treatment with atmospheric pressure plasma torch, *International Journal of Adhesion and Adhesives, 26*, pp. 345-354.

[29] **Kocevski, S., Yagneswaran, S., Xiao, F., Punith, V., Smith, D. W., and Amirkhanian, S.** (2012). Surface modified ground rubber tire by grafting acrylic acid for paving applications, *Construction and Building Materials, 34*, pp. 83-90.

[30] **Rahman, M. A., Sartore, L., Bignotti, F., and Di Landro, L.** (2013). Autonomic self-healing in epoxidized natural rubber, *ACS Applied Materials & Interfaces, 5*, pp. 1494-1502.

[31] **Rubber, M.** (2016, August, 09). *Rubber Chemistry*. Available: http://laroverket.com/wpcontent/uploads/2015/03/rubber_chemistry.pdf

[32] **John, S. D. and Charles, P. R.** (2014). Textile Reinforcing Materials and Their Adhesive Systems Used in Rubber," in *Raw Materials Supply Chain for Rubber Products*, ed: Carl Hanser Verlag GmbH & Co. KG, pp. 115-154.

[33] **Chanda, M.** (2013). *Introduction to polymer science and chemistry: a problem-solving approach*: CRC Press.

[34] **Wei, Q.** (2009). *Surface modification of textiles:* Elsevier.

[35] **Luo, S. and Van Ooij, W. J.** (2002). Surface modification of textile fibers for improvement of adhesion to polymeric matrices: a review, *Journal of Adhesion Science and Technology, 16*, pp. 1715-1735.

[36] **Donelli, I., Freddi, G., Nierstrasz, V. A., and Taddei, P.** (2010). Surface structure and properties of poly-(ethylene terephthalate) hydrolyzed by alkali and cutinase, *Polymer Degradation and Stability, 95*, pp. 1542-1550.

[37] **Liu, X.-D., Sheng, D.-K., Gao, X.-M., Li, T.-B., and Yang, Y.-M.** (2013). UV-assisted surface modification of PET fiber for adhesion improvement, *Applied* Surface *Science, 264*, pp. 61-69.

[38] **Yoshioka, T., Motoki, T., and Okuwaki, A.** (2001). Kinetics of hydrolysis of poly (ethylene terephthalate) powder in sulfuric acid by a modified shrinking-core model, *Industrial & Engineering Chemistry Research, 40*, pp. 75-79.

[39] **Michielsen, S.** (2003). Surface modification of fibres via graft-site amplifying polymers, *Georgia Institute of Technology, INJ Fall*, pp. 41-45.

[40] **Liu, Y., He, T., and Gao, C.** (2005). Surface modification of poly (ethylene terephthalate) via hydrolysis and layer-by-layer assembly of chitosan and chondroitin sulfate to construct cytocompatible layer for human endothelial cells, Colloids *and surfaces B: Biointerfaces, 46*, pp. 117-126.

[41] **Raslan, W., El-Khatib, E., El-Halwagy, A., and Ghalab, S.** (2011). Low Temperature Plasma/Metal Salts Treatments for Improving Some Properties of Polyamide 6 Fibres, *Journal of Industrial Textiles, 40*, pp. 246-260.

[42] **Janca, J., Stahel, P., Buchta, J., Subedi, D., Krcma, F., and Pryckova, J.** (2001). A plasma surface treatment of polyester textile fabrics used for reinforcement of car tires, *Plasmas and Polymers, 6*, pp. 15-26.

[43] **Biswas, M. K., Shayed, M., Hund, R., and Cherif, C.** (2013). Surface modification of Twaron aramid fiber by the atmospheric air plasma technique, *Textile Research Journal, 83*, pp. 406-417.

[44] **Armağan, O. G., Kayaoglu, B. K., Karakas, H. C., and Guner, F. S.** (2013). Adhesion strength behaviour of plasma pre-treated and laminated polypropylene nonwoven fabrics using acrylic and polyurethane-based adhesives, *Journal of Industrial Textiles, 43*, pp. 396-414.

[45] **Song, J.** (2004) *Fatigue of cord-rubber composites for tires*, The Pennsylvania State University.

[46] **Yilmaz, B.** (2010). Effects of disturbing parameters on the stability of latex and resorcinol formaldehyde latex based adhesives, *The Journal of Adhesion, 86*, pp. 430-446.

[47] **Li, S.** (2012) United States Patent: *Adhesion composition and textile materials and articles treated therewith.*

[48] **Darwish, N., Shehata, A., Abou-Kandil, A. I., Abd El-Megeed, A., Lawandy, S., and Saleh, B.** (2013). A novel promoter for enhancing adhesion between natural rubber and brass-plated steel cords, *International Journal of* Adhesion *and Adhesives, 40*, pp. 135-144.

[49] **Jincheng, W., Yuehui, C., and Zhaoqun, D.** (2005). Research on the adhesive property of polyethylene terephthalate (PET) cord and nitrile-butadiene rubber (NBR) system, *Journal of Industrial Textiles, 35*, pp. 157-172.

[50] **Choi, S.-S. and Kim, O.-B.** (2013). Influence of rubber and fabric cord on deformation of a fabric cord-inserted rubber composite by thermal

aging, Journal *of Industrial and Engineering Chemistry, 19*, pp. 650-654.

[51] **Choi, S.-S. and Kim, O.-B.** (2014). Influence of specimen directions on recovery behaviors from circular deformation of polyester cord-inserted rubber composites, *Journal of Industrial and Engineering Chemistry, 20*, pp. 202-207.

[52] **Louis, A., Noordermeer, J., Dierkes, W., and Blume, A.** (2014) Technologies for Polymer Cord/Rubber Adhesion in Tire Applications," presented at the 186th Technical Meeting of Rubber Division, ACS, Nashville, Tennessee, USA.

[53] **Shi, X., Lian, C., Shang, Y., and Zhang, H.** (2015). Evolution of the dynamic fatigue failure of the adhesion between rubber and polymer cords, *Polymer Testing, 48*, pp. 175-182.

[54] **de Lange, P. J., Akker, P. G., Willemsen, S., and Datta, R. N.** (2009). The effect of oily finish components on the adhesion between aramid fibers and rubber, *Journal of Adhesion Science and Technology, 23*, pp. 139-149.

[55] **Darwish, N., Lawandy, S., El-Shazly, S. A., and Abou-Kandil, A.** (2000). Effect of bonding systems on the adhesion of nitrile rubber to nylon cord, *Polymer*-Plastics *Technology and Engineering, 39*, pp. 793-806.

[56] **Kardar, P., Ebrahimi, M., and Bastani, S.** (2008). Study the effect of nano-alumina particles on physical–mechanical properties of UV cured epoxy acrylate via nano-indentation, *Progress in Organic Coatings, 62*, pp. 321-325.

[57] **Salleh, N. G. N., Alias, M. S., Gläsel, H., and Mehnert, R.** (2013). High performance radiation curable hybrid coatings, *Radiation Physics and* Chemistry, *84*, pp. 70-73.

[58] **Job, L. and Joseph, R.** (1999). Studies on rubber-to-nylon tire cord bonding, *Journal of Applied Polymer Science, 71*, pp. 1197-1202.

[59] **Jones, I. and Stylios, G. K.** (2013). *Joining textiles: Principles and applications:* Elsevier.

[60] **Damico, D. J.** (2005). *Advances in Adhesives, Adhesion Science, and Testing*: ASTM International.

[61] **Cognard, P.** (2006). *Handbook of adhesives and sealants: general knowledge,* application *of adhesives, new curing techniques* vol. 2: Elsevier.

[62] **da Silva, L. F., Öchsner, A., and Adams, R. D.** (2011). *Handbook of adhesion* technology: Springer Science & Business Media.

[63] **Mittal, K.** (2015). Advances *in Contact Angle, Wettability and Adhesion, Volume Two*: John Wiley & Sons.

[64] **Nitowski, G. A.** (1998) Topographic and Surface Chemical Aspects of the Adhesion of Structural Epoxy Resins to Phosphorus Oxo Acid Treated Aluminum Adherends," Doctor of Philosophy Materials Engineering

Science, Virginia Polytechnic Institute and State University, Blacksburg, Virginia, USA.

[65] **Bracco, G. and Holst, B.** (2013). *Surface Science Techniques*: Springer Science & Business Media.

[66] **Shim, E.** (2010) Coating and laminating processes and techniques for textiles, in *Smart* Textile *Coatings and Laminates*, pp. 10-41.

[67] **Lynta, J. and Rani, J.** (1999) Studies on adhesives for bonding rubber to rubber and rubber to textiles, Cochin University of Science & Technology.

[68] **Mattson, C.** (2016, August, 09). *The Physics of Adhesives*. Available: http://ffden2.phys.uaf.edu/webproj/212_spring_2014/Connor_Mattson/connor_mattson/physics.html

[69] **Shim, E.** (2013) Bonding requirements in coating and laminating of textiles, in *Joining Textiles: Principles and Applications*, pp. 309-350.

[70] **Giessmann, A.** (2012). *Coating substrates and textiles: A practical guide to coating* and *laminating technologies*: Springer Science & Business Media.

[71] **Singha, K.** (2012). A review on coating & lamination in textiles: processes and applications, *American* Journal *of Polymer Science, 2*, pp. 39-49.

[72] **Bayramoğlu, G., Kahraman, M. V., Kayaman-Apohan, N., and Güngör, A.** (2007). The coating performance of adipic acid modified and methacrylated bisphenol-A based epoxy oligomers, *Polymers for Advanced Technologies, 18*, pp. 173-179.

[73] **Davidson, R.** (2001). Radiation *curing* vol. 12: iSmithers Rapra Publishing.

[74] **Decker, C., Viet, T. N. T., Decker, D., and Weber-Koehl, E.** (2001). UV-radiation curing of acrylate/epoxide systems, *Polymer, 42*, pp. 5531-5541.

[75] **Golaz, B., Michaud, V., Leterrier, Y., and Månson, J.-A.** (2012). UV intensity, temperature and dark-curing effects in cationic photo-polymerization of a cycloaliphatic epoxy resin, *Polymer, 53,* pp. 2038-2048.

[76] **Schnabel, W.** (2007). *Polymers and light: fundamentals and technical* applications: John Wiley & Sons.

[77] **Bajpai, M., Shukla, V., and Kumar, A.** (2002). Film performance and UV curing of epoxy acrylate resins, *Progress in Organic Coatings, 44*, pp. 271-278.

[78] **Sung, S. and Kim, D. S.** (2013). UV-curing and mechanical properties of polyester–acrylate nanocomposites films with silane-modified antimony doped tin oxide nanoparticles, *Journal of Applied Polymer Science, 129*, pp. 1340-1344.

[79] **Firdous, H. and Bajpai, M.** (2010). UV curable heat resistant epoxy acrylate coatings, *Chemistry and Chemical Technology, 4*, pp. 205-216.

[80] **Eksik, O., Tasdelen, M. A., Erciyes, A. T., and Yagci, Y.** (2010). In situ synthesis of oil-based polymer/silver nanocomposites by photoinduced

electron transfer and free radical polymerization processes, *Composite Interfaces*, *17*, pp. 357-369.

[81] **Xie, J., Zhang, N., Guers, M., and Varadan, V. K.** (2002). Ultraviolet-curable polymers with chemically bonded carbon nanotubes for microelectromechanical system applications, *Smart Materials and Structures, 11*, pp. 575.

[82] **Bayramoğlu, G., Kahraman, M. V., Kayaman-Apohan, N., and Güngör, A.** (2006). Synthesis and characterization of UV-curable dual hybrid oligomers based on epoxy acrylate containing pendant alkoxysilane groups, *Progress in* Organic *Coatings, 57*, pp. 50-55.

[83] **Kahraman, M. V., Bayramoğlu, G., Kayaman-Apohan, N., and Güngör, A.** (2007). UV-curable methacrylated/fumaric acid modified epoxy as a potential support for enzyme immobilization, *Reactive and Functional* Polymers, *67*, pp. 97-103.

[84] **Dillman, B. F.** (2013) The kinetics and physical properties of epoxides, acrylates, and hybrid epoxy-acrylate photopolymerization systems, Doctor of Philosophy, Chemical and Biochemical Engineering, The University of Iowa.

[85] **Green, W. A.** (2010). Industrial *photoinitiators: A technical guide*: CRC Press Boca Raton (FL).

[86] **Mishra, M. and Yagci, Y.** (2008). *Handbook of Vinyl Polymers: Radical Polymerization, Process, and Technology:* CRC press.

[87] **Fink, J. K.** (2013). *Reactive Polymers Fundamentals and Applications: A Concise Guide to Industrial Polymers*: William Andrew.

[88] **Url-1** <*http://mcdowellscienceexam.weebly.com/heat.html*>, date retrieved 13.09.2016.

[89] **Kunwong, D., Sumanochitraporn, N., and Kaewpirom, S.** (2011). Curing behavior of a UV-curable coating based on urethane acrylate oligomer: the influence of reactive monomers, *Sonklanakarin Journal of Science and Technology, 33*, pp. 201.

[90] **Pitchaimari, G., Sarma, K. S. S., Varshney, L., and Vijayakumar, C. T.** (2014). Influence of the reactive diluent on electron beam curable funtionalized N-(4-hydroxyl phenyl) maleimide derivatives – Studies on thermal degradation kinetics using model free approach, *Thermochimica Acta, 597*, pp. 8-18.

[91] **da Silva, W. M., Ribeiro, H., Neves, J. C., Sousa, A. R., and Silva, G. G.** (2015). Improved impact strength of epoxy by the addition of functionalized multiwalled carbon nanotubes and reactive diluent, *Journal of Applied Polymer Science, 132*, pp. 425-437.

[92] **Baştürk, E., İnan, T., and Güngör, A.** (2013). Flame retardant UV-curable acrylated epoxidized soybean oil based organic–inorganic hybrid coating, Progress *in Organic Coatings*, *76*, pp. 985-992.

[93] **Chittavanich, P., Miller, K., and Soucek, M.** (2012). A photo-curing study of a pigmented UV-curable alkyd, *Progress in Organic Coatings*, *73*, pp. 392-400.

[94] **Craver, C. and Carraher, C.** (2000). *Applied Polymer Science: 21st Century:* Elsevier.

[95] **Golaz, B., Michaud, V., and Månson, J.-A.** (2013). Photo-polymerized epoxy primer for adhesion improvement at thermoplastics/metallic wires interfaces, *Composites Part A: Applied Science and Manufacturing, 48*, pp. 171-180.

[96] **Moon, J. H., Shul, Y. G., Hong, S. Y., Choi, Y. S., and Kim, H. T.** (2005). A study on UV-curable adhesives for optical pick-up: II. Silane coupling agent effect, *International Journal of Adhesion and Adhesives, 25*, pp. 534-542.

[97] **Chiang, T. H. and Hsieh, T.-E.** (2008). A study of UV-curable epoxide resins containing thermal accelerator–Tertiary amines, *Reactive and Functional* Polymers*, 68*, pp. 601-612.

[98] **Agarwal, N., Varma, I. K., and Choudhary, V.** (2006). Methacrylate/acrylate terminated derivatives of diglycidyl hexahydrophthalate: Synthesis, structural, and thermal characterization, *Journal of Applied Polymer Science, 99*, pp. 2414-2420.

[99] **Yang, G., Liu, H., Bai, L., Jiang, M., and Zhu, T.** (2008). Preparation and characterization of novel poly (vinyl ester resin) monoliths, *Microporous and* Mesoporous *Materials, 112*, pp. 351-356.

[100] **Mansour, S., Mostafa, N., and Abd-El-Messieh, L.** (2007). Electrical and positron annihilation study on epoxy and epoxy acrylate composites, *European Polymer Journal*, *43*, pp. 4770-4782.

[101] **Mandal, B. M.** (2013). *Fundamentals of Polymerization*. Singapore: World Scientific Publishing Co.

[102] **Alyamac, E., Gu, H., Soucek, M. D., Qiu, S., and Buchheit, R. G.** (2012). Alkoxysilane oligomer modified epoxide primers, *Progress in Organic Coatings, 74*, pp. 67-81.

[103] **Pham, H. Q. and Marks, M. J.** (2004) Epoxy resins, in *Kirk-Othmer Encyclopedia of* Chemical *Technology*. vol. 10, ed: John Wiley & Sons, Inc., pp. 347-471.

[104] **Qian, X., Song, L., Hu, Y., and Yuen, R. K.** (2013). Thermal degradation and flammability of novel organic/inorganic epoxy hybrids containing organophosphorus-modified oligosiloxane, *Thermochimica Acta, 552*, pp. 87-97.

[105] **Sandler, S. R., Karo, W., Bonesteel, J., and Pearce, E. M.** (1998). *Polymer* Synthesis *and Characterization: A Laboratory Manual*: Academic Press.

[106] **Srivastava, A., Agrawal, S., and Rai, J.** (2002). Kinetics of esterification of cycloaliphatic epoxies with methacrylic acid, *Journal of Applied Polymer* Science, *86*, pp. 3197-3204.

[107] **Chattopadhyay, D. K., Panda, S. S., and Raju, K. V. S. N.** (2005). Thermal and mechanical properties of epoxy acrylate/methacrylates UV cured coatings, *Progress in Organic Coatings, 54*, pp. 10-19.

[108] **ASTM** (2007). *Standard test method for neutralization number by color indicator titration* (ASTM D974) ed: ASTM International.

[109] **Cheng, W., Chih, Y., and Lin, C.** (2005). Formulation and characterization of UV-light-curable electrically conductive pastes, *Journal of Adhesion Science and Technology, 19*, pp. 511-523.

[110] **Pascault, J.-P. and Williams, R. J.** (2009). Epoxy *Polymers*: John Wiley & Sons.

[111] **Pham, H. and Marks, M.** (2005) Epoxy Resins, Ullmann's Encyclopedia of Industrial Chemistry. *13*, ed: Wiley–VCH Verlag GmbH & Co. KGaA.

[112] **Rayss, J., Gorgol, A., Podkościelny, W., Widomski, J., and Chołyk, M.** (1998). Influence of the fused silica surface dehydroxylation on the adhesion of epoxyacrylate protective coatings used for optical fibers, *Journal of Adhesion Science and Technology, 12*, pp. 293-303.

[113] **Wang, X., Wang, B., Xing, W., Tang, G., Zhan, J., Yang, W., Song, L., and Hu, Y.** (2014). Flame retardancy and thermal property of novel UV-curable epoxy acrylate coatings modified by melamine-based hyperbranched polyphosphonate acrylate, *Progress in Organic Coatings, 77*, pp. 94-100.

[114] **Choudhary, V., Agarwal, N., and Varma, I. K.** (2006). Evaluation of bisacrylate terminated epoxy resins as coatings, *Progress in Organic Coatings*, 57, pp. 223-228.

[115] **Qian, X., Tai, Q., Song, L., and Yuen, R.** (2014). Thermal degradation and flame-retardant properties of epoxy acrylate resins modified with a novel flame retardant containing phosphorous and nitrogen, *Fire Safety Science, 11*, pp. 883-894.

[116] **Xing, W., Jie, G., Song, L., Wang, X., Lv, X., and Hu, Y.** (2011). Flame retardancy and thermal properties of epoxy acrylate resin/alpha-zirconium phosphate nanocomposites used for UV-curing flame retardant films, *Materials Chemistry and Physics, 125*, pp. 196-201.

[117] **Macarie, L. and Ilia, G.** (2010). Poly (vinylphosphonic acid) and its derivatives, *Progress in Polymer Science, 35*, pp. 1078-1092.

[118] **Salzinger, S., Seemann, U. B., Plikhta, A., and Rieger, B.** (2011). Poly (vinylphosphonate) s synthesized by trivalent cyclopentadienyl lanthanide-induced group transfer polymerization, *Macromolecules, 44*, pp. 5920-5927.

[119] **Opwis, K., Wego, A., Bahners, T., and Schollmeyer, E.** (2011). Permanent flame retardant finishing of textile materials by a photochemical immobilization of vinyl phosphonic acid, *Polymer Degradation and Stability, 96*, pp. 393-395.

[120] **Alam, M., Akram, D., Sharmin, E., Zafar, F., and Ahmad, S.** (2014). Vegetable oil based eco-friendly coating materials: A review article, *Arabian* Journal *of Chemistry, 7*, pp. 469-479.

[121] **Miao, S., Wang, P., Su, Z., and Zhang, S.** (2014). Vegetable-oil-based polymers as future polymeric biomaterials, *Acta Biomaterialia, 10*, pp. 1692-1704.

[122] **Li, F. and Larock, R. C.** (2000). Thermosetting polymers from cationic copolymerization of tung oil: synthesis and characterization, *Journal of Applied Polymer Science, 78*, pp. 1044-1056.

[123] **Li, F. and Larock, R. C.** (2003). Synthesis, structure and properties of new tung oil-styrene-divinylbenzene copolymers prepared by thermal polymerization, *Biomacromolecules, 4*, pp. 1018-1025.

[124] **Thames, S. F. and Yu, H.** (1996). Synthesis, characterization, and application of Lesquerella oil and its derivative in water-reducible coatings, *JCT, Journal of* Coatings *Technology, 68*, pp. 63-67.

[125] **Wicks Jr, Z. W., Jones, F. N., Pappas, S. P., and Wicks, D. A.** (2007). Organic *Coatings: Science and Technology*: John Wiley & Sons.

[126] **Wutticharoenwong, K. and Soucek, M. D.** (2010). Synthesis of Tung-Oil-Based Reactive Diluents, *Macromolecular Materials and Engineering, 295*, pp. 1097-1106.

[127] **Thanamongkollit, N., Miller, K. R., and Soucek, M. D.** (2012). Synthesis of UV-curable tung oil and UV-curable tung oil based alkyd, *Progress in Organic* Coatings, *73*, pp. 425-434.

[128] **Goud, V. V., Patwardhan, A. V., Dinda, S., and Pradhan, N. C.** (2007). Epoxidation of karanja (Pongamia glabra) oil catalysed by acidic ion exchange resin, *European Journal of Lipid Science and Technology, 109*, pp. 575-584.

[129] **Karak, N.** (2012). *Vegetable oil-based polymers: properties, processing and* applications: Elsevier.

[130] **Lligadas, G., Ronda, J. C., Galia, M., and Cadiz, V.** (2013). Renewable polymeric materials from vegetable oils: a perspective, *Materials Today, 16*, pp. 337-343.

[131] **Mungroo, R., Pradhan, N. C., Goud, V. V., and Dalai, A. K.** (2008). Epoxidation of canola oil with hydrogen peroxide catalyzed by acidic ion exchange resin, *Journal of the American Oil Chemists' Society, 85*, pp. 887-896.

[132] **Saremi, K., Tabarsa, T., SHakeri, A., and Babanalbandi, A.** (2012). Epoxidation of soybean oil, *Ann. Biol. Res, 3*, pp. 4254-4258.

[133] **Shen, L., Haufe, J., and Patel, M. K.** (2009). Product overview and market projection of emerging bio-based plastics PRO-BIP 2009, *Report for European* Polysaccharide *Network of Excellence (EPNOE) and European Bioplastics, 243*, pp. 1-226.

[134] **Wang, F., Hu, J., and Tu, W.** (2008). Study on microstructure of UV-curable polyurethane acrylate films, *Progress in Organic Coatings, 62,* pp. 245-250.

[135] **Kim, E.-H., Jung, Y.-G., and Paik, U.** (2009). Holographic grating formation in PVB doped polymer dispersed liquid crystal based on PUA, *Thin Solid Films, 518,* pp. 1424-1429.

[136] **Barszczewska-Rybarek, I. M.** (2014). Characterization of urethane-dimethacrylate derivatives as alternative monomers for the restorative composite matrix, *Dental Materials, 30,* pp. 1336-1344.

[137] **Çanak, T. Ç. and Serhatlı, İ. E.** (2013). Synthesis of fluorinated urethane acrylate based UV-curable coatings, *Progress in Organic Coatings, 76,* pp. 388-399.

[138] **Çanak, T. Ç., Kiraylar, E., and Serhatli, E.** (2016). Preparation and Application of Urethane Acrylate Coatings for Enhanching Mechanical Properties of Coagulated Surfaces, *Karaelmas Fen ve Mühendislik Dergisi, 6,* pp. 359-368.

[139] **Yanılmaz, M., Erbay, B. T., Serhatli, E., and Sarac, A. S.** (2013). Synthesis of urethane acrylate based electromagnetic interference shielding materials, Journal *of Applied Polymer Science, 127,* pp. 4957-4966.

[140] **Türel Erbay, B. and Serhatlı, I. E.** (2013). Synthesis of bis[(4-hydroxyethoxy)phenyl]sulfone containing urethane acrylates and their applications, *Progress in Organic Coatings, 76,* pp. 1-10.

[141] **Lei, G., Angeli, S., Kristol, D., and Snyder, W.** (1987). Preparation of new blocked diisocyanate for dental application, *Journal of Polymer Science Part A: Polymer Chemistry, 25,* pp. 607-615.

[142] **Zhou, X. Q., Cao, Y. M., and Tian, J. L.** (2011). Synthesis and Properties of Waterborne UV Polyurethane in *Advanced Materials Research,* pp. 1087-1092.

[143] **Wang, S. J., Wang, Y. L., Yang, P. F., and Li, T. D.** (2012). Preparation of Polyurethane-Poly (butyl acrylate) Hybrid Latexes via Miniemulsion Polymerization in *Applied Mechanics and Materials,* pp. 3938-3941.

[144] **Bai, Y., Chen, Y., Wang, Q., and Wang, T.** (2014). Poly (vinyl butyral) based polymer networks with dual-responsive shape memory and self-healing properties, *Journal of Materials Chemistry A, 2,* pp. 9169-9177.

[145] **Dhaliwal, A. K. and Hay, J. N.** (2002). The characterization of polyvinyl butyral by thermal analysis, *Thermochimica Acta, 391,* pp. 245-255.

[146] **Lian, F., Wen, Y., Ren, Y., and Guan, H.** (2014). A novel PVB based polymer membrane and its application in gel polymer electrolytes for lithium-ion batteries, *Journal of Membrane Science, 456,* pp. 42-48.

[147] **Olabisi, O. and Adewale, K.** (2015). *Handbook of Thermoplastics, Second* Edition: CRC Press.

[148] **ASTM** (2014). *Standard Practices for Evaluating the Resistance of Plastics to Chemical Reagents* (ASTM D543-14) ed: ASTM International.

[149] **Kabza, K. G., Gestwicki, J. E., and McGrath, J. L.** (2000). Contact angle goniometry as a tool for surface tension measurements of solids, using Zisman plot method. A physical chemistry experiment, *Journal of Chemical Education, 77,* pp. 63.

[150] **ASTM** (2015). *Standard Test Method for Peel Resistance of Adhesives (T-Peel Test)* (ASTM D1876-08) ed: ASTM International.

[151] **ASTM** (2012). *Standard Test Method for Measuring Minimum Oxygen Concentration to Support Candle-Like Combustion of Plastics* (ASTM D2863-13) ed: ASTM International.

[152] **Nemati, M., Eslam, H. K., Talaeipour, M., Bazyar, B., and Samariha, A.** (2015). Effect of Nanoclay on Flammability Behavior and Morphology of Nanocomposites from Wood Flour and Polystyrene Materials, *BioResources, 11*, pp. 748-758.

[153] **Desroches, M., Escouvois, M., Auvergne, R., Caillol, S., and Boutevin, B.** (2012). From vegetable oils to polyurethanes: synthetic routes to polyols and main industrial products, *Polymer Reviews, 52,* pp. 38-79.

[154] **Yildiz, Z., Gungor, A., Onen, A., and Usta, I.** (2016). Synthesis and characterization of dual-curable epoxyacrylates for polyester cord/rubber applications, *Journal of Industrial Textiles, 46,* pp. 596-610.

[155] **Cramer, N. B. and Bowman, C. N.** (2001). Kinetics of thiol–ene and thiol–acrylate photopolymerizations with real-time fourier transform infrared, Journal *of Polymer Science Part A: Polymer Chemistry, 39,* pp. 3311-3319.

[156] **Çanak, T. Ç., Kaya, K., and Serhatlı, I. E.** (2014). Boron containing UV-curable epoxy acrylate coatings, *Progress in Organic Coatings, **77***, pp. 1911-1918.

[157] **Pan, G., Du, Z., Zhang, C., Li, C., Yang, X., and Li, H.** (2007). Synthesis, characterization, and properties of novel novolac epoxy resin containing naphthalene moiety, *Polymer, 48*, pp. 3686-3693.

[158] **TS EN ISO** (2012). *Textiles - Tests for colour fastness - Part C06: Color fastness to domestic and commercial laundering* (TS EN ISO 105-C06) p. 7.

[159] **Yildiz, Z., Onen, A., and Gungor, A.** (2016). Preparation of flame retardant epoxyacrylate-based adhesive formulations for textile applications, *Journal of* Adhesion *Science and Technology, 30*, pp. 1765-1778.

[160] **De Cupere, V. and Rouxhet, P.** (2002). Surface crystallization of poly (ethylene terephtalate) studied by atomic force microscopy, *Polymer, 43*, pp. 5571-5576.

[161] **Yoshii, T., Yoshida, H., and Kawai, T.** (2005). Effect of structural relaxation of glassy PET on crystallization process observed by the simultaneous DSC–XRD and DSC–FTIR, *Thermochimica Acta, 431*, pp. 177-181.

[162] **Zhou, X., Chen, K., and Yi, H.** (2014). Synthesis and application of a formaldehyde-free flame retardant for bamboo viscose fabric, *Textile Research* Journal, *84*, pp. 1515-1527.

[163] **Zarshenas, K., Raisi, A., and Aroujalian, A.** (2015). Surface modification of polyamide composite membranes by corona air plasma for gas separation applications, *RSC Advances*, *5*, pp. 19760-19772.

[164] **Wang, Q. and Shi, W.** (2006). Photopolymerization and thermal behaviors of acrylated benzenephosphonates/epoxy acrylate as flame retardant resins, *European Polymer Journal*, *42*, pp. 2261-2269.

[165] **Laoutid, F., Bonnaud, L., Alexandre, M., Lopez-Cuesta, J.-M., and Dubois, P.** (2009). New prospects in flame retardant polymer materials: from fundamentals to nanocomposites, *Materials Science and Engineering: R: Reports*, *63*, pp. 100-125.

[166] **Li, B. and Xu, M.** (2006). Effect of a novel charring–foaming agent on flame retardancy and thermal degradation of intumescent flame retardant polypropylene, *Polymer Degradation and Stability*, *91*, pp. 1380-1386.

[167] **Kabza, K. G., Gestwicki, J. E., and McGrath, J. L.** (2000). Contact angle goniometry as a tool for surface tension measurements of solids, using Zisman plot method. A physical chemistry experiment, *Journal of Chemistry Education*, *77*, pp. 63.

[168] **Yuan, Y. and Lee, T. R.** (2013) Contact angle and wetting properties, in *Surface* science *techniques*, ed: Springer, pp. 3-34.

[169] **Wagner, T., Manhart, A., Deniz, N., Kaltbeitzel, A., Wagner, M., Brunklaus, G., and Meyer, W. H.** (2009). Vinylphosphonic Acid Homo-and Block Copolymers, *Macromolecular Chemistry and Physics*, *210*, pp. 1903-1914.

[170] **Stemmelen, M., Pessel, F., Lapinte, V., Caillol, S., Habas, J. P., and Robin, J. J.** (2011). A fully biobased epoxy resin from vegetable oils: From the synthesis of the precursors by thiol-ene reaction to the study of the final material, *Journal of Polymer Science Part A: Polymer Chemistry*, *49*, pp. 2434-2444.

[171] **Saithai, P., Lecomte, J., Dubreucq, E., and Tanrattanakul, V.** (2013). Effects of different epoxidation methods of soybean oil on the characteristics of acrylated epoxidized soybean oil-co-poly (methyl methacrylate) copolymer, Express *Polymer Letters*, *7*, pp. 910-924.

[172] **Milchert, E. and Smagowicz, A.** (2009). The influence of reaction parameters on the epoxidation of rapeseed oil with peracetic acid, *Journal of the American* Oil *Chemists' Society*, *86*, pp. 1227-1233.

[173] **İşeri-Çağlar, D., Baştürk, E., Oktay, B., and Kahraman, M. V.** (2014). Preparation and evaluation of linseed oil based alkyd paints, *Progress in Organic Coatings*, *77*, pp. 81-86.

[174] **Ugur, M., Kılıç, H., Berkem, M., and Güngör, A.** (2014). Synthesis by UV-curing and characterisation of polyurethane acrylate-lithium salts-based

polymer electrolytes in lithium batteries, *Chemical Papers, 68*, pp. 1561-1572.

[175] **Liu, C. G., Zhou, Y. H., and Hu, L. H.** (2012). Novel Biobased Materials from Tung Oil-Based Monomer and Tung Oil-Modified Unsaturated Polyester in *Advanced Materials Research*, pp. 121-124.

[176] **Huang, K., Liu, Z., Zhang, J., Li, S., Li, M., Xia, J., and Zhou, Y.** (2014). Epoxy monomers derived from tung oil fatty acids and its regulable thermosets cured in two synergistic ways, *Biomacromolecules, 15*, pp. 837-843.

[177] **Gerbase, A. E., Petzhold, C. L., and Costa, A. P. O.** (2002). Dynamic mechanical and thermal behavior of epoxy resins based on soybean oil, *Journal of the* American *Oil Chemists' Society, 79*, pp. 797-802.

[178] **Saikia, D., Wu, H.-Y., Pan, Y.-C., Lin, C.-P., Huang, K.-P., Chen, K.-N., Fey, G. T., and Kao, H.-M.** (2011). Highly conductive and electrochemically stable plasticized blend polymer electrolytes based on PVdF-HFP and triblock copolymer PPG-PEG-PPG diamine for Li-ion batteries, *Journal of Power Sources, 196*, pp. 2826-2834.

[179] **Yildiz, Z., Onen, H. A., and Gungor, A.** (2015) Synthesis of Phosphorus Containing Bio-Based Adhesives For Textile Applications, presented at the 15th AUTEX World Textile Conference, Bucharest, Romania, June 10-12.

[180] **Pérez-Limiñana, M. A., Arán-Aís, F., Torró-Palau, A. M., Orgilés-Barcel, C., and Martín-Martínez, J. M.** (2007). Influence of the hard-to-soft segment ratio on the adhesion of water-borne polyurethane adhesive, *Journal of* Adhesion *Science and Technology, 21*, pp. 755-773.

[181] **Dusek, K., Spirkova, M., and Havlicek, I.** (1990). Network formation of polyurethanes due to side reactions, *Macromolecules, 23*, pp. 1774-1781.

[182] **Mishra, A. K., Narayan, R., and Raju, K.** (2012). Structure–property correlation study of hyperbranched polyurethane–urea (HBPU) coatings, Progress *in Organic Coatings, 74*, pp. 491-501.

[183] **Semsarzadeh, M. and Navarchian, A.** (2003). Effects of NCO/OH ratio and catalyst concentration on structure, thermal stability, and crosslink density of poly (urethane-isocyanurate), *Journal of Applied Polymer Science, 90*, pp. 963-972.

[184] **Tsai, Y., Fan, C.-H., and Wu, J.-H.** (2016). Synthesis, microstructures and properties of amorphous poly (ethylene terephthalate-co-tricyclodecanedimethylene terephthalate), *Journal of Polymer Research, 23*, pp. 1-9.

[185] **Huang, J. and Zhang, L.** (2002). Effects of NCO/OH molar ratio on structure and properties of graft-interpenetrating polymer networks from polyurethane and nitrolignin, *Polymer, 43*, pp. 2287-2294.

[186] **Desai, S., Thakore, I., Sarawade, B., and Devi, S.** (2000). Effect of polyols and diisocyanates on thermo-mechanical and morphological properties of polyurethanes, *European Polymer Journal, 36*, pp. 711-725.

[187] **Liao, F., Zeng, X.-r., Li, H.-q., Lai, X.-j., and Zhao, F.-c.** (2012). Synthesis and properties of UV curable polyurethane acrylates based on two different hydroxyethyl acrylates, *Journal of Central South University, 19*, pp. 911-917.

[188] **Morones, P. G., Tavizón, S. F., Hernández, E. H., Vega, C. A. G., and Santillán, A. D. L.** (2016). Hybridization of graphene sheets with polyethylene terephthalate through the process of in situ polymerization aided by ultrasound, *RSC Advances, 6*, pp. 18413-18418.

[189] **Tan, S. Z., Wang, Y., Zhang, Y. F., and Zhou, W. L.** (2012). Preparation of a Novel Prepolymer of Polyurethane Acrylate, *Advanced Materials Research, 554*, pp. 153-156.

[190] **Yu, Y., Liao, B., Jiang, S., Li, G., and Sun, F.** (2015). Synthesis and characterization of photosensitive-fluorosilicone–urethane acrylate prepolymers, *Designed Monomers and Polymers, 18*, pp. 199-209.

[191] **Deepak, V., Rajan, J., and Asha, S.** (2006). Hydrogen bonding and rate enhancement in the photoinduced polymerization of telechelic urethane methacrylates based on a cycloaliphatic system: Tricyclodecane dimethanol, *Journal of Polymer Science Part A: Polymer Chemistry, 44*, pp. 4384-4395.

[192] **Satav, S. S., Karmalkar, R. N., Kulkarni, M. G., Mulpuri, N., and Sastry, G. N.** (2007). Hydrogen bonding in trivinyl monomers: Implications for inclusion complexation and polymerization, *Macromolecules, 40*, pp. 1824-1830.

[193] **Fernandez, M., Fernandez, M., and Hoces, P.** (2006). Synthesis of poly (vinyl butyral) s in homogeneous phase and their thermal properties, *Journal of* Applied *Polymer Science, 102*, pp. 5007-5017.

[194] **Liu, C. D., Huang, C. K., Wu, S. Y., Han, J. L., and Hsieh, K. H.** (2010). Nanometer-thick patterned conductive films prepared through the self-synthesis of polythiophene derivatives, *Polymer International, 59*, pp. 517-522.

[195] **Hajian, M., Reisi, M. R., Koohmareh, G. A., and Jam, A. R. Z.** (2012). Preparation and characterization of polyvinylbutyral/graphene nanocomposite, Journal *of Polymer Research, 19*, pp. 1-7.

[196] **Jaw, K.-S., Hsu, C.-K., and Lee, J.-S.** (2001). The thermal decomposition behaviors of stearic acid, paraffin wax and polyvinyl butyral, *Thermochimica* Acta, *367*, pp. 165-168.

[197] **Beyler, C. L. and Hirschler, M. M.** (2002). Thermal decomposition of polymers, *SFPE Handbook of Fire Protection Engineering, 2*, pp. 110-131.

[198] **Chattopadhyay, D. and Webster, D. C.** (2009). Thermal stability and flame retardancy of polyurethanes, *Progress in Polymer Science, 34*, pp. 1068-1133.

[199] **Peng, Y. and Sui, Y.** (2006). Compatibility research on PVC/PVB blended membranes, *Desalination, 196*, pp. 13-21.

[200] **Shen, F., Lu, X., Bian, X., and Shi, L.** (2005). Preparation and hydrophilicity study of poly (vinyl butyral)-based ultrafiltration membranes, *Journal of* Membrane *Science, 265*, pp. 74-84.

[201] **Bandeira, L. C., Ciuffi, K. J., Calefi, P. S., Nassar, E. J., Silva, J. V., Oliveira, M., Maia, I. A., Salvado, I. M., and Fernandes, M. H. V.** (2012). Effect of calcium phosphate coating on polyamide substrate for biomaterial applications, *Journal of the Brazilian Chemical Society, 23*, pp. 810-817.

[202] **Cheval, N., Gindy, N., Flowkes, C., and Fahmi, A.** (2012). Polyamide 66 microspheres metallised with in situ synthesised gold nanoparticles for a catalytic application, *Nanoscale Research Letters, 7*, pp. 1.

[203] **Kirov, K. R. and Assender, H. E.** (2005). Quantitative ATR-IR analysis of anisotropic polymer films: surface structure of commercial PET, *Macromolecules, 38*, pp. 9258-9265.

[204] **Smith, B. C.** (1998). *Infrared spectral interpretation: a systematic approach*: CRC press.

[205] **Vijayakumar, S. and Rajakumar, P.** (2012). Infrared spectral analysis of waste pet samples, *International Letters of Chemistry, Physics and Astronomy, 4*, pp. 58-65.

[206] **Lu, Q. W., Hoye, T. R., and Macosko, C. W.** (2002). Reactivity of common functional groups with urethanes: models for reactive compatibilization of thermoplastic polyurethane blends, *Journal of Polymer Science Part A: Polymer Chemistry, 40*, pp. 2310-2328.

[207] **Tyagi, A. K., Choudhary, V., and Varma, I.** (1991). Effect of reactive diluents on curing behaviour and thermal stability of urethane methacrylate, *Die* Angewandte *Makromolekulare Chemie, 189*, pp. 105-115.

[208] **Galagan, Y. and Su, W.-F.** (2008). Reversible photoreduction of methylene blue in acrylate media containing benzyl dimethyl ketal, *Journal of Photochemistry and Photobiology A: Chemistry, 195*, pp. 378-383.

CURRICULUM VITAE

Name Surname **:** Zehra YILDIZ

Place and Date of Birth **:** Ankara, 17/04/1986

E-Mail **:** zehra.yildiz@marmara.edu.tr

EDUCATION:

B.Sc. : 2004-2008, Marmara University, Technical Education Faculty, Department of Textile Technology Education
M.Sc. : 2009-2011, Marmara University, Institute of Sciences and Technology, Department of Textile Technology Education

PROFESSIONAL EXPERIENCE AND REWARDS:

- 2008-2009 – R&D Department in Tavsanli Tekstil San. ve Tic. Ltd. Sti., Bursa, TURKEY
- 03/2009-Current – Research Assistant in Marmara University, Faculty of Technology. Department of Textile Engineering, Istanbul, TURKEY
- 10/2015-10/2016 – Visiting Researcher in Georgia Institute of Technology, School of Materials Science and Engineering, Atlanta, Georgia, USA

PUBLICATIONS AND PRESENTATIONS ON THE THESIS:

- **Z. Yildiz,** A. Gungor, H. A. Onen, and I. Usta, "Synthesis and characterization of dual-curable epoxyacrylates for polyester cord/rubber applications," Journal of industrial textiles, vol. 46, pp. 596-610, 2016.
- **Z. Yildiz,** H. A. Onen, and A. Gungor, "Preparation of flame retardant epoxyacrylate-based adhesive formulations for textile applications," Journal of adhesion science and technology, vol. 30, pp. 1765-1778, 2016.
- **Z. Yildiz,** H. A. Onen, “Dual-Curable PVB Based Adhesive Formulations for Cord/Rubber Composites: The Influence of Reactive Diluents,” International Journal of Adhesion and Adhesives, Accepted on January 2017, In Press.
- **Z. Yildiz,** H. A. Onen, A. Gungor, Y. Wang, K. Jacob, “Synthesis and application of dual-curable PVB based adhesive formulations for cord/rubber applications,” Journal of Adhesion Science and Technology, Accepted on January 2017, doi: 10.1080/01694243.2017.1289828, In Press.
- **Z. Yildiz,** M. H. Ugur, A. Gungor, H. A. Onen, Y. M. Sahin, “Synthesis and Application of UV-Curable Tung Oil Based Adhesive Formulations,” Under Review in International Journal of Adhesion and Adhesives.
- **Z. Yildiz,** H. A. Onen, A. Gungor, Y. Wang, K. Jacob, “Effects of NCO/OH Ratio and Reactive Diluent Type on the Adhesion Strength of Polyurethane methacrylates for Cord/Rubber Composites,” Submitted to Polymer-Plastics Technology and Engineering on December 2016.
- **Z. Yildiz,** H. A. Onen, A. Gungor, “Synthesis of Phosphorus Containing Bio-Based Adhesives For Textile Applications,” Oral presentation in 15th AUTEX World Textile Conference, (June 10-12, 2015), Bucharest, Romania.
- **Z. Yildiz,** H. A. Onen, A. Gungor, Y. Wang, K. Jacob, “Preparation of Dual-Curable Adhesive Formulations by Composition of Acrylic Reactive Diluents for Cord/Rubber Applications”, Oral presentation in 17th AUTEX World Textile Conference, (May 29-31, 2017), Corfu, Greece.

SOME OF OTHER PUBLICATIONS AND PRESENTATIONS:

- Gungor, I. Usta, **Z. Yildiz,** M. H. Ugur, O. Atak, “Electromagnetic Shielding Effectiveness and Electrical Properties of UV Cured E-Glass Fibre Reinforced Composites Containing Textile Surface/MWCNT/PANI/Cu Wire”, Poster presentation in 11th World Textile Conference AUTEX 2011, Mulhouse, France.
- A. Gungor, I. Usta, M. H. Ugur, **Z. Yildiz,** E. Sancak, C. Macit, “Electromagnetic Shielding and Electrical Properties of Polyurethane Acrylate/E-Glass Composites in the 3-13 GHz Frequency Range,” Poster presentation in XXX URSI General Assembly and Scientific Symposium of International Union of Radio Science, 2011, Istanbul, Turkey.
- **Z. Yildiz,** M. H. Ugur, C. Macit, I. Usta, A. Gungor, “The Effect of Polivinyl Butyral Binder on Electromagnetic Shielding Effectiveness of UV-Cured Polyurethane Acrylate/Copper Wire/E-Glass Fabric Composites,” Poster presentation in RadTech Europe 2011, Basel, Switzerland.

- **Z. Yildiz,** I. Usta, A. Gungor, "Electrical Properties and Electromagnetic Shielding Effectiveness of Polyester Yarns with Polypyrrole Deposition", Textile Research Journal, vol. 82(20), pp. 2137-2148, 2012.
- **Z. Yildiz,** I. Usta, A. Gungor, “Investigation of the Electrical Properties and Electromagnetic Shielding Effectiveness of Polypyrrole Coated Cotton Yarns”, Fibres & Textiles in Eastern Europe, vol. 21, 2(98), pp. 32-37, 2013.
- **Z. Yildiz,** O. Atak, A. Gungor, H. A. Onen, I. Usta, “The Effect of Various Dopant Types for Chemical Oxidation Polymerization of Pyrrole on Electromagnetic Shielding, Electrical Conductivity and Thermal Properties of Cotton Fabrics”, Oral presentation in 2nd International Conference on Value Addition and Innovation in Textile (Covitex) 2013, Faisalabad, Pakistan.
- **Z. Yildiz,** I. Usta, A. Gungor, H. A. Onen, “Investigation of Polypyrrole Coated Cotton Fabrics as Electromagnetic Shielding Material,” Oral presentation in 6th International Istanbul Conference on Future Technical Textile (FTT 2014). Istanbul, Turkey.
- H. Tieshi, S. Qunyan, **Z. Yildiz,** C. Kedi, Y. Wang, “Ultrafine Carbon Fibers with Hollow-Porous Multilayered Structure for Supercapacitors,” Electrochimica Acta, Accepted 14 November 2016, In Press, http://dx.doi.org/10.1016/j.electacta.2016.11.083.